PL–TR–
95–3006

Residual Strength and Life Prediction of Composite Laminates

S. Subramanian
K.L. Reifsnider
W.W. Stinchcomb

Virginia Polytechnic Institute and State University
Engineering Science and Mechanics Department
Blacksburg VA 24061

July 1995

Final Report

Approved for Public Release; Distribution is Unlimited

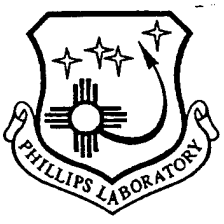

PHILLIPS LABORATORY
Propulsion Directorate
AIR FORCE MATERIEL COMMAND
EDWARDS AIR FORCE BASE CA 93524–7160

NOTICE

When U.S. Government drawings, specifications, or other data are used for any purpose other than a definitely related Government procurement operation, the fact that the Government may have formulated, furnished, or in any way supplied the said drawings, specifications, or other data, is not to be regarded by implication or otherwise, or in any way licensing the holder or any other person or corporation, or conveying any rights or permission to manufacture, use or sell any patented invention that may be related thereto.

FOREWORD

This report was prepared by Virginia Polytechnic Institute and State University, Blacksburg, VA, under MIPR, for Operating Location AC, Phillips Laboratory, Edwards AFB, CA 93524–7048. Project Manager for Phillips Laboratory was Dr. C.T. Liu.

This report has been reviewed and is approved for release and distribution in accordance with the distribution statement on the cover and on the SF Form 298.

Chi Tsuh Liu

C.T. LIU
Project Manager

Stephen L. Rodgers

STEPHEN L. RODGERS
Director
Propulsion Science Division

Ranney G. Adams

RANNEY G. ADAMS, III
Public Affairs Director

95-098

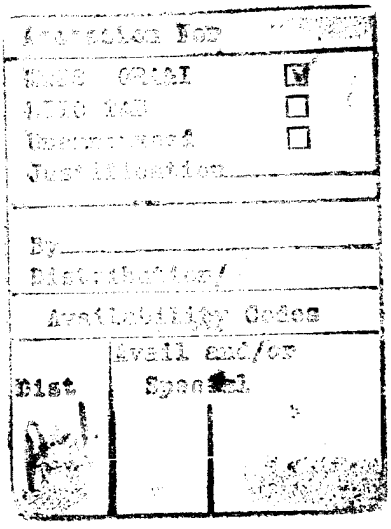

REPORT DOCUMENTATION PAGE

Form Approved
OMB No 0704-0188

1. AGENCY USE ONLY (LEAVE BLANK)	2. REPORT DATE	3. REPORT TYPE AND DATES COVERED
	July 1995	Final Report

4. TITLE AND SUBTITLE

Residual Strength and Life Prediction of Composite Laminates

5. FUNDING NUMBERS

C:
PE: 61102F
PR: 921B
TA: 00CD

6. AUTHOR(S)

S. Subramanian, K.L. Reifsnider, W.W. Stinchcomb

7. PERFORMING ORGANIZATION NAME(S) AND ADDRESS(ES)

Virginia Polytechnic Institute and State University
Engineering Science and Mechanics Department
Blacksburg VA 24061

8. PERFORMING ORGANIZATION REPORT NUMBER

9. SPONSORING/MONITORING AGENCY NAME(S) AND ADDRESS(ES)

AFFTC/RKFE
Phillips Laboratory
Edwards AFB CA 93524-1185

10. SPONSORING/MONITORING AGENCY REPORT NUMBER

PL-TR-95-3006

11. SUPPLEMENTARY NOTES

COSATI CODE(S): 20/11; 21/09/02

12a. DISTRIBUTION/AVAILABILITY STATEMENT

Approved for Public Release; Distribution is Unlimited

12b. DISTRIBUTION CODE

A

13. ABSTRACT (MAXIMUM 200 WORDS)

A systematic study was conducted to examine the influence of fiber-matrix interphase on the mechanical properties of composite laminates. Three material systems having the same carbon fibers and toughened epoxy matrix, but with different interphases were used in this study. The fibers used in the 810 A and 820 A systems received 100% and 200% surface treatments respectively, and were sized with epoxy material. The 810 O system was manufactured with 100% surface treated fiber that were sized with a thermoplastic material. Results indicate that the 810 O system had significantly greater longitudinal tensile strength and failure strain compared to the 810 A and 820 A systems. The 810 O laminates have longer fatigue lives at higher load levels and shorter fatigue lives at lower load levels compared to the 810 A laminates. The 820 A laminates have longer life compared to the other two materials systems. The cross-ply laminates from the three material systems exhibit different damage mechanisms and failure modes under monotonic tensile and fatigue loading. A micromechanics model was developed to investigate the role of the interphase on the tensile strength of unidirectional laminates. A new parameter called the 'efficiency of the interface', is introduced in the model. A simple scheme that uses the experimentally determined tensile modulus of unidirectional laminates in a concentric cylinders model, is described to estimate the interfacial efficiency. The tensile fatigue performance of cross-ply laminates is predicted using this micromechanics model in a cumulative damage scheme. The predicted fatigue lives and failure modes agree well with experimental results.

14. SUBJECT TERMS

Fatigue, composites, strength and life prediction, micromechanics, durability

15. NUMBER OF PAGES

16. PRICE CODE

17. SECURITY CLASSIFICATION OF REPORT	18. SECURITY CLASSIFICATION OF THIS PAGE	19. SECURITY CLASSIFICATION OF ABSTRACT	20. LIMITATION OF ABSTRACT
Unclassified	**Unclassified**	**Unclassified**	**SAR**

TABLE OF CONTENTS

LIST OF FIGURES

LIST OF TABLES

1.0 INTRODUCTION AND OBJECTIVE

Although the concept of fiber reinforced composite materials has been around for a long time, there has been an upsurge of interest in this class of materials over the last two decades. This has primarily been due to the demands placed on materials performance by advanced technology in the aerospace industry. In order to satisfy the requirements of the aerospace industry, materials engineers have been actively pursuing the goal of creating new material systems which possess high specific strength and stiffness. In this effort, man has turned to nature to draw on its expertise in creating the most optimized systems for different purposes. Natural wood, the human bone, etc. are some common examples of " fibrous composites " created by nature to best meet the requirements placed on these structures. In creating newer material systems, materials engineers have combined high strength and stiffness fibers with softer, less strong matrix materials to form composite materials with high specific strength and stiffness. During the last decade, a great deal of attention has been focussed on improving the performance of the two basic constituents of the composite material, namely, the fiber and matrix. Stronger, stiffer and lighter fibers are being developed towards this end. The performance of the matrix is being improved by developing tougher, damage tolerant matrices. However, in the last few years, the role of the third constituent of the composite called the "Interphase/Interface", has also received a great deal of attention. Composites engineers are currently seeking to answer the following question: ***" Can the performance of the composite system be improved by tailoring the interphase/interface region? ".*** It must be admitted that the composites community is far from having a simple answer to this question, but numerous investigations are being carried out to better understand the role of fiber-matrix interface/interphase in the performance of advanced composites. Results from these investigations indicate that the mechanical properties of composite materials can be significantly improved by altering the fiber-matrix interphase. A detailed review of the recent literature on the characterization of the interphase and its effects on the mechanical properties of composites is provided in Reference [1].

The objective of the present study is to investigate the influence of the fiber-matrix interphase on the damage characteristics and performance of cross-ply laminates under monotonic and long-term (fatigue and creep) loading. Three material systems having the same Apollo graphite fibers and HC9106-3 toughened epoxy matrix, but with different fiber surface treatments (100 % and 200 %) and sizing (Bisphenol-A (unreacted epoxy) and Polyvinylpyrrolidone (thermoplastic)) were used in this study. A $(0,90_3)_s$ cross-ply laminate configuration was used to study the performance of these material systems.

The objective of this work is to study the influence of fiber-matrix interphase on the damage and performance characteristics of graphite/toughened epoxy laminates under monotonic and fatigue and creep long term loading. Some of the specific objectives of this study are highlighted below :

- To establish the formation of different fiber-matrix interphases by varying the fiber surface treatments and sizing using qualitative and quantitative interphase characterization techniques.
- To evaluate the effect of the interphase on the unidirectional properties such as longitudinal and transverse stiffness and strength.
- To investigate the influence of the interphase on the damage characteristics and strength of $(0,90_3)_s$ laminates under monotonic loading. Various non-destructive techniques such as edge replication, x-ray radiography, acoustic emission etc. are used to document the progression of damage in the cross-ply laminate.
- To evaluate the role of fiber-matrix interphase on the damage progression and life of cross-ply laminates subjected to tension-tension fatigue loading.
- To construct analytical models including the effect of interphase, to predict the various damage mechanisms such as matrix cracking, fiber-matrix debonding and fiber fracture.
- To develop a cumulative damage scheme (that uses the models developed to predict the various damage mechanisms) and estimate the fatigue life of cross-ply laminates.

2.0 MATERIAL SYSTEM AND TEST PROCEDURE

2.1 Material System

Material used in this study was obtained from McDonnell Aircraft Co., through Dexter Hysol. Three material systems having the same high modulus Apollo carbon fibers (manufactured by Courtoulds Research) and HC 9106-3 toughened epoxy matrix, but with different fiber sizing and surface treatment, were used to study the effects of interphase. For convenience, these are designated 810 A, 820 A and 810 O systems. Table I shows the description of the fiber, sizing and matrix used in the three material system. The fibers used in the 810 A and 810 O systems received 100 % surface treatments, while those used in the 820 A system received 200 % surface treatment. The 'A' and 'O' represent the two different sizing used in the fibers. Lesko et al. [2] have identified these sizings with permission from the manufacturers. The "A" sizing is an unreacted Bisphenol-A epoxy and the "O" sizing is Polyvinylpyrrolidone (PVP), a thermoplastic material. The exact process used to get the sizing material on the fiber surface is not known (proprietary information). In general, after receiving the surface treatment, the fiber tows are passed through a bath containing the sizing material dissolved in some solvent. The fibers are coated with a thin layer of sizing material as they come out of this bath. The solvent is then removed by drying the fibers. It is interesting to note that the individual fibers are not coated with sizing material. Only tows of fiber are coated. The fiber sizing results in improved handleabilty. The sizing material (usually a polymer) also acts as a site for nucleation of polymer cross-linking, and results in better bonding between fiber and matrix.

2.2 Laminate Configuration and Specimen Geometry

Laminates were manufactured by Dexter Hysol as 6" x 6" panels using an autoclave processing method in the following lay-ups : $(0,90_3)_s$, $(0)_{12}$ and $(0)_8$. All panels were inspected for manufacturing flaws using an ultrasonic C-scan technique. The fiber volume fraction in each panel were determined using the IsoPropyl Alcohol (IPA) technique. A complete description of the IPA technique is given in Reference [3]. It must be noted that this technique does not measure the void fraction present in the system. The average fiber volume fractions in the $(0)_8$, $(0)_{12}$, and $(0,90_3)_s$ panels are given in Table II. All panels had fiber volume fractions between 56 % and 59 %. Specimens measuring 6" long and 1" wide were cut from the $(0,90_3)_s$ panels using a diamond saw for static and fatigue test. 6" long and 0.5" wide specimen were cut from the 8 ply and 12 ply unidirectional laminates. The 8 ply panels were cut along the fiber direction for longitudinal tensile test specimen, and the 12 ply panels were cut perpendicular to the fiber direction for transverse tensile test specimen. From all three material systems, small pieces of unidirectional laminates were cut and mounted in room temperature curing epoxy. After curing, the specimens were polished on a polishing wheel. These polished specimens were used for the etching and scanning electron microscopy studies.

2.3 Test Procedure

2.3.1 Quasi-Static Testing

All quasi-static tensile tests were performed on a 20 kip servo-hydraulic MTS test machine under load control mode. A loading rate of 3300 lbs /min was used for all tests on $(0,90_3)_s$ laminates. The loading rate used in the transverse tension tests on $(90)_{12}$ laminates was 200 lbs /min, while a loading rate of 5000 lbs/min was used in the unidirectional longitudinal tensile tests on $(0)_8$ laminates. A data collection software (developed in-house) was used to collect and store the load and strain data. 1" long, 0.5" wide and 0.1" thick glass/epoxy end tabs were used in the longitudinal tensile tests on $(0)_8$ laminates. The end tabs and the specimen surfaces were sanded using a 100 grit sandpaper, before gluing the end tabs to the specimen using a room temperature glue (3M#DP-460 Epoxy). In order to minimize grip

section damage in the $(90)_{12}$ and cross-ply $(0,90_3)_s$ laminates, two layers of 60 grit sandpaper with the grit side facing the specimen, were used. At least 1" on each end of the specimen was inserted into the gripping region. A grip pressure of 500 psi was used for the $(0,90_3)_s$ laminates and $(0)_8$ laminates, while a grip pressure of 50 psi was used for the $(90)_{12}$ transverse tensile tests. Strain measurement was done using a 1.0" MTS extensometer. Aluminum V-notched tabs were glued 1" apart, on the specimen using a silicone rubber glue. The knife edges of the extensometer were placed in the V-notch of each tab, and the extensometer was held in position using rubber bands. At least three specimens from each material system were loaded continuously until failure, to obtain the static strength, stiffness and strain to failure of the laminates.

2.3.2 Tensile Fatigue Testing

All fatigue tests were performed on a 20 kip servo-hydraulic MTS test machine under load control mode. Two 60 grit sand papers were used on each end of the specimen to prevent grip section damage. At least 1" of specimen was gripped on either end. A grip pressure of 500 psi was for all tests. Strain measurement was done using a 1.0" extensometer (procedure described in detail in the previous section). The dynamic stiffness was calculated using the dynamic strain (ε) that was monitored continuously as a function of cycles. In order to compare the results at different load levels, the stiffness was normalized with the initial secant modulus E_o. Since the tests were conducted under load control mode, the normalized stiffness E/E_o was obtained simply by calculating the ratio of the dynamic strain and the initial strain ($\varepsilon/\varepsilon_o$).

Fatigue tests were conducted at three load levels, with the maximum load corresponding to 85, 80, and 75 % of the static strength of the $(0,90_3)_s$ laminate. All tests were conducted at a frequency of 10 Hz, and an R ratio of 0.1. Since the 820 A laminates exhibited run-outs (life greater than 1 million cycles was termed run-out) below the 80 % load level, tests on this material system were conducted at 90%, 85% and 80% load levels.

In addition to these tests, one cross-ply specimen from each material system was fatigued at two load levels for a specific number of cycles. The specimen was removed from the testing machine and x-rayed to document the damage.

2.3.3 Interphase Characterization Testing

Etching and scanning electron microscopy

The permanganic etching technique described in reference [84] was used to characterize the interphase in the three material system used in this study. The etchant was prepared following the procedure detailed below. One gram of ground potassium permanganate ($KMnO_4$) was added to 40 ml of 85% orthophosphoric acid (H_3PO_4) and 10 ml of distilled water. This solution was stirred for 15 minutes, and the liquid was decanted off the remaining undissolved potassium permanganate. A polished section of the specimen was immersed in freshly prepared etching solution for 5 minutes. While submerged in the solution, the sample was continuously shaken. After etching for 5 minutes, the sample was washed thoroughly in cold running water. The etched sample was then coated with gold using a sputter coater and observed under the SEM at high magnifications. The 5 minute etching time was found (by trial and error method) to be adequate for the material system used in this study.

Table I Description of the three material systems used in this study.

	810 A	820 A	810 O
Fiber	Apollo	Apollo	Apollo
Matrix	HC 9106-3	HC 9106-3	HC 9106-3
Surface Treatment	100 %	200 %	100 %
Sizing	Bisphenol-A	Bisphenol-A	PolyVinylPyrrolidone

Table II Fiber volume fractions in the various laminates (estimated using IPA technique).

Laminate	810-A	820-A	810-O
$(0,90_3)_s$	55.90	57.07	57.16
$(0)_8$	56.44	56.83	58.13
$(0)_{12}$	57.46	58.27	57.41

3.0 RESULTS AND DISCUSSION

3.1 INTERPHASE CHARACTERIZATION RESULTS

3.1.1 Etching and scanning electron microscopy

Specimens from each of the three material systems were polished and etched using the technique described in the previous chapter. The etched samples were observed under the SEM at high magnifications. Figure 1 shows the scanning electron micrograph of an etched 810 A sample at 20000 X magnification. The fiber used in 810-A material appears to have an irregular shape, with numerous striations visible on the fiber surface. The figure shows an 810 A fiber surrounded by matrix material, with a dark band (that has been etched away) of interphase region between the fiber and the matrix. As mentioned earlier, the function of the etchant is to preferentially etch any uncross-linked material that is present in the system. Looking at figure 1, it may be concluded that the Bisphenol-A sizing (unreacted epoxy) forms an interphase around the fiber, that essentially consists of uncross-linked polymeric material. The interphase formed in the 810 A system is continuous as evidenced by the discountinuous dark band around the fiber (figure 1). This is not very surprising, considering that the sizing material did not contain any hardening agent. Any cross-linking of the sizing material would be due to diffusion of curing agent from the matrix material. Also seen in the figure are numerous dark spots in the matrix material. It has been reported in an earlier study [5] that the PolyEtherSupfone (PES) toughener material phase separates out in the HC 9106-3 matrix material. Since PES is a thermoplastic material (linear chain polymer), it is easily attacked by the etchant used in this study. Based on this, it is claimed that the dark regions in the matrix material represent the etched PES phase in the matrix.

Figure 2 shows the scanning electron micrograph of an etched 810-O sample at 20000 X magnification. The morphology of the interphase revealed in figure 2 is different from that seen in figure 1. It is seen that the fibers in the 810-O system are surrounded by a dark region. This uncross-linked region is surrounded by material that has a gradient morphology. The matrix material near the interphase has a different morphology than the bulk material. The presence of PVP sizing appears to have affected the cure chemistry of the matrix material near the interphase. The matrix material near the interphase is less cross linked. It is also interesting to note that the interphase formed in the 810 O system appears to be continuous and more well defined compared to that in the 810 A system. It is thus concluded that the use of different sizing results in material systems with distinctly different interphases.

In order to determine if there is any preferential distribution of PVP in the 810 O system, some of the etched samples were observed under an optical microscope at low magnification. Figure 3 shows the etched 810 O sample at 390 X magnification. The etched regions appear as dark areas in the photograph. It is seen clearly that the distribution of PVP is highly non-uniform across the specimen section. It appears that some fibers have excess PVP around them, while others do not have any coating. It is also interesting to note the high concentration of PVP at ply and tow boundaries. Since the sizing process essentially consists of pulling a fiber tow through a bath of sizing material, it is hypothesized that in the 810 O system, the fibers on the outside of the tow get coated well with PVP, while the fibers inside the tow do not receive any PVP coating. It must be emphasized here that this non-uniform distribution of PVP must be borne in mind while interpreting the results that will be presented in the following chapters. The author wishes to reiterate that the interphase morphology shown in figure 2 is not representative of the interphase present in the entire laminate. This leads one to believe that the effects of different fiber sizing could be either due to the changes in the morphology of the fiber-matrix interphase in some fibers (micro level effects) or due to a meso level effect (such as bundling of fibers, interleaving effect).

The scanning electron micrograph of an etched 820-A sample shown in figure 4 reveals fewer striations on the fibers compared to the 100 % surface treated fibers. The figure also shows that the diameter of the 200 % surface treated fibers are smaller. This is not very surprising, considering that the surface treatment process is known to remove surface layers from the fibers. This removal of surface

material could contribute to the reduction in fiber diameter. It is also interesting to note that the dark spots in the matrix that were seen in the 810 A and 820 A system are also seen in the 820 A system. As mentioned earlier, these represent the PES toughener material present in the matrix. What is most striking is the absence of any well defined interphase region near the fiber in this figure. The 200 % surface treated system does not have a low cross-link density region near the fiber surface which was seen in the other two material systems. The matrix appears to have the same morphology at regions near and away from fiber surface. It appears that the 200 % surface treatment imparted to the fiber results in enhanced chemical activity near the fiber surface. This could have resulted in complete cross-linking of the matrix material near the fiber surface. This is somewhat surprising considering that the 200 % surface treated fibers have also been sized with Bisphenol-A epoxy material. This unreacted epoxy sizing produced a discontinuous interphase in the 810 A system. There is no evidence of formation of an interphase with morphology different from that of the bulk matrix material in the 820 A system. The present results indicate that the role of fiber sizing is influenced by the level of surface treatment on the fibers.

Comparing figures 1,2 and 4 it could be said that the region near the fiber surface constituting the interphase has different morphology in the three systems. The 810 A system has a discontinuous region around the fiber which is made of uncross-linked polymeric material. In the 820 A system, this region with uncross-linked polymeric material is absent. In the 810 O system, in addition to the presence of a region with uncross-linked polymeric material, the morphology of the matrix material near the fiber is different. It appears that the cure chemistry of the matrix material near the fiber is affected by the presence of PVP, resulting in a significantly different interphase.

3.1.2 Single Fiber Fragmentation Test (SFFT)

The single fiber fragmentation tests were performed by Drzal et al at Michigan State University under contract from the Air Force. These results are reported in reference [6]. Since the same material system was used in the present study, their results are discussed in this section. Due to the restrictions on the publication of these results, the numerical values of Interfacial shear strength (ISS) are not reported here. All the results are normalized with respect to the ISS of the 810 A system. Detailed description of the test procedure and data reduction technique are provided in reference [6].

The results from SFFT on the 810 A, 820 A and 810 O system are summarised in Table III. Results indicate that the ISS of the 810 A and 820 A material system are almost identical. However, the 810 O system possesses a significantly lower ISS. It is also interesting to note that the failure modes are different for the three material system. The 810 O system exhibits 'interfacial failure', while the 810 A system indicates a mixed 'interfacial/matrix failure'. The 820 A system in contrast to the other two material system appears to exhibit a predominantly 'matrix failure'. It is noted that the system with the highest ISS exhibits a predominantly matrix failure, while the system with low ISS exhibits interfacial failure.

Table III Normalized Interfacial Shear Strength and failure modes (SFFT) [6].

810 A		810 O		820 A	
Normalized I.S.S	Failure Mode	Normalized I.S.S	Failure Mode	Normalized I.S.S	Failure Mode
1.00	Interface/ Matrix	0.79	Interface	1.02	Matrix

3.2 UNIDIRECTIONAL LAMINATE TEST RESULTS

3.2.1 Longitudinal Tensile Test

Quasi-static tests were conducted on three specimens from each of the three material systems. The average of three test results are listed in Table IV. The shows the initial stiffness, strength and strain to failure values for the three material systems. The data indicate that varying fiber surface treatment level from 100 % to 200 % does not alter the longitudinal stiffness significantly. However, the strength and strain to failure of the laminate reduces with the increase in surface treatment level. Comparison of the results for the epoxy sized 810 A and PVP sized 810 O system reveals surprising differences. The 810 O system has a significantly greater strain to failure value. It is interesting to note that the strain to failure of the 810 O fiber (obtained from the manufacturer) is 1.66 %. The 810 O unidirectional laminates have strain to failure values close to the failure strain of the fiber. This indicates that the failure of the unidirectional laminate is controlled by the global strain to failure of the fiber. The local stress concentration effects do not play an important role in the laminate strength. The strength of the 810 O laminate is 10 % greater than that of the 810 A laminate. It is thus seen that by varying the interfacial bonding, the fiber dominated properties such as longitudinal strength and strain to failure can be affected significantly. Results shown in Table IV also indicates that the longitudinal stiffness of the 810 O laminate is significantly lower than that of the 8810 laminate. There is a 16% reductions in the stiffness value going from a Biphenol-A sized fiber system to a PVP sized system. This is surprising considering that the fiber volume fraction in all the panels were almost identical. Varying the interfacial bonding was not expected to change a fiber dominated property such as longitudinal stiffness. There are a couple of explanations that could explain this phenomenon. It is possible that the sizing process results in degradation in the fiber stiffness, which manifests as a reduction in longitudinal stiffness of the laminate. However, this appears less likely, because the sized fibers were tested and the stiffness of these fibers were only 5% lower than that of the 8810 A fibers. It is also possible that the sizing process could have resulted in the breaking of the carbon fibers.

Table IV Longitudinal tensile properties of unidirectional $(0)_8$ laminates.

PROPERTY	810 A	810 O	820 A
STIFFNESS (MSI)	27.75 (0.37)	23.43 (0.86)	28.5 (0.21)
TENSILE STRENGTH (KSI)	407 (6.02)	444 (16.42)	400 (3.27)
FAILURE STRAIN (%)	1.31 (0.04)	1.66 (0.05)	1.28 (0.02)

* Values in paranthesis represent the C.O.V

The presence of broken fibers in the composite could result in reduced longitudinal stiffness. However, since the 810 A, 820 A and 810 O fibers were sized, it could be argued that the sizing process

would have resulted in similar damage to the fibers in all three material systems. The only other explanation for the reduced modulus is that there is ineffective load transfer from the matrix to the fiber in the 810 O system, due to the PVP sizing. It is hypothesized that the interphase in the 810 O system results in inefficient load transfer from the matrix to the fiber. This results in the fiber carrying less load. Since the load carrying capacity of the fiber is not fully utilized, the stiffness of the unidirectional laminate is lower. At the present moment, there is no conclusive evidence to back up this claim. However, there are indirect evidences that point to this scenario. It may be recalled that the stiffness of the unidirectional 810 O system was found to be about 10 % lower than the 810 A system in the meso-indentation tests. It must also be pointed out that Lesko et al [7], working with the same material system, have reported similar reduction in unidirectional compressive stiffness. In his work with notched cross-ply laminates, Swain [3] has also observed that the stiffness of the 810 O system was significantly lower than that of the 810 A system. In a recent study, Subramanian et al [8] have reported that the dynamic mechanical characteristics of the 810 O laminates are different from those of the 810 A laminates. They have reported that the storage modulus of the 810 O unidirectional laminates are significantly lower than that of the 810 A laminates. All these results and the results from $(0,90_3)_s$ laminates that will be discussed in the following chapters indicate that the longitudinal stiffness of the unidirectional laminates with PVP sizing is lower than that of the 810 A laminates under tensile and compressive loading.

Figure 5 shows a comparison of typical stress-strain curves for the 810 A, 810 O and 820 A systems. The figure indicates that the stress-strain curves are non-linear for all three material system. This kind of non-linear stress-strain behavior has been reported previously for graphite/epoxy composites by many investigators [9,10]. This has been attributed to the non-linear stress-strain behavior of the carbon fibers.

Figure 6 shows a comparison of the photographs of failed specimen from the three material system. The figure indicates that the 810 A and 820 A system exhibit a brittle failure, with very little longitudinal splitting. However, the 810 O laminate appears to have more of a "broom failure", with evidence of relatively more longitudinal splitting. This difference in failure modes will be discussed in more detail in the following chapters, where the same trend is seen in the cross-ply laminates under quasi-static and fatigue loading.

Based on the behavior of the unidirectional laminates, the following conclusions are made. The failure of the 810 A and 820 A system is controlled by local stress concentration effects in the vicinity of the broken fibers. This is because of the good fiber-matrix bonding that is seen in these systems. The good bonding precludes the formation of longitudinal splits/debonds near the broken fibers, resulting in the stress concentration effects near broken fibers controlling the final failure of the laminate. In the 810 O system, the lower fiber-matrix bond strength results in the formation of local splits/debonds in the vicinity of the broken fibers, thus reducing the effects of stress concentration in the adjacent fibers. This effectively decouples the broken fiber and isolates it, resulting in a global strain controlled failure of the laminate. The weaker fiber-matrix bonding is probably responsible for the unusually high strain to failure of the 810 O unidirectional laminate.

3.2.2 Transverse Tensile Test

The transverse tensile strength of the three material systems used in this study was obtained from the test on $(90_{12})_8$ laminates. The stiffness, strength, and strain to failure for the three material systems obtained from 5 tests are displayed in Table V. Before discussing the results, it must be pointed out that the C-Scan of the 810 O panel indicated that the quality of the 810 O panel was not very good. However, due to lack of availability of any other panels, the specimen from this panel was tested. The results must

be interpreted with this in mind. The results indicate that the stiffness of all three material systems are almost identical. However, the strength of the 820 A system is highest, while that of the 810 O system is the lowest. It is also interesting to note that the scatter in the strength data is high in the 810 O laminates. The low strength and the greater scatter in the data could be either due to the poor quality of the panel, or due to the PVP sizing used in the material. As will be seen in the next chapter, the data from the cross-ply laminates indicate that the transverse strength of the 810 O laminate is indeed lower, and the scatter in the data is also due to the PVP sizing. As mentioned earlier, the sizing process results in nonuniform distribution of sizing in the 8810 O system. Only the fibers on the outside of the tow received PVP coating. If the interphase in the 810 O system is weak, then the nonuniform distribution of PVP could result in a nonuniform distribution of strength in the 90° ply. This would manifest itself as greater scatter in the strength data. It is thus claimed that the "normal strength" of the interphase formed by PVP in the 810 O system is lower than that in the 810 A system. Similarly, it could be said that the "normal strength" of the interphase with 200% surface treatment is greater than that of the 100% surface treated 8810 A system.

Figure 7 shows a comparison of the stress-strain diagrams for the three material systems. The stress-strain curve is linear up to failure. As mentioned earlier, the stiffness of the three material systems was almost identical. The stiffness of the 8810 A system was the highest, while that of the 820 A system was the lowest. This is surprising because it was expected that the change in interphase would result in changes in the transverse modulus which is a matrix dominated property. In this investigation, the laminates with different interphases possess similar transverse moduli.

Table V Transverse tensile properties of unidirectional $(90)_{12}$ laminates.

PROPERTY	810 A	810 O	820 A
STIFFNESS (MSI)	1.24 (0.04)	1.22 (0.02)	1.20 (0.02)
TENSILE STRENGTH (KSI)	8.70 (0.45)	8.07 (1.98)	10.80 (3.35)
FAILURE STRAIN (%)	0.70 (0.05)	0.66 (0.18)	0.86 (0.27)

* Values in paranthesis represent the C.O.V

3.3 QUASI-STATIC TEST RESULTS : CROSS-PLY LAMINATES

3.3.1 Strength Results

Results from quasi-static tests on $(0,90_3)_s$ cross-ply laminates of the three material systems used in this study are discussed in this chapter. The average values of stiffness (as measured by elastic modulus

E_{xx}), strength, and strain to failure from three tests are shown in the Table VI. The stiffness values reported in the table represent the initial stiffness of the cross-ply laminates obtained by a linear least squares fit of the data between 0 and 1000 lbs (22 ksi). The results indicate that the stiffness of the 810 A laminates are the highest, while the stiffness of the 810 O laminates are significantly lower than that of the 810 A and 820 A laminates. These results are consistent with the unidirectional longitudinal laminate test results discussed in the previous chapter. The 810 O material has the lowest stiffness in both configurations, 0° unidirectional and $(0,90_3)_s$ cross-ply laminates. A simple classical lamination theory based analysis shows that a 16 % change in E_{11} would result in a 10 % change in longitudinal stiffness (E_{xx}) in a $(0,90_3)_s$ laminate. This is consistent with the observed 10 % stiffness reduction in the 810 O laminates, compared to that of the 810 A laminates. The stiffness of the 820 A laminate is 2.5 % lower than that of the 810 A laminate, which is not considered to be experimentally significant.

The tensile strengths of 810 A and 810 O laminates are almost identical, with the 810 O laminates having a 3 % higher strength. This is surprising considering that the 810 O system has a 10 % greater longitudinal strength compared to that of the 810 A system. The strain to failure of the 810 O laminate however is significantly higher. The failure strain of the 810 O laminate is 16 % higher than that of the 810 A laminate. This is consistent with the unidirectional longitudinal strength results. A direct comparison between the unidirectional tensile results and the cross-ply results is made because in the cross-ply laminate, once transverse crack saturation occurs, most of the load is carried by the 0° ply. The failure of the laminate is essentially controlled by the failure of the 0° plies. It is interesting to note that the strain to failure of the cross-ply laminate with PVP sizing is approximately 1.6 %, which is very close to the strain to failure of the unidirectional laminate and the fiber used in this material system. This indicates that the failure of the 810 O laminate is controlled by the strain to failure of the fiber.

Comparison of the strength of 810 A and 820 A laminates reveal that the 820 A laminate has a significantly lower strength and strain to failure. This is indicative of a brittle local stress concentration controlled failure in the 0° ply of the laminate. Ivens et al. [11] have reported similar results in their study with $(0_2,90_2)_s$ graphite/toughened epoxy laminates. Their results indicate that increasing surface treatment levels result in increased bond strength, and also increased notch sensitivity. They have attributed the reduced cross-ply strength at higher surface treatment levels to the increased notch sensitivity. The results in this study follow the trends observed by Ivens et al. [11]. The low strength of the 820 A laminate could be due to increased fiber-matrix bond strength and notch sensitivity.

Table VI Tensile properties of $(0,90_3)_s$ laminates.

PROPERTY	810 A	810 O	820 A
STIFFNESS (MSI)	7.78 (0.12)	7.01 (0.10)	7.57 (0.12)
TENSILE STRENGTH (KSI)	107 (2.16)	111 (4.58)	95.27 (2.16)
FAILURE STRAIN (%)	1.36 (0.02)	1.60 (0.06)	1.23 (0.02)

* Values in paranthesis represent the C.O.V

A comparison of typical stress-strain curves of the three material systems is shown in figure 8. The figure shows that the stress-strain curve of the 820 A laminate is approximately linear to failure. However, the stress-strain curves for 810 A and 810 O laminates exhibit non-linearities close to failure. This is indicative of damage accumulation in the laminate in the form of delaminations and fiber fractures. The 810 O laminate appears to undergo greater amount of damage prior to failure, as evidenced by the high strain to failure.

3.3.2 Damage Analysis

The damage accumulation in the cross-ply laminates of the three material systems was monitored using numerous NDE techniques and the results are discussed in this section. Two specimens from each material system were loaded incrementally, with edge replication being performed at each load level. After edge replication was performed, the specimen was unloaded, and the stiffness was measured by reloading the specimen upto 1000 lbs. The variation of crack density and the corresponding stiffness reductions are plotted as a function of applied load level in figures 9 through 12. The results of the 810 A laminates are compared separately to those of the 820 A laminates and 810 O laminates in order to bring out the influence of fiber surface treatment level and fiber sizing. Figure 9 shows the variation of transverse crack density as a function of applied load in the 810 A and 820 A laminates. The transverse crack density was determined from the crack data on the edge replicas. Data from two tests on each system are presented in the figure. The figure shows that the curves for the two systems are very similar. The onset of matrix cracking occurs slightly early in the 820 A system, and the number of cracks (per inch) at saturation is also slightly lower in the 820 A laminates. Figure 10 shows the crack density data for the 810 A and 810 O laminates. As is evident from the figure, there is a significant difference in the matrix cracking characteristics of the two systems with different sizing. The onset of matrix cracking occurs very early in the 810 O laminate. The results indicate that the onset of transverse cracking occurs at approximately 26 ksi in the 810 O laminate; but the first transverse crack appears at approximately 41 ksi in the 810 A laminates. ***By changing the fiber sizing, a 45 % increase in stress to onset of transverse cracking is achieved.*** This is a significant change considering that the sizing material forms less than 1 weight percent of the composite. The figure also indicates that the matrix cracking in the 810 A laminate occurs over a small range of stress values. The saturation of matrix cracking occurs in the 810 A laminates at a stress level of approximately 65 ksi. In contrast, the matrix cracking in the 810 O laminate occurs over a wider range of stress levels. The saturation of matrix cracking occurs at a stress level of around 58 ksi. The saturation crack spacing in the 810 A laminate is 0.05 inches, which is higher than the 0.043 inches saturation spacing in the 810 O laminate.

These results are consistent with some observations reported in the previous section. The onset of transverse cracking in the three material system is controlled by two factors; the strength of the 90° ply and the local stresses in the 90° ply. Consider the 810 O and 810 A cross-ply laminate loaded in the axial direction. Since the stiffness of the 0° ply in the 810 O system is lower than that in the 810 A system, the axial stress in the 90° ply of the 810 O system would be greater than that in the 810 A system, for the same external applied load. This would account for some reduction in the stress to onset of matrix cracking. Also, the transverse strength of the 810 O laminate is lower than the transverse strength of the 810 A laminate. This would also result in early transverse cracking in the cross-ply laminate. It is concluded that a combination of increased stress and lower strength in the 90° ply results in early transverse cracking in the 810 O cross-ply laminates.

There are two schools of thought that subscribe to different views, to explain the progressive cracking in cross-ply laminates. According to some researchers, matrix cracking is accompanied by the strain energy release. Once a matrix crack forms, the strain energy required to form the next crack is

greater [12-14]. Hence the next crack forms at a higher load level. According to the other school of thought, the progressive matrix cracking is due to the statistical variation in the local strength in the ply (or in other words, statistical distribution of flaws in the material) [15,16]. If there are fewer flaws or weak sites in the material, then the matrix cracking would occur over small load range. If however, there are more flaws in the material, then the matrix cracking would occur over a larger load range. In the 810 O system, it was observed that the distribution of PVP is non-uniform. Also the transverse strength data indicated greater scatter. This indicates that the distribution of local strength (flaws) in the 90° ply of the cross-ply laminate could have a large scatter. There could be regions in the 90° ply with very high and very low local strengths. If this is indeed the case, then onset of matrix cracking would occur very early, at sites with low strengths. Also, due to the wide distribution of local strength, the progressive cracking would occur over a larger load range. This is exactly what is seen in the 810 O laminate.

The matrix cracking results discussed in the previous paragraph could also be used to make qualitative estimates of the interfacial strength of the material system. It can be argued that if the presence of PVP results in a strong interface, then matrix cracking would initiate at regions away from the tow boundaries which has high PVP concentration. This would mean that matrix cracking would occur at regions where the fiber is bonded directly to the matrix. The interface in this region is similar to that present in the 810 A material system. This would mean that the onset of matrix cracking should occur at similar load levels in the 810 A and 810 O laminates. The experimental results however indicate otherwise. The first matrix crack appears at a significantly lower load level in the 810 O laminate. This leaves one with no choice but to conclude that the interphase formed in the 810 O laminate is the weak link. It is thus concluded that the "interfacial normal strength" of the 810 O system is lower than that of the 810 A system.

Figure 11 shows the variation of stiffness in the 810 A and 820 A cross-ply laminates as a function of applied load. The data for the 810 A and 820 A laminates are similar. This is not very surprising considering that the crack density curves for these two laminates were almost identical. The maximum stiffness reduction for the 810 A and 820 A laminates is approximately 7 %. The horizontal line in the figure indicates the amount of stiffness reduction in the two systems predicted by a complete ply discount method. The experimental data suggests that the 90° plies in both the 810 A and 820 A laminates carry load even after the saturation crack spacing is achieved. It is also observed that the onset of stiffness reduction coincides with the onset of transverse matrix cracking.

The variation in stiffness as a function of applied load for the 810 A and 810 O laminates are plotted in figure 12. The figure reveals that the stiffness reduction starts at a very low load level in the 810 O laminates. The early stiffness reduction is consistent with the early onset of transverse cracking observed in this material system. It is also noted that the 810 O laminate undergoes 10 % stiffness reduction before transverse crack saturation occurs. This is higher than the 7 % stiffness reduction in the 810 A laminate. The greater stiffness reduction is mainly due to the greater number of matrix cracks seen in the 810 O laminate. The horizontal lines in the figure indicate the amount of stiffness reduction in the two systems predicted by a complete ply discount method. The experimental data suggest that the 90° plies in both the 810 A and 810 O laminates carry load even after the saturation crack spacing is achieved.

In order to detect the damage in the 0° plies and interlaminar damage in the laminate, x-ray radiography was performed on one specimen from each material system. One specimen from each system was loaded upto 2000, 3000 and 4000 lbs, and x-rayed at each of these load levels. Details of the damage analysis results can be found in reference [17]. Results indicate that the 810 O laminate exhibits greater damage in the form of transverse matrix cracking, longitudinal splitting and local delaminations, compared to the 810 A laminate. Also, the 820 A laminate undergoes lesser damage prior to final failure, compared to the 810 A laminate.

One specimen from each material system was load monotonically upto failure, and the acoustic emission signals were monitored. These results are discussed in greater detail in reference [17]. It would suffice to mention that the acoustic emmission results support the earlier observations on the damage accumulation in these composites (x-ray radigraphy and edge replication results). In addition to the greater damage in the 810 O system in the form of matrix cracking, longitudinal splitting and local delaminations, this mterial system also exhibits more fiber fractures prior to final failure. It is also interesting to note that the 820 A system exhibits least number of fiber fractures, compared to the 810 A and 810 O systems. It is thus observed that the damage modes and failure mechanisms in the cross-ply laminates with altered interphases are vastly different.

3.4 FATIGUE CHARACTERIZATION OF CROSS-PLY LAMINATES

3.4.1 Fatigue S-N Characterization

Results from fatigue tests on $(0,90_3)_8$ laminates at various load levels are discussed in this section. The fatigue lives of the 810 A, 820 A and 8810 O systems at the three load levels are displayed in Figure 13. The lines represent linear least squares approximations. For comparison purpose, the fatigue lives are plotted against the normalized stress levels ($\sigma_{max}/\sigma_{ult}$) in Figure 13a. Results indicate that the fatigue lives of 810 O laminates are greater at higher normalized load levels, while the 810 A laminates have longer lives at lower normalized load levels. The 820 A laminates have the longest lives at all normalized load levels. The 810 A and 820 A laminates exhibit run outs at 75 % and 80 % load levels respectively (fatigue lives greater than 1 million cycles are termed run outs). The 810 O laminates possess lives less than 1 million cycles at all three load levels. However, it must be borne in mind that the static strength of the 820 A laminate was significantly lower than that of the other two systems. Hence, at the same normalized stress level ($\sigma_{max}/\sigma_{ult}$), the 820 A laminate is subjected to a lower absolute applied stress level. This is seen clearly from figure 13b which shows the fatigue lives of these laminates at various load levels. The 820 A laminates have the lowest fatigue lives at any given stress level. Also, the slope of the S-N curve of the 810 O laminate is significantly greater than that of the other two material systems. **Results indicate that cross-ply laminates of materials with the same fiber and matrix, but with different interphase, exhibit varied fatigue response.** This observation is even more surprising if we consider that the strength and life of $(0,90_3)_s$ is essentially determined by the 0° ply in the laminate. **This means that the fatigue response of the fiber dominated 0° ply, in the cross-ply laminate configuration, is sensitive to the interfacial bonding condition.** It is believed that the damage mechanisms and failure modes in the 810 A, 820 A and 810 O cross-ply laminates are vastly different which results in significantly altered fatigue performance characteristics in these materials. This claim is supported by the damage analysis results which are discussed in the following section.

3.4.2 Damage Analysis

Stiffness degradation has been used as a non destructive testing parameter to measure damage in laminated composites in a number of previous studies [18-20]. In this study, dynamic stiffness reduction was monitored for one specimen at each load level, as a function of cycles. The normalized stiffness (E/E_o) is plotted against the normalized life (N/N_f) in Figures 14,15 and 16 for the 810 A, 820 A and 810 O cross-ply laminates respectively. Results indicate that the damage evolution, as indicated by stiffness reduction, is significantly different for the three material system. Figure 14 reveals two distinct stages in the life of the 810 A laminates. Most of the stiffness reduction occurs in the first stage, during the first 10 % of the life of the specimen. The stiffness remains relatively unchanged throughout the remaining life.

At all load levels, the maximum stiffness reduction is 7-9 %. The 810 A specimens do not exhibit any accelerated damage near the end of the life, and appear to fail suddenly, in a brittle fashion. The stiffness reduction curves for the 820 A laminates at the three load levels are plotted in Figure 15. The 820 A laminates also show two distinct stages, with most of the stiffness reduction occurring in the first 10 % of the life of the laminate. The stiffness does not change appreciably after the first 10 % of the life. The total stiffness reduction in the 820 A laminates range between 3 and 8 %. Figure 16 shows that there are three distinct phases in the life of the 810 O laminates at all three load levels. Significant damage occurs in the first stage of the life of the laminate that lasts 10-20 % of the life. The stiffness change occurring in this stage is significantly higher than that measured in the 810 A and 820 A laminates. In the second stage, which continues until 90 % of the life, there is no appreciable damage occurring in the laminate. The stiffness reduces by about 2-3 % during the second stage which spans 70-80 % of the life of the laminate. In the third stage, during the last 10 % of the life, an appreciable amount of damage occurs in the laminate, as indicated by the rapid reduction in stiffness of the laminate before final failure occurs. This third stage is observed at all three load levels in the 810 O system. It is also interesting to note that the total stiffness reduction in the 810 O laminate before failure occurs ranges between 13 and 20 %. This is significantly higher than the stiffness reduction observed in the 810 A and 820 A laminates. It should be noted that the 13-20 % reduction in stiffness is significantly greater than the 12 % stiffness reduction predicted by a total ply discount theory. This leads one to believe that there is significant damage occurring the 0° ply of the 810 O cross-ply laminate in the form of fiber fractures. The presence of local delaminations on the 0/90 interface (to be discussed in the next section) could also account for some of the stiffness reduction in these laminates. It is concluded that the higher stiffness reduction in the 810 O laminate is due to the greater amount of damage in the form of matrix cracking, fiber-matrix debonding, local delaminations and fiber fracture. In sharp contrast to the failure process of 810 A and 820 A laminates, the 810 O laminates exhibit accelerated accumulation of damage at the end of the life.

In order to get a better understanding of the damage mechanisms, one specimen from each material system was fatigued at different load levels for specific number of cycles and removed for penetrant enhanced x-radiography. Figure 17 shows the x-ray radiograph of 810 A laminates at 80 % and 75 % load levels after 50,000 cycles and 1 million cycles respectively. The two dark, rectangular areas in the radiographs are the extensometer mounting tabs. The x-ray radiograph reveals numerous transverse cracks in the 810 A laminates at both load levels. The 810 A laminates have 21 and 28 transverse cracks/inch at 80 % and 75 % load levels. A few longitudinal splits are also present in the 0° ply of the 810 A laminates at both load levels. There are however no local delaminations on the 0/90 interface at both the load levels. The x-ray radiograph of the 810 A laminate after 50,000 cycles at the 80 % load level reveals an edge delamination. There is no edge delamination present in the 810 A laminate after 1 million cycles at 75 % load level. The x-ray radiographs of the 810 O laminates after 50,000 cycles and 200,000 cycles at 80 % and 75 % load levels respectively are displayed as Figure 18. The figure reveals 21 and 30 transverse cracks/inch at the 80 % and 75 % load levels respectively. In sharp contrast to the 810 A laminates, the 810 O laminates exhibit extensive longitudinal splitting at both load levels. The longitudinal splits do not extend throughout the length of the specimen and appear to be local splits/debonds. These longitudinal splits are dispersed throughout the 0° ply of the 810 O laminate. It is also interesting to note that numerous local delaminations are present on the 0/90 interface at both load levels. These local delaminations appear at intersections of the 90° and 0° ply cracks. The x-ray radiographs of 820 A laminates after 250,000 cycles and 1 million cycles at 85 % and 80 % load levels respectively are shown in Figure 19. The figure reveals 29 transverse cracks/inch at both load levels. In addition to the transverse cracks, numerous longitudinal cracks in the 0° ply are also seen in the laminates at both load levels. However, it appears that the longitudinal cracks in the 820 A laminates are longer

than those seen in the 810 O laminates. The 820 A laminates do not reveal any edge or local delaminations at both load levels. Comparing the x-ray radiographs in figures 17,18 and 19, it is clear that the damage mechanisms in the cross-ply laminates of the three material systems used in this study are significantly different.

Based on the damage analysis results, one can speculate on the strength of the fiber-matrix interphase under fatigue loading. The presence of numerous distributed longitudinal splits in the 810 O laminates leads one to believe that the interphase in this system is weaker under fatigue loading. The absence of appreciable longitudinal splits in the 810 A cross-ply laminates can be interpreted as an indication of good fiber-matrix bond in this material system. These results are consistent with the quasi-static test results discussed in the previous chapter. This leads one to believe that the performance of the interphase in these two material system are qualitatively similar under static and fatigue loading. The 820 A laminates however exhibit surprisingly different behavior under static and fatigue loading. There was no evidence of longitudinal splitting in these laminates under static loading even at very hig load levels. In sharp contrast, the 820 A laminates exhibit appreciable amount of longitudinal splitting at all load levels under fatigue loading. This leads to the question of the behavior of the interphase under static and fatigue loading. One is forced to ask the question **" Does the interphase behave differently under static and fatigue loading conditions ?"** The results from the present study do not provide a definitive answer to this question. However, there is reason to suspect that the behavior of the interphase could be different under static and fatigue loading. More systematic studies need to be performed to conclusively establish the significance and relevance of this issue.

Figures 20, 21 and 22 show the photographs of failed 810 A, 820 A and 810 O laminates fatigued at different load levels. The figure indicates that the 810 A laminate exhibits catastrophic brittle failure, with little evidence of longitudinal splitting in the 0° ply. The 820 A laminate exhibits a brittle failure with some evidence of longitudinal splitting. In contrast, when the 810 O laminate fails, the outer 0° ply shatters completely, resulting in a brush like failure. The failed specimens indicate that the failure of the 810 A and 820 A laminates are controlled by local stress concentration effects in the 0° ply, while the 810 O laminates exhibits a global failure. Since significant stiffness reduction occurs at all three load levels in the 810 O laminates prior to final failure, and the strain in the laminate exceeds 1.5 %, it can be said that the failure of the 810 O laminates is controlled by global strain to failure in the 0° ply.

From the stiffness reduction results, damage analysis, and the appearance of the failed specimen, it is concluded that the fatigue failures of the 810 A and 820 A systems are controlled by stress concentration effects near broken fibers in the 0° ply. In the 810 O system, there is more damage in the 0° ply in the form of longitudinal splitting and local delamination. It appears that these damage modes provide an energy absorbing mechanism and reduce the local stress concentration effects near broken fibers. The final failure of the 810 O cross-ply laminate is controlled by the global strain in the 0° ply. More about these effects will be discussed in the tensile strength modelling section.

The damage analysis and fatigue life results presented in this section indicate clearly that the damage mechanisms and failure modes in cross-ply laminates of the three material system used in this study are vastly different. Since the same fiber and matrix were used in these material systems, the changes could be attributed to the presence of the different interphases. **One is left with no choice but to believe that changes in fiber-matrix bonding conditions effected through subtle changes in the form of varied fiber surface treatment levels and sizing (which constitute < 1 % of the composite), alter the damage mechanisms and failure modes of cross-ply laminates under fatigue loading. This results in fatigue lives that are different by orders of magnitude.** It must however be admitted that the exact mechanism by which these changes are brought about is not fully known at the present moment.

In this section, a brief discussion is provided to explain the varied fatigue behavior (Figure 13) of the 810 A, 820 A and 810 O laminates based on the damage analysis results. It is well known that in a $(0,90_3)_s$ cross-ply laminate configuration, the final failure of the laminate is controlled by the failure of the 0° ply. The 90° ply undergoes early cracking during the first 10 % of the life, and as a result most of the load is carried by the 0° ply. Thus, in order to predict the strength and life of the laminate, the strength and life of the 0° ply needs to be estimated accurately. Recent analytical investigations [21,22] have revealed that the strength of unidirectional 0° laminate is controlled by two factors ; the stress concentration effects near broken fibers and the ineffective length. The strength reduces as the stress concentration factor increases and as the ineffective length increases. The damage analysis results indicate that the 810 O and 820 A laminates (to a lesser extent) exhibit more longitudinal splitting compared to the 810 A laminates. The effect of these splits on the stress concentration factors and ineffective length are different. The presence of longitudinal splits reduce the stress concentration effects near broken fibers and increase the ineffective length (details in the modelling section). This means that the presence of splits would improve strength and life of the laminate when stress concentration effects control the failure, and reduce the strength and life when ineffective length controls the final failure. It is postulated that in the material system used in this study, failure at high load levels (greater than 80 %) are controlled by stress concentration effects and at lower load levels, the ineffective length controls the failure. The S-N curves of the three material system can be explained using this hypothesis. Comparing the S-N curves of the 810 A and 810 O laminates, it could be said that at high load levels, the presence of longitudinal splits reduce the stress concentration effects in 810 O laminates. This results in longer fatigue lives in 810 O laminates, compared to the 810 A laminates, at higher load levels. At lower load levels, the distributed longitudinal splitting results in increased ineffective length in the 810 O laminates. The lower fatigue life of 810 O laminates at the lower load level could be attributed to this. Comparing the S-N curves for the 810 A and 820 A laminates, it can be said that the 820 A laminates have longer lives at higher load levels because of the longitudinal splits and lower absolute load levels applied in these tests (due to the lower static strength of the laminates). However, as was seen in the 810 O laminates, the slope of the S-N curve of the 820 A laminate is greater than that of the 810 A laminate. This is probably due to the presence of greater number of longitudinal splits, at lower load levels, in the 820 A laminates. These longitudinal splits increase the ineffective length and reduce the strength and life of the laminate.

The results from this study could be generalized and the following conclusion could be made. The presence of longitudinal splits result in the shifting of the S-N curve of the cross-ply laminate (whose failure is controlled by 0°ply) to the right. The longitudinal splits also appear to increase the slope of the S-N curve, resulting in poor performance under low-load long-life situations.

4.0 STATIC STRENGTH AND FATIGUE LIFE PREDICTION MODELS

In order to predict the influence of fiber-matrix interphase on the long term behavior of cross-ply laminates, a few strength and damage prediction models were developed in this study. These include models that consider the effect of an interphase at a micro-level and at a ply level. These models were used in a cumulative damage scheme to predict the fatigue lives of cross-ply laminates. The cumulative damage scheme is based on the philosophy used in the 'Critical Element Model' proposed by Reifsnider and Stinchcomb [23]. The damage progression in a cross-ply laminate has been studied extensively by numerous researchers [24-26]. It is well established that the main damage mechanisms in this laminate configuration include the transverse matrix cracking, longitudinal splitting, and delaminations (both local and free edge). The final failure of this laminate is controlled by the tensile failure of the 0° ply in the laminate. It is also well established in the literature that the failure of the 0° ply is essentially controlled by the accumulation of fiber fractures in the ply [27,28]. Hence, in order to predict the strength and life of cross-ply laminates, the accumulation of matrix damage (transverse, longitudinal cracks and delamination) as well as the accumulation of fiber fractures need to be predicted accurately. In this study, a model that includes the effect of fiber-matrix interphase, has been developed, to predict the tensile strength of the unidirectional laminates. In order to predict the accumulation of transverse matrix cracks, the 1-D shear lag model proposed by Reifsnider [29] has been modified to include the effects of an interphase. Results from these two models have been used in a cumulative damage scheme to predict the fatigue life of cross-ply laminates. These modelling efforts will be discussed in three sections. In the first section, the tensile strength prediction model is described and some salient features of this model are highlighted. In the next section, the shear lag model used to predict the progressive transverse cracking in cross-ply laminates is described. Finally, these models are used in a cumulative damage scheme to predict the damage evolution and life of cross-ply laminates under fatigue loading. The damage and fatigue life predictions are compared with experimental values.

4.1 Unidirectional Tensile Strength Prediction Model

The tensile failure of unidirectional composites has been studied by numerous researchers [30-32] in the past two decades. It is well recognized that the tensile failure of unidirectional laminates is best described by a cumulative damage process. The final failure results from the accumulation of damage in the form of fiber fractures in the unidirectional laminate. The properties of the fiber and matrix such as strength and stiffness, have been shown to influence the tensile strength of the unidirectional laminate significantly. Some recent experimental [33,34] and analytical efforts [22,27] have, however, brought out the importance of the role of the fiber-matrix bonding (also referred to as the interface/interphase) in determining the tensile failure process. Based on these models, it is clear that the tensile strength of the unidirectional laminate is dependent on the ineffective length and the stress concentration effects near fiber fractures. Recently, Reifsnider et al. [22,27] realized that the assumption of a perfectly elastic matrix may not reflect the physics of the problem accurately. The high shear stresses in the matrix material near broken fibers could lead to local matrix plasticity and/or fiber matrix debonding. They also observed that both the ineffective length and stress concentration factors could vary as a function of the number of fiber fractures. Based on this, they constructed a model that considers elasto-plastic matrix deformation near fiber fractures. They estimated the ineffective length and stress concentration factors using shear lag analysis and used this in Batdorf's model to predict the tensile strength. This model shows that when the fiber-matrix bond strength is low, debonding occurs. Under these conditions, the failure of the laminate is controlled by the ineffective length. However, when the fiber-matrix bond strength is high, elastic failure

(controlled by stress concentration effects near broken fibers) is observed. In the elastic failure regime, higher bond/yield strength results in greater stress concentrations, leading to reduced strength. When the failure is accompanied by debonding/yielding, higher bond/yield strength reduces the ineffective length and hence increases the tensile strength. **This analysis clearly indicates that, generally speaking, when elastic failure occurs, the tensile strength reduces with increasing fiber-matrix bond strength values. However, when interfacial debonding occurs in the material, the tensile strength increases with increasing interfacial strength values. The model predicts the existence of an optimum interfacial strength value for which the tensile strength is maximum.**

Using this scheme, the authors were able to predict a maximum of 7-8 % changes in tensile strength for graphite/epoxy laminates. Recent experimental efforts [11,33,34], however, have shown that by changing fiber surface treatment and sizing in graphite/epoxy laminates, 40-50 % changes in tensile strength could be obtained. However, these experimental results must be interpreted with some degree of caution. Higher levels of surface treatment are known to remove weak outer carbon fiber layers and improve fiber-matrix bonding. But, during this process, the fiber strength could also be degraded significantly. This could result in lowered tensile strength at higher surface treatment levels. However, in the authors opinion, the model described in reference [22] captures the qualitative trends reported in references [11,33,34], but does not predict the actual changes in strengths observed experimentally. This could be due to one or a combination of the following reasons. This model considers perfect bonding between fiber and matrix prior to interfacial debonding. There is some experimental evidence that shows that this may not be true. The longitudinal stiffness of the unidirectional laminate calculated assuming perfect bonding (using the rule of mixtures) appears to over predict the stiffness values in laminates where poor fiber-matrix bonding is observed. In their study with AU4, AS4 and AS4C fibers in Epon 828 matrix, Madhukar and Drzal [35] have observed over 10 % increase in longitudinal modulus going from an untreated AU4 system to a surface treated AS4 system. They have also reported a 5 % increase in tensile modulus in the AS4C laminates compared to the AS4 laminates. Similarly, Ivens et al [11] have reported upto 20 % increase in longitudinal modulus of $(0_2,90_2)_s$ laminates going from an untreated system to a 100 % surface treated system. Since the transverse modulus of a unidirectional graphite/epoxy composite is almost 20 time lower than its longitudinal modulus, it can be easily shown that the contribution of the 90° ply to the overall stiffness of the cross-ply laminate used in their study is less than 5 %. This being the case, the 20 % stiffness change between the untreated and 100 % surface treated system must be a direct consequence of stiffness changes in 0° ply. Ivens et al have used the argument of unbonded fibers proposed by Gresczuk [36] to explain this behavior. They claim that the reduction in longitudinal stiffness could be due to a certain volume fraction of fibers not being bonded to the matrix material. In the present study, 16 % reduction in the longitudinal modulus of unidirectional laminates were observed going from a Bisphenol-A sized fiber to a PVP sized fiber system. These and numerous other investigations indicate that the longitudinal modulus of unidirectional laminates could be altered by a significant amount by varying the interphase. In the authors's opinion, this indicates that the longitudinal stiffness of unidirectional laminate is influenced significantly by the nature of bonding that exists between the fiber and matrix. In systems with good bonding, the matrix transfers the load to the fiber effectively and the stiffness of the laminate approaches the value predicted by a rule of mixtures. The assumption of perfect bonding between fiber and matrix is valid under those conditions. However, when the bonding between the fiber and the matrix is poor (as in the case of untreated fiber systems and also in the systems with certain sizings), there could be inefficiency in the load transfer between the matrix and the fiber. This could result in a discontinuity in displacement between the fiber and the matrix. Since the matrix does not transmit all the load into the fiber, the stiffness of the laminate is reduced. Under such conditions, the perfect bonding assumption is not valid. Hence, while modelling

interphase problems, the perfect bonding assumption must be used with caution. The model in reference [22] uses a perfect bonding assumption. This could be one reason for the difference in the experimental and predicted tensile strength values.

In the model developed in reference [22], it is assumed that the matrix material undergoes plastic deformation even after the first fiber fracture. However, it is often observed that the first fiber fracture occurs at load levels that are almost half the failure loads. At such load levels, the interface may not fail. In order to accurately predict the tensile strength, the failure of the interface should be checked after each fiber fracture. If the interface does not fail, then elastic analysis must be performed. If interfacial failure occurs before the final failure of the laminate, then a plastic analysis must be performed

In this study, the tensile strength prediction model proposed in reference [22] is modified to account for some of the factors discussed in this section. A brief description of the model is given below. Following the work of Gao and Reifsnider [22], the broken fibers are assumed to form a central core with a layer of matrix material around it. The nearest neighboring row of fibers are assumed to be arranged such that it forms a concentric cylinder around the central core of broken fibers. Concentric cylinders of matrix material and average composite material are assumed to be wrapped around this. Figure 23 shows a schematic of the arrangement described above. The nomenclature used in this chapter is described in Appendix 1. The calculation of the geometric parameters and the average properties of the central core are described in Appendix 2. The force equilibrium equations for the central core of broken fibers and the adjacent fibers are written in the following form

$$E_f \pi r_f^2 \frac{d^2 u_f}{dx^2} + 2\pi r_f \tau_{m1} = 0 \tag{1}$$

$$n_i E_{f2} \pi r_{f2}^2 \frac{d^2 u_{f2}}{dx^2} + 2\pi r_m \tau_{m2} + 2\pi r_{f2} \tau_{m3} = 0 \tag{2}$$

where

$$\tau_{m1} = \left(\frac{u_{m2} - u_{m1}}{b} \right) G_i$$

$$\tau_{m2} = \left(\frac{u_{m1} - u_{m2}}{b} \right) G_i \tag{3}$$

$$\tau_{m3} = \left(\frac{u_c - u_{m2}}{b} \right) G_i$$

In writing these relationships, it is assumed that the displacement varies linearly in the radial direction, in the matrix material. Assuming that the displacement in the fiber and matrix at the fiber-matrix interface is discontinuous, and that the displacement in the average composite is uniform, the following expressions can be written

$$u_c = \frac{\sigma_a x}{E_x} \tag{4}$$

$$u_{m1} = \eta\, u_{f1} \tag{5}$$

$$u_{m2} = \eta\, u_{f2} \tag{6}$$

where η is the 'efficiency factor' that determines how well the load is transferred from the matrix into the fiber. $\eta = 1$ indicates perfect bonding and good load transfer at the interface, while $\eta = 0$ indicates complete debonding with no transfer of load from the matrix into the fiber. It must be mentioned here that this 'efficiency factor' may be estimated using the measured tensile modulus of the unidirectional laminate. A detailed description of the procedure used for estimating the 'efficiency factor' from the longitudinal modulus is given in Appendix 3.

Using equations 4,5 and 6, the equilibrium equations (1 and 2) are written in the following form

$$\frac{d^2 u_{f1}}{dx^2} + k_1\, u_{f1} + k_2\, u_{f2} = 0 \tag{7}$$

$$\frac{d^2 u_{f2}}{dx^2} - k_3\, u_{f2} + k_4\, u_{f1} + k_5\, x = 0 \tag{8}$$

where

$$k_1 = -\frac{2\, r_{f1}\, \eta\, G_i}{b\, E_{f1}\, r^2_{f1}}$$

$$k_2 = -k_1 \tag{9}$$

$$k_3 = \frac{2\, r_m\, \eta\, G_i}{n_i\, b\, E_{f2}\, r^2_{f2}} + \frac{2\, r_{f2}\, \eta\, G_i}{n_i\, b\, E_{f2}\, r^2_{f2}}$$

$$k_4 = \frac{2\, r_m\, \eta\, G_i}{n_i\, b\, E_{f2}\, r^2_{f2}}$$

$$k_5 = \frac{2\, r_{f2}\, \eta\, G_i\, \sigma_a}{n_i\, b\, E_{f2}\, r^2_{f2}\, E_x}$$

Equations 7 and 8 have to be solved subject to the following boundary conditions

$$\left(\frac{du_{f1}}{dx}\right)_{x=0} = 0 \tag{10}$$

$$\left(u_{f2}\right)_{x=0} = 0 \tag{11}$$

The solution to the problem is obtained as

$$u_{f2} = D_1 e^{-\alpha x} + D_2 e^{-\beta x} + D_3 x \qquad (12)$$

$$u_{f2} = D_1 e^{-\alpha x} + D_2 e^{-\beta x} + D_3 x$$

The constants are given by equation 13 and α and β are given by equation 14 shown below.

$$C_3 = \frac{-k_2 k_5}{k_1 k_3 + k_2 k_4}$$

$$D_3 = -C_3$$

$$C_1 = \left(-\frac{k_2}{\alpha^2 + k_1}\right) D_1$$

$$C_2 = \left(-\frac{k_2}{\beta^2 + k_1}\right) D_2 \qquad (13)$$

$$D_1 = \frac{C_3}{\left[\frac{\beta k_2}{\beta^2 + k_1}\right]}$$

$$D_2 = -D_1$$

$$\alpha, \beta = \left[\frac{(k_3 - k_1) +\_ \sqrt{(k_1 + k_3)^2 + 4 k_2 k_4}}{2}\right]^{1/2} \qquad (14)$$

The strains and stresses in the central core and the adjacent fibers are obtained using the strain-displacement and constitutive relationships as

$$\varepsilon_{f1} = \frac{du_{f1}}{dx} \; ; \; \sigma_{f1} = E_{f1} \varepsilon_{f1}$$

$$\varepsilon_{f2} = \frac{du_{f2}}{dx} \; ; \; \sigma_{f2} = E_{f2} \varepsilon_{f2} \qquad (15)$$

The elastic stress concentration factor in the adjacent fiber is then written as

$$C_i = \left(\sigma_{f2}\right)_{x=0} \tag{16}$$

The elastic ineffective length is obtained by determining the length over which the inner core recovers 99 % of the applied stress. It is obtained by solving the following equation for x

$$\sigma_{f1}(x) = 0.99\ \sigma_a \tag{17}$$

Having obtained the elastic stress concentration factor (C_i) and the elastic ineffective length(δ_i), the corresponding plastic stress concentration factor C^*_i and the plastic ineffective length (δ^*_i) are obtained using the following approximation. It is assumed that the matrix exhibits an elastic-perfectly plastic behavior. If the average shear stress in the interphase exceeds the interfacial shear strength, the interface is assumed to debond. Once debonding occurs, the shear stress in the matrix is assumed to be constant over the region defined as the plastic ineffective length, and zero elsewhere. The plastic stress concentration factor is estimated by calculating the average stress in the adjacent fiber as follows

$$\overline{\sigma_{f2}} = \frac{1}{\delta}\int_0^{\delta} \sigma_{f2}\, dx \tag{18}$$

$$C^*_i = \frac{\overline{\sigma_{f2}}}{E_{f2}\ D_3} \tag{19}$$

It turns out that the plastic stress concentration factor calculated in this manner is 1. In order to estimate the plastic ineffective length, the force balance argument is used to obtain

$$\delta^*_i = \frac{\overline{\sigma_{f1}}\ r_{f1}}{2\ \eta\ \tau_i} \tag{20}$$

where $\overline{\sigma_{f1}}$ is the average stress in the inner core and is given by

$$\overline{\sigma_{f1}} = \frac{E_{f1}}{\delta}\int_0^{\delta} \varepsilon_{f1}\, dx \tag{21}$$

$$\overline{\sigma_{f1}} = \frac{E_{f1}}{\delta}\left(C_3\ \delta - C_1 - C_2\right) \tag{22}$$

Note that in writing the force balance equation, it has been assumed that due to interfacial debonding, the shear stress in the matrix is not equal to the interfacial shear strength, but is multiplied by the 'efficiency factor' η. This is because once debonding occurs, the stress transfer occurs essentially by means of friction. It is expected that the stress transfer in this region after debonding occurs will not be perfect. The shear stress is multiplied by the efficiency factor to reflect this behavior. Knowing the stress

concentration factors and ineffective lengths (elastic and plastic) for the different fiber breakages (i-plets), the tensile strength is predicted following Batdorf's analysis.

Batdorf has shown that the stress level at which the first fiber fracture occurs (singlet) is given by

$$\sigma_1 = \left(\frac{1}{NL}\right)^{\frac{1}{m}} \sigma_0 \tag{23}$$

where N = Total number of fibers in the specimen
L = Normalized length of the specimen
m = Weibull strength shape factor for the fiber
σ_0 = Weibull strength location parameter for the fiber

The stress level at which the subsequent fiber fractures occur is given by

$$\sigma_i = \left(\frac{1}{NL\,\pi\, n_{i-1}\, \lambda_{i-1}}\right)^{\frac{1}{im}} \sigma_0 \qquad i = 2,3,..... \tag{24}$$

where

$$\lambda_i = 2\,\delta_i \left[\frac{C_i^{m+1} - 1}{(C_i - 1)\,(m+1)}\right] \tag{25}$$

and n_i are the number of nearest neighbors around a core of i broken fibers. The number of nearest neighbors are estimated assuming that the fibers are arranged in a hexagonal packed system.

The procedure used for estimating the tensile strength is detailed below. The stress required for breaking the first fiber is first estimated using equation 23. At this stress level, the average shear stress in the matrix region is estimated by integrating the shear stress in the matrix over the elastic ineffective length as follows

$$\overline{\tau_m} = \frac{1}{\delta}\int_0^{\delta} \left(\frac{u_{2m} - u_{1m}}{b}\right) G_i\, dx \tag{26}$$

$$\overline{\tau_m} = \frac{G_i\,\eta}{\delta b}\left[\frac{(D_1 - C_1)}{\alpha} + \frac{(D_2 - C_2)}{\beta}\right] \tag{27}$$

It is assumed that interfacial debonding occurs when the average shear stress in the matrix exceeds the interfacial shear strength. Subsequent fiber failure loads are calculated using equation 24. At each load level, it is checked to see if interfacial failure occurs. The elastic stress concentration factors (SCF) and ineffective lengths are used in equation 24 until interfacial failure is observed. Once interfacial failure occurs, the plastic SCF and ineffective lengths are used in equation 24 to predict subsequent fiber fractures. If there is no interfacial failure until instability occurs, then the final failure is classified as elastic failure. If debonding occurs prior to final failure, the failure is termed plastic.

Using the model described above, the tensile strength and the failure mode of unidirectional laminates can be predicted. It must be mentioned here that the prediction scheme requires that the Weibull strength parameters for the fiber be known. It is also required to normalize the lengths used in the analysis with a characteristic length value. In this study, all the lengths are normalized by a factor of $100*r_f$. The typical radius of a carbon fiber is around 5 microns. The factor $100*r_f$ is chosen because 500 microns is very close to the typical critical length value obtained for graphite/epoxy composites using the single fiber fragmentation test. Parametric studies were conducted to investigate the influence of various parameters on the failure mode and tensile strength of unidirectional graphite/epoxy composites. The results from these studies are discussed below. The following parameters were used in all the calculations discussed in this section.

$N =$ 1 Million (Total number of fibers)

$L' =$ 5 inch (Length of the specimen)

$l =$ $100*r_f$ (Normalization length)

$r_f =$ 5 microns (Fiber radius)

$v_f =$ 0.60 (Volume fraction)

$\sigma_0 =$ 500 ksi (Fiber strength Weibull location parameter)

$E_f =$ 44 msi (Fiber stiffness)

$E_x =$ $E_c*(\eta)^{0.66}$ (where E_x is the composite stiffness, E_c is the composite stiffness predicted using the rule of mixtures and η is the efficiency factor) [This relationship was obtained using the CCM detailed in Appendix 3]

Using these parameters, the influence of the interfacial shear strength, efficiency factor, matrix shear modulus, and Weibull strength shape factor on the tensile strength of the unidirectional laminate was investigated. In all the figures, the tensile strength of the laminate has been normalized with the Weibull location parameter σ_0. Figure 24 shows the variation of normalized tensile strength with the interfacial shear strength for different values of Weibull shape factor (m). The figure shows clearly that the tensile strength increases with 'm'. The figure also indicates that high interfacial strengths result in elastic failures, while low interfacial strengths result in plastic failures. In the elastic failure range, the strength of the unidirectional laminate is independent of the interfacial shear strength. This is because the elastic stress concentration factors and ineffective lengths used to estimate the strength are independent of the interfacial shear strength. When the interfacial shear strength is low, early debonding occurs. Under these conditions, the tensile strength reduces rapidly as the interfacial shear strength decreases. For intermediate interfacial shear strength values, the transition from elastic to plastic failure is observed. In this region, even though the failure is plastic, the plastic ineffective length is small and the failure is still controlled by the stress concentration factor. Since debonding reduces the stress concentration factor, the tensile strength increases with reducing interfacial strength values. It is thus observed that when the failure is controlled by stress concentration effects, interfacial debonding increases the tensile strength. This makes physical sense in that debonding results in decoupling the broken fiber from the rest of the composite and alleviates the stress concentration effects. However, when the plastic ineffective length controls the failure, debonding reduces the tensile strength. This is because the plastic ineffective length increases with debonding very rapidly, and the tensile strength reduces with increasing ineffective length. In figure 25, the variation of tensile strength as a function of the efficiency factor η is plotted for various values of 'm'. It is observed that when the failure is elastic, the tensile strength reduces with increasing η. However, when the composite material failure is preceded by interfacial failure, the trends are reversed. Tensile strength in this regime increases with increasing values of η. It is also interesting to note that as the value of 'm' increases, the tensile strength increases. Since the tensile strength is low for small values of 'm', the shear stress in the matrix material is low, and hence most of the failures are elastic. For high

values of 'm', the shear stresses in the matrix are significantly higher. This results in early debonding at the interface and most failures are plastic. It is also noted that elastic failure occurs when η is large and plastic failure occurs when η is small. Let us take a moment to consider the physical significance of η. As mentioned earlier, large values of η indicates effective load transfer at the interface (good bonding) and low values of η results in ineffective load transfer which is indicative of poor fiber-matrix bonding. This means that when fiber-matrix bonding is good, elastic failure (controlled by SCF) occurs, and poor bonding results in plastic failure accompanied by fiber-matrix debonding.

The variation of tensile strength as a function of the interfacial shear strength for two different values of η are shown in figure 26. The figure reveals that for a given value of η, an optimal interfacial shear strength value exists, for which the tensile strength of the composite is maximum. However, it is observed that the optimal interfacial strength value is a function of η. As η reduces, the optimal interfacial strength value and the maximum tensile strength achievable increases.

Based on the predictions of this model, it is claimed that the interface can be characterized completely by the two parameters η and τ. For example, changes in the interfacial conditions effected through fiber surface treatment and sizing can be fully represented using these two parameters. Knowing these two parameters, the tensile strength of the unidirectional laminate can be predicted. It is also interesting to note that by varying these two parameters slightly, the tensile strength of the unidirectional laminate could be altered significantly. This is especially true when the failure mode changes from elastic to plastic or vice-versa.

Using the scheme described, the tensile strength of the 810 A, 820 A and 810 O laminates were estimated. It must be mentioned here that most of the data necessary for the strength prediction are not available. However, since the same fiber and matrix material has been used in the three systems, and only the interphase has been changed, the necessary values were assumed but kept constant for the three systems. Only the interfacial shear strength and efficiency factor values were altered to reflect the changes in interphase. This enables us to compare the predicted values of tensile strength with the experimental values. It must be mentioned here that as far as possible, most of the values used in the model were assumed to be typical values used for most graphite/epoxy composites. Some of the properties used in the strength prediction model are listed below

$N =$ 1 Million (Total number of fibers)
$L =$ 5 inch (Length of the specimen)
$l =$ $100*r_f$ (Normalization length)
$r_f =$ 5 microns (Fiber radius)
$v_f =$ 0.60 (Volume fraction)
$\sigma_0 =$ 1000 ksi (Fiber strength Weibull location parameter)
$m =$ 5
$E_f =$ 44 msi (Fiber stiffness)
$E_x =$ $E_c*(\eta)^{0.66}$ (where E_x is the composite stiffness, E_c is the composite stiffness predicted using the rule of mixtures and η is the efficiency factor)
G_m = 0.18 msi

810 A		**820 A**		**810 O**	
η	= 0.9	η	= 0.95	η	= 0.77
τ_m	= 14 ksi	τ_m	= 14 ksi	τ_m	= 12 ksi

The above properties were chosen based on experimental data on these material systems. The experimental results indicate that the interface is weakest in the 810 O system and strongest in the 820 A system. Hence, the ISS of the 810 O was assumed to be lower than that of the other two systems. Also,

the experimental data from unidirectional laminate tests indicate that the stiffness of the 820 A laminates is very close to the values predicted by the rule of mixtures. The experimental values diverge very significantly for the 810 O system. Using the procedure described in Appendix 3, the efficiency factors for the three systems were estimated. **It must be emphasized that these values are based on experimental data on these material systems and were not chosen arbitrarily.**

Using the properties listed above, the tensile strength of the three material systems were predicted. Table VII shows the predicted and experimental tensile strength values for the three material systems. The table also shows the predicted failure modes and number of i-plets formed before final failure occurs. The model predicts that the 810 A and 820 A laminates do not exhibit interfacial failure prior to final failure. However, the 810 O system exhibits plastic failure. It may be recalled that the non-destructive testing results for the cross-ply laminates indicated similar results. The NDE results revealed that the 810 A and 820 A laminates exhibit less interfacial debonding and the failed specimen suggest that the failure is elastic. In sharp contrast, the 810 O laminate exhibits extensive fiber-matrix debonding and the failed specimen suggests a global strain controlled failure. These observations are consistent with the predictions shown in Table VII. The AE results indicate that the number of fiber fractures in the 0° ply of the cross-ply laminate is highest in the 810 O laminate and lowest in 820 A laminates. The tensile strength model predicts the observed trends very well. Maximum fiber fractures are predicted by the tensile strength prediction model in the 810 O system, followed by the 810 A and 820 A system respectively. It is thus seen that the failure modes and the tensile strength values predicted by the model agree very well with the experimental values.

4.2 Prediction of matrix cracking and damage in cross-ply laminates

Numerous models are available in the literature to predict the onset of transverse matrix cracking in laminated composites. Most of these models use modified forms of shear lag analysis to estimate the stresses in the laminate with a transverse crack [37-42]. These stresses are used in some stress/strain/strain energy based failure criterion to predict the onset of transverse matrix cracks in laminated composites.

In this study, the one dimensional shear lag model proposed by Reifsnider [37] has been used to determine the saturation crack spacing and the stress state in the cross-ply laminates with transverse matrix cracks. A novel scheme that uses the Weibull strength parameters of the 90° ply is used in conjunction with the shear lag analysis results to predict the onset and progression of transverse matrix cracks. It is well known that the strength of the 90° ply is dependent on the volume of the 90° ply. It has been observed that as the volume of the 90° ply increases, the strength reduces. This behavior has been explained using the following arguments. As the volume of the 90° ply increases, the number of flaws present in the ply also increases. The presence of a greater number of flaws increases the probability of failure and reduces the strength of the laminate. In the present model, similar arguments are used to account for the changes in the transverse cracking characteristics due to changes in volume of the 90° ply. A brief description of the model is given in the next section. First, a brief description of the shear lag model is provided. This is followed by a description of the scheme that uses the results from shear lag analysis to predict the onset and progression of matrix cracking.

The one dimensional shear lag model proposed by Reifsnider [37] has been used to study the matrix cracking behavior in $(0,90_3)_s$ cross-ply laminates. Since detailed descriptions of the problem formulation and solution technique are available in the literature [37], the discussion here will be limited. The schematic of the matrix cracking problem to be solved using the shear lag analysis is shown in figure 27. The figure shows a transverse matrix crack in the 90° ply constrained by 0° plies on either side. The

thickness of the 90° ply and the 0° ply are denoted by 'a' and 'c' respectively. It is assumed that the stresses are transferred from the 90° ply to the 0° ply through a shear transfer mechanism over a small region. This region is assumed to have a thickness of 'b'. Let U_0 and U_{90} represent the axial displacement of the 0° ply and the 90° ply respectively. The force equilibrium equations for the 0° ply and the 90° ply are written as

$$A \frac{d^2 u_{90}}{dx^2} + (u_0 - u_{90}) = 0 \tag{28}$$

$$B \frac{d^2 u_0}{dx^2} + (u_{90} - u_0) = 0 \tag{29}$$

where

$$A = \frac{E_{90}\, b}{2\, E_x\, a}$$
$$B = \frac{E_0\, b\, c}{E_x\, a^2} \tag{30}$$

Equations 28 and 29 are solved subject to the following boundary conditions

$$\left(\frac{d_{u90}}{dx}\right)_{x \geq \infty} = 1 \tag{31}$$

$$\left(\frac{d\, u_0}{dx}\right)_{x \geq \infty} = 1 \tag{32}$$

$$\left(\frac{d\, u_{90}}{dx}\right)_{(x=0)} = 0 \tag{33}$$

$$(u_0)_{(x=0)} = 0 \tag{34}$$

Assume a solution of the following form

$$u_{90} = x + C_1\, e^{-\alpha x} + C_2\, e^{-\beta x} \tag{35}$$

$$u_0 = x + C_1 D_1 e^{-\alpha x} + C_2 D_2 e^{-\beta x} \quad (36)$$

Substituting the assumed displacement functions in the equilibrium equation (equations 28 and 29), the constants are obtained using the boundary conditions (Details available in refence [1].)

Having obtained the complete solution, the stresses in the 90° ply and the 0° ply are written as

$$\sigma_{90} = \frac{\sigma_a E_{90}}{E_x}\left[1 - \alpha C_1 e^{-\alpha x} - \beta C_2 e^{-\beta x}\right] \quad (37)$$

$$\sigma_0 = \frac{\sigma_a E_0}{E_x}\left[1 - \alpha C_1 D_1 e^{-\alpha x} - \beta C_2 D_2 e^{-\beta x}\right] \quad (38)$$

It was reported earlier that the accumulation of transverse matrix cracks occurs over a range of applied external load. It was observed that gradual accumulation of transverse matrix cracks in the 90° ply of the cross-ply laminate occurs as the applied external load is increased incrementally, until a Characteristic Damage State (CDS) is reached. Beyond this, the transverse crack density does not change as the applied external load increases. The matrix cracking is accompanied by reduction in the axial stiffness of the laminate. Experimental data indicated that the onset and rate of accumulation of transverse cracks was different for the three material system examined. It must be mentioned that when the applied load level is significantly greater than the load level at which CDS is achieved, new transverse cracks appear at locations between the existing cracks. In this analysis, only the transverse cracking characteristics before the CDS is reached, is modeled. The onset and progression of transverse cracking in the cross-ply laminate is predicted using the results from the shear lag analysis (described in the previous section) and the Weibull strength parameters for the 90° laminate.

The shear lag analysis is used to determine the saturation crack spacing and the characteristic damage state (CDS). The saturation crack spacing (SCS) is the distance from the crack face, over which 99.9 % of the applied external stresses are recovered in the 90° ply of the laminate. The CDS is obtained by calculating the reciprocal of the SCS (CDS = 1/SCS). The CDS essentially represents the number of cracks/inch in the 90° ply of the laminate, when saturation of transverse matrix cracking occurs. This is a function of the material properties and laminate configuration.

It is claimed that the accumulation of transverse matrix cracks occur over a range of applied external load because of the non-uniform distribution of flaws/defects in the 90° ply. The distribution of flaws would essentially result in a non-uniform distribution of local strength in the 90° ply. Due to the spatial distribution of strength in the 90° ply, the transverse cracks would form at different locations in the 90° ply, at different applied load levels. Under these assumptions, matrix cracks would occur at locations in the 90° ply where the local stresses exceed the local strength. It is postulated that the spatial distribution of local strength in the 90° ply is directly related to the Weibull strength parameters of 90° laminates. The shape factor (α) and location parameter (β) for the 90° laminate can be obtained by fitting the experimental transverse strength data with a two parameter Weibull fit. The Weibull shape factor α indicates the distribution of the strength about the mean value, and β is a measure of the mean strength. In this study, only 5 specimens were tested from each material system under a transverse tensile loading mode. The data were fitted with a two parameter Weibull distribution, and the corresponding α and β values (Maximum Likelihood Parameter estimates) for the three material system are located in Table VIII. The data clearly indicates that the spread in the strength is more in the 810 O and 820 A laminates. Also,

the location parameter (β) is highest for the 820 A system and lowest for the 810 O system. Since very few tests were performed, the values of α and β obtained from the transverse test data may not be accurate. However, the trends obtained from these results are used to estimate the values α and β to be used in the model. The assumed values of α and β used in this analysis are shown in Table IX. Using these values of α and β in conjunction with the results from the shear lag analysis, the onset and progression of matrix cracking is predicted.

For an applied external stress σ_a, the strain (ε_{90}) in the 90° ply is calculated using CLT. Knowing the Weibull strength parameters for the 90° laminate, the probability of failure of the 90° ply in the cross-ply laminate at a strain level ε_{90} is written as

$$p(\varepsilon_{90}) = 1 - \exp\left(-\frac{\varepsilon_{90}}{\beta}\right)^{\alpha} \tag{39}$$

It is postulated that the number of transverse matrix cracks/inch at a strain level ε_{90} is related to the probability of failure of the 90° ply in the cross-ply laminate by the following linear relationship

$$n_{cr} = n_{CDS}\, p(\varepsilon_{90}) \tag{40}$$

where n_{cr} is the number of cracks at any applied external stress σ_a, n_{CDS} is the number of cracks in the 90° ply when saturation of matrix cracking occurs, and $p(\varepsilon_{90})$ is the probability of failure of the 90° ply in the cross-ply laminate at that strain level. This functional representation essentially indicates that when the probability of failure of the 90° ply is less than 1 %, there is no transverse matrix cracking. As the probability of failure increases, the number of transverse matrix cracks also increase. When the probability of failure is 100 %, saturation of matrix cracking occurs (the Characteristic Damage State is reached).

It is well known that the formation of transverse matrix cracks is accompanied by a stiffness reduction in the laminate. The presence of transverse cracks reduces the load carrying capacity of the 90° ply. This results in a reduction in the stiffness of the 90° ply and the whole laminate. In order to estimate the reduction in stiffness of the 90° ply and the laminate due to the formation of a single transverse crack, results from the shear lag analysis are used. The stiffness reduction scheme proposed by Lim and Hong [42] is used in this analysis. The average strain in the 0° ply, in the presence of a single transverse crack in the 90° ply is determined as

$$\overline{\varepsilon_0} = \frac{\sigma_a}{l\, E_x} \int_0^l (1 - \alpha\, C_1\, D_1\, e^{-\alpha x} - \beta\, C_2\, D_2\, e^{-\beta x})\, dx \tag{41}$$

which yields

$$\overline{\varepsilon_0} = \frac{\sigma_a}{l\, E_x} (l + C_1\, D_1\, (e^{-\alpha l} - 1) + C_2\, D_2\, (e^{-\beta l} - 1)) \tag{42}$$

It is assumed that the crack occurs at a constant applied external load and the constitutive relations for the uncracked and cracked laminates are written as

$$\sigma_x = \varepsilon_0\, E_x \qquad \textit{(Uncracked laminate)} \tag{43}$$

$$\sigma_x = \overline{\varepsilon_0}\,\overline{E_x} \qquad \textit{(Cracked laminate)} \tag{44}$$

Combining equations 40, 41 and 42, the stiffness reduction due to the formation of a single transverse matrix crack in the 90° ply of the cross-ply laminate is written as

$$\frac{\overline{E_x}}{E_x} = \frac{l}{l + C_1 D_1 (e^{-\alpha l} - 1) + C_2 D_2 (e^{-\beta l} - 1)} \tag{45}$$

where $\overline{E_x}$ is the stiffness of the laminate in the presence of a single transverse crack, E_x is the undamaged initial stiffness of the laminate, l is the distance over which the stresses are perturbed due to the presence of the crack, and the other parameters such as α, β, C_1, C_2, D_1 and D_2 are shear lag parameters defined earlier. Having estimated the stiffness reduction in the laminate, the stiffness reduction in the 90° ply can be estimated easily using CLT (assuming that the stiffness of the 0° ply does not change). Since a cross-ply laminate is used in this study, this can be estimated by using the rule of mixtures in the following way

$$\overline{E_{90}} = \frac{\overline{E_x} - E_0 v_0}{v_{90}} \tag{46}$$

where E_0 is the axial stiffness of the 0° ply, v_0 and v_{90} are the volume fractions of the 0° and 90° plies in the laminate respectively.

The variation of transverse matrix crack density with the applied load is given by equation 40 and the corresponding stiffness reduction in obtained from equation 45. The accumulation of damage in the cross-ply laminate is predicted using these equations as follows. The applied external load is increased incrementally and the load level required to initiate the first transverse crack is calculated using equation 40. The stiffness reduction associated with the formation of the first crack is then estimated using equation 45. Using the reduced stiffness, the shear lag analysis is performed and the new values of α, β, C_1, C_2, D_1 and D_2 are calculated. Using these values, the load level required to initiate the next crack and the corresponding stiffness reduction are calculated. This procedure is repeated until the saturation of matrix cracking is achieved.

Using the cumulative damage scheme described in the previous paragraph, the matrix cracking characteristics of 810 A, 820 A and 810 O laminates predicted. The material properties used in the model to predict this are displayed in Table X. The variation of transverse matrix crack density and the associated stiffness reduction for the 810 A and 810 O laminates predicted using this scheme are compared with the experimental data in figures 28 and 29. The figures show good correlation between the experimental and predicted values. The model predicts the early onset of transverse cracking in the 810 O laminate very well. It also predicts a greater number of transverse matrix cracks in the 810 O laminate when saturation occurs. This compares well with the experimental data. It is also interesting to note that even though the load level at which onset of matrix cracking occurs is significantly different for the 810 A and 810 O laminates, the difference in the load level at which saturation of matrix cracking occurs is not much. It is concluded that the differences in the load required to initiate the transverse matrix cracking is due to a combination of reduction in the stiffness of the 0° ply and the greater distribution in the strength of the transverse (90°) ply. This analysis brings out the importance of the Weibull strength parameters in the onset and progression of transverse matrix cracking very well. It is observed that even when the average transverse strength of the 90° ply in two material systems is not very different, the onset of matrix cracking in the 90° ply could occur very early if the distribution of strength

in the 90° ply is not uniform. As was mentioned earlier, the distribution of PVP in the 810 O laminate was uneven. It was observed that fibers on the outside of the tow had excess amounts of PVP and those on the inside of the tow had lesser or no PVP. This could have resulted in the wider distribution of strength (weak links) in the 810 O laminates. This is confirmed by the greater scatter in the transverse strength data of the 810 O laminates and the early onset of matrix cracking in the cross-ply laminate.

The experimental and predicted variation of transverse crack density and stiffness reduction in the 810 A and 820 A laminates are displayed as figures 30 and 31. It is again observed that the predictions correlate well with the experimental data. It is noted that even though the average transverse strength ofthe 820 A laminate is greater than the 810 A laminate, the onset of transverse cracking occurs at almost the same load levels in the two material system. This is due to the greater variation in the transverse strength of the 820 A laminate that is reflected by the lower value of α for this system. The horizontal lines in figures 29 and 31 indicate the stiffness reduction predicted using the ply discount method which assumes the stiffness of the 90° ply is zero. The experimental data and the present analysis indicate that the 90° ply carries load even after saturation of matrix cracking occurs.

4.3 Fatigue Life Prediction

Numerous models have been forwarded in recent years for predicting the long-term behavior of laminated composite materials. Some of the commonly used methods have been discussed in the literature review section. In this study, a cumulative damage scheme based on the Critical Element Model [23] has been used to predict damage and fatigue life of cross-ply laminates. This model uses a semi-empirical approach, where the results from the damage analysis are used in conjunction with the models described earlier, to predict the long-term behavior of cross-ply laminates. Figure 32 shows a schematic of the outline of the critical element model. The laminate is considered to be composed of sub-critical elements and critical elements. The sub-critical elements are defined as those elements that undergo damage during fatigue loading, but the failure of these elements does not result in the final failure of the laminate. In contrast, the primary load carrying member in the laminate, is designated as the critical element. The failure of the whole laminate is controlled by the failure of this element. In $(0,90_3)_s$ laminates, the 90° ply is the sub-critical element, and the 0° ply is the critical element. It is assumed that most of the damage occurs in the sub-critical element, while the final failure of the laminate is considered to coincide with the failure of the critical element. The damage in the sub-critical element results in degradation of properties (eg. stiffness) and this results in redistribution of stresses. Based on the damage in the sub-critical element, the stresses in the critical element are calculated as a function of cycles. The critical element itself would exhibit time dependent property degradation (eg. strength degradation of 0° ply under fatigue loading represented by the S-N curve for the 0° ply, damage in the 0° ply in the form of interfacial damage, etc). This is obtained from experiments performed on 0° laminates. After each block of loading cycles, the stress and strength of the critical element are used in an appropriate failure function (eg. maximum stress/strain, Tsai-Hill etc) to predict the failure of the critical element. It is assumed that the failure of the laminate coincides with the failure of the critical element. The fatigue life is defined by the number of cycles required for the failure of the critical element.

The damage analysis results discussed earlier indicate that transverse matrix cracking, creep deformation in the 90° ply and local delaminations on the 0/90 interface are the main damage mechanisms associated with the sub-critical element. In the critical element, other than the strength reduction in the 0° ply characterized by the S-N curve of the 0° laminate, fiber-matrix debonding is observed in some laminates. Based on these experimental observations, a cumulative damage scheme is constructed to predict the fatigue life of cross-ply laminates. A schematic of the cumulative damage

scheme is shown in figure 33. A detailed description of the scheme is provided in this section. The variation of the transverse crack density as a function of cycles is determined experimentally for the three material systems at different load levels. In order to construct a master curve, independent of the applied load level, the crack density is multiplied by a factor $\left[1 - \left(\frac{\sigma_{max}}{\sigma_{static}}\right)\right]$ and plotted against the number of cycles. These data are fitted with a power law curve to obtain a single master curve that describes the variation of crack density as a function of cycles. The master curves for the three material systems are shown in figure 34. The master curve that describes the variation in crack density in the different material system at different load levels (in the form of a power law curve) is provided as an input to the model. Using the shear lag model and the crack density variation provided as an input, the stiffness reduction in the 90° ply is calculated after each block of cycles. The stiffness reduction in the 90° ply due to creep (determined experimentally and discussed in detail in [1]) is also input into the model in the form of a power law curve. The total stiffness reduction in the 90° ply (due to damage and creep) after each block of cycles is estimated by adding the individual components. The stiffness of the entire laminate is then calculated using the rule of mixtures (equation 30). Classical Lamination Theory is used to calculate the stresses and strains in the 0° ply (using the damaged properties of the 90° ply), after each block of cycles. It must be mentioned here that this scheme neglects the interaction between the damage and creep phenomena.

The S-N curves for the 0° laminates of the three material system used in this study were not available. Hence, an S-N curve was assumed for each of the three material systems. Since the same fiber and the same matrix material were used, the same S-N curve was used for the three material systems. It must be mentioned here that the insitu S-N curve of the 0° ply in the cross-ply laminate could be different from that of the 0° laminate. This is because of the transverse stresses that are present in the 0° ply of the cross-ply laminate. These transverse stresses could initiate debonding in the 0° ply. As mentioned earlier, the debonding in the 0° ply would result in a reduction in the efficiency of load transfer from the matrix to the fiber and vice-versa. This is accounted for by varying the efficiency factor η in the 0° ply as a function of cycles. Since there is no direct way to experimentally determine this variation, a polynomial function is assumed to describe the variation of η as a function of cycles. The polynomial describing the variation of η with cycles was used in conjunction with the tensile strength model to predict the insitu tensile strength variation of the 0° ply as a function of cycles. The predicted tensile strength is then used in the assumed S-N curve of the 0° ply to estimate the degradation of the insitu tensile strength of the 0° ply as a function of cycles.

The tensile strength and the tensile stress estimated thus are used in a maximum strain failure criterion after each block of cycles to check for the failure of the critical element. If the critical element fails, then the calculation is terminated and the number of cycles at which this occurs is assumed to be the fatigue life.

The influence of fiber-matrix interphase is included in the present model in a number of different levels. Different creep stiffness reduction curves and crack density variation curves are input into the model for the three material system with different interphases. The calculation of stiffness reduction using the shear lag model also includes the effects of interphase at a lamina level. The influence of interphase on the behavior of the critical element is also included in this model. This is done by varying the efficiency factor η which reflects the interfacial bonding condition.

In this section, the rationale behind using some specific forms of equations (which were not generated experimentally) to predict the fatigue life of cross-ply laminates with different interphase is discussed. The S-N curve for the 0° laminate was not experimentally generated because of the lack of

availability of specimens for testing. As mentioned earlier, since the same fiber and matrix material were used in the three material systems, and since the influence of the interphase is introduced in the model through the efficiency factor η, the same S-N curve equation was used for all three material systems. An equation that is consistent with the typical S-N curves of graphite/epoxy 0° laminates was used. It was experimentally observed that the debonding characteristics in the 0° ply of the three material system were significantly different. This was used as a guide while choosing the functional relationships describing the variation of η as a function of cycles. It was reported earlier that the 810 O laminates exhibit extensive debonding in the 0° ply, while the 810 A laminates exhibit very few debonds. The 820 A laminates revealed intermediate amount of debonding in the 0° ply. In order to reflect this, it was assumed that η remains unchanged in the 810 A laminates and 820 A laminates. The stiffness reduction data also indicate these trends. As was mentioned in the tensile strength modeling section, the interfacial efficiency (η) is directly related to the longitudinal stiffness. Degradation in η results in a reduction in the longitudinal modulus of the 0° ply of the laminate. Hence, the experimentally measured stiffness reduction data can be used directly to estimate the changes in η as a function of cycles. The stiffness reduction data indicate that there is very little stiffness reduction in the 810 A and 820 A systems after the first 10 % of the life. Also, the amount of stiffness reduction is small, indicating that it is primarily due to matrix cracking in the 90° ply. This indicates that there is no significant stiffness reduction in the 0° ply of the laminate. Hence, it is assumed that η remains constant under fatigue loading in these two material systems. In contrast, there is significantly greater amount of stiffness reduction in the 810 O laminate. Also, there is appreciable stiffness reduction occuring in the laminate after the intial stiffness drop in the first 10 % of the life. This indicates that the stiffness of the 0° ply reduces as a function of cycles in this material system. In order to reflect this, a linear stiffness reduction equation is used for the 810 O system. The assumed variations of η as a function of cycles are shown in figure 35. The variation of tensile strength with η for the three material system, predicted by the model is depicted in figure 36. Note that the 810 A and 820 A system are represented by the same curve because all the parameters for these two systems used in the model are identical. However, the interfacial shear strength for the 810 O system was assumed to be lower than that of the 810 A and 820 A system. This results in a different curve for the 810 O laminate. The figure suggests that the tensile strength increases initially as η reduces. However, for small values of η, the strength starts reducing significantly. Combining the relationship that describes the variation in η with cycles and the relationship that describes the variation in tensile strength with η, the variation in tensile strength with cycles can be obtained. This is combined with the assumed S-N curve to obtain the variation of insitu strength of the 0° ply of the three material systems.

Using these experimental data along with the assumed functional relationships described earlier, the fatigue lives of the 810 A, 820 A and 810 O laminates are predicted at various applied load levels. All the equations used for the three material system are listed in Table XI.

A comparison of the experimental and predicted fatigue lives for the three material systems at the different load levels is shown in figures 37 through 39. The figures show good correlation between experimental and predicted fatigue lives. Some of the experimental observations that are predicted well by the model and some limitations of the model are listed below

- The fatigue lives of the 820 A laminates are higher than those of the 810 A and 810 O laminate at all three load levels.
- The 810 A laminates have lower life at 85 % load level and higher life at 75 % load level compared to the 810 O laminate.
- The S-N curve for the 810 O laminate has the highest slope, followed by the 820 A and 810 A laminates.

It must be pointed out that in order to obtain better estimates of fatigue lives and minimize the assumptions involved in the life prediction scheme, the following approach should be used.

- The S-N curves for the 0° laminates must be obtained experimentally.
- The variation of η as a function of cycles should be experimentally determined. It must be mentioned here that a method that involves the measurement of hysteresis loss as a function of cycles has been used in ceramic matrix composites to measure the effect of sliding friction at fiber-matrix debonds. This could yield quantitative information about the extent of debonding in the material. This method could be used to obtain the variation of η as a function of cycles.
- The interaction between damage and creep must be experimentally characterized and used in the model.

Based on the experimental results and the predictions from the model, it is claimed that the presence of interfacial debonding influences the fatigue behavior in the following manner. In general, the presence of fiber-matrix debonding reduces the stress concentration effects and increases the ineffective length. In the high stress, low life situation, the stress concentration effects control the laminate failure. The presence of debonds in the 0° ply alleviates the stress concentration effects in this regime and increases the fatigue life of the 810 O laminates. In the low load, long life regime, the ineffective length controls the final failure. The presence of debond increases the ineffective length and reduces the fatigue life under these conditions. This is reflected in the greater slope of the S-N curve of the 810 O laminates. It can thus be concluded that for the material system under investigation, the presence of fiber-matrix debonds in the 0° ply shifts the S-N curve to the right and also increases the slope of the S-N curve. Depending upon the extent of debonding, the fatigue lives of the cross-ply laminates are altered differently.

Table VII Comparison of experimental and predicted unidirectional static strength

	Strength (ksi) (Expt)	Strength (ksi) (Pred)	Fiber Fractures (Expt)	Fiber Fractures (Predicted i-plets)	Debonding (Expt)	Debonding (Pred)
810 A	407	392	Few	18	None	No
810 O	444	432	Numerous	25	Extensive	Yes
820 A	400	388	Very Few	18	None	No

Table VIII Weibull strength parameters for the 810 A, 820 A and 810 O 90° laminates estimated from experimental transverse strength results

	810 A	810 O	820 A
α	22.2	4.3	4.0
β (%)	0.719	0.726	0.992

Table IX Weibull strength parameters for the 810 A, 820 A and 810 O 90° laminates used in the shear lag model.

	810 A	810 O	820 A
α	9	5	6
β (ksi)	0.718	0.655	0.833

Table X Material properties for 810 A, 820 A and 810 O material system used for static damage prediction

	810 A	810 O	820 A
E_{11} (msi)	27	24	27
E_{22} (msi)	1.24	1.22	1.2
G_{12} (msi)	0.7	0.7	0.7
ν_{12}	0.3	0.3	0.3
E_{xx} (msi)	7.68	6.91	7.68
G_m (msi)	0.15	0.15	0.15
t_{ply} (in)	0.0055	0.00525	0.0055
b (in)	0.00055	0.000525	0.00055

Table XI Equations for the 810 A, 820 A and 810 O material system used in the fatigue damage and life prediction model

810 A	810 O	820 A
$n[1-(\sigma_{max}/\sigma_{ult})] = 2\ (N)^{0.08}$	$n[1-(\sigma_{max}/\sigma_{ult})] = 2\ (N)^{0.09}$	$n[1-(\sigma_{max}/\sigma_{ult})] = 0.4\ (N)^{0.2}$
$\varepsilon_0^{fat} = \varepsilon_0^{st}\ (1.02 - 0.013\ \ln(N)^{0.9}$	$\varepsilon_0^{fat} = \varepsilon_0^{st}\ (1.02 - 0.013\ \ln(N)^{0.9}$	$\varepsilon_0^{fat} = \varepsilon_0^{st}\ (1.02 - 0.013\ \ln(N)^{0.9}$
$\eta = 0.95$	$\eta = 0.89 - 1.8*10^{-8}*N - 1.02*10^{-14}*N^2 - 3*10^{-18}*N^3$	$\eta = 1 - 0.05\ \ln(N)$
$\varepsilon_0^{st} = 0.014$	$\varepsilon_0^{st} = 0.73 + 0.62*\eta - 0.39*\eta^2$	$\varepsilon_0^{st} = 1.25 - 1.48*\eta + 3.15*\eta^2 - 1.92*\eta^3$
$E_{90}^{crp} = E_{90}\ [1.03\ (t)^{-0.008}]$	$E_{90}^{crp} = E_{90}\ [1.09\ (t)^{-0.020}]$	$E_{90}^{crp} = E_{90}\ [1.03\ (t)^{-0.008}]$

n = Number of transverse cracks/in

N = Number of cycles

t = Time (sec)

η = Efficiency factor

E_{90} = Unidirectional transverse stiffness (msi)

E_{90}^{crp} = Unidirectional transverse stiffness including creep effects (msi)

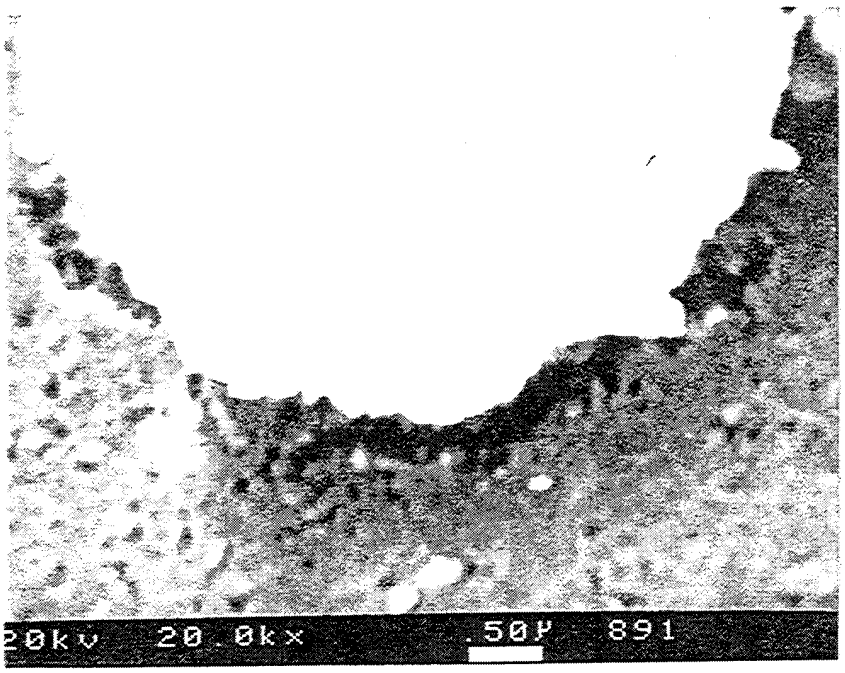

Figure 1 Scanning electron micrograph of an etched 810 A specimen (20000 X)

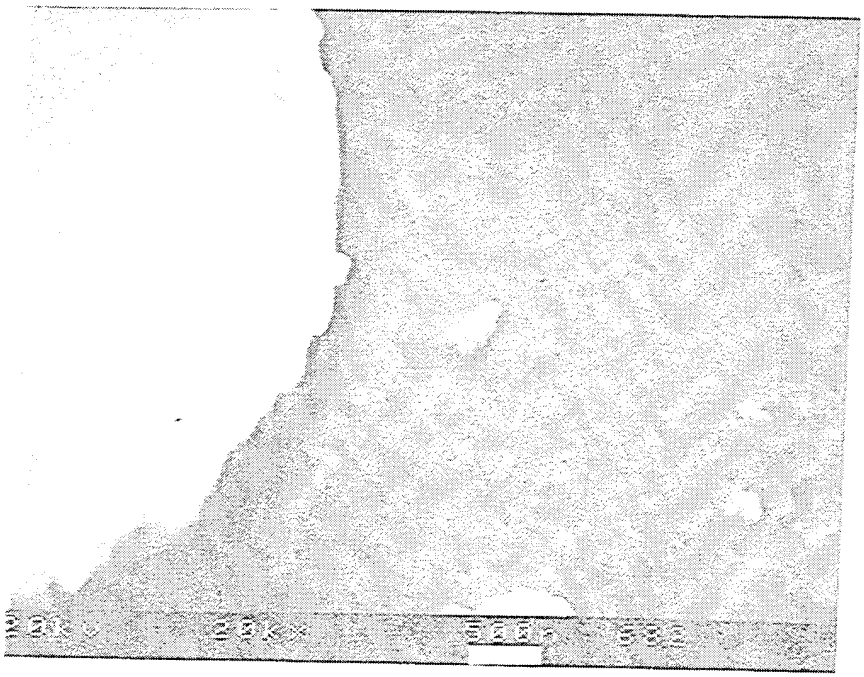

Figure 2 Scanning electron micrograph of an etched 810 O specimen (20000 X)

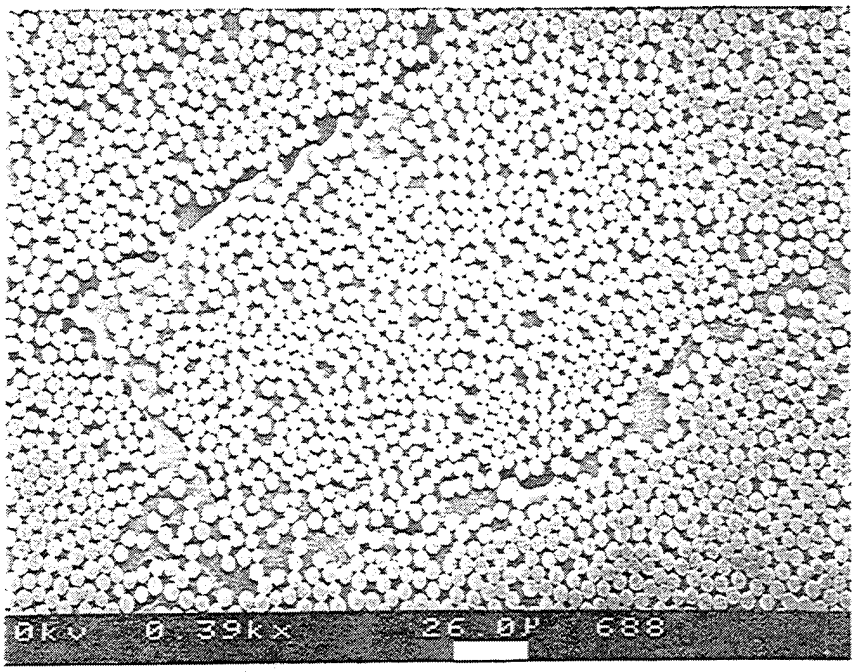

Figure 3 Optical micrograph of an etched 810 O specimen (500 X)

Figure 4 Scanning electron micrograph of an etched 820 A specimen (20000 X)

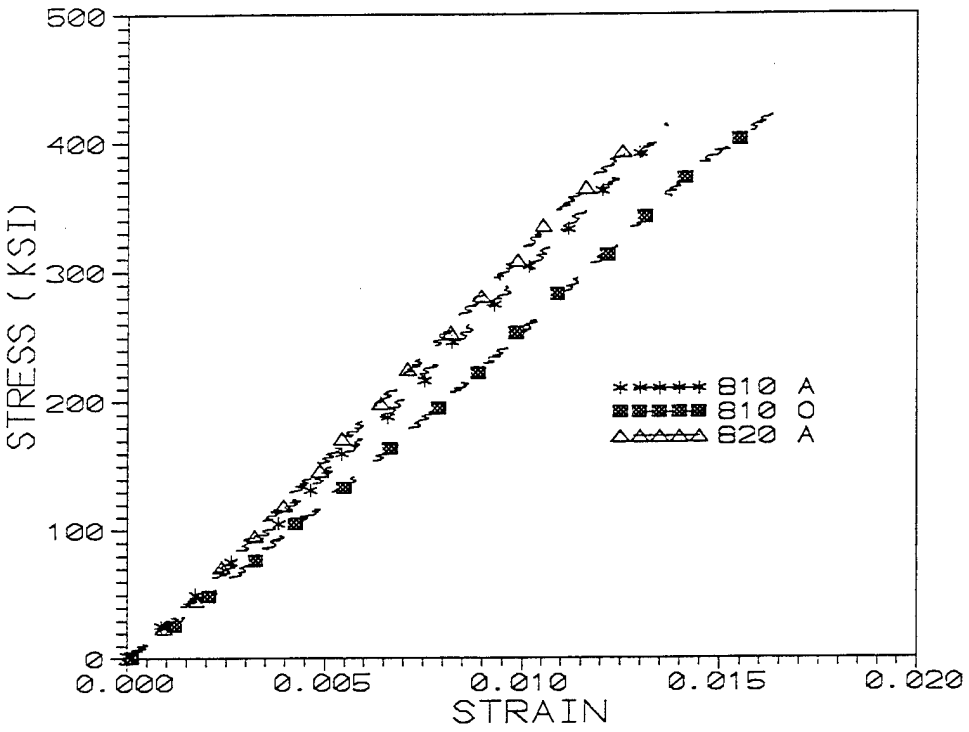

Figure 5 Typical stress-strain diagrams of $(0)_8$ unidirectional 810 A, 820 A and 810 laminates.

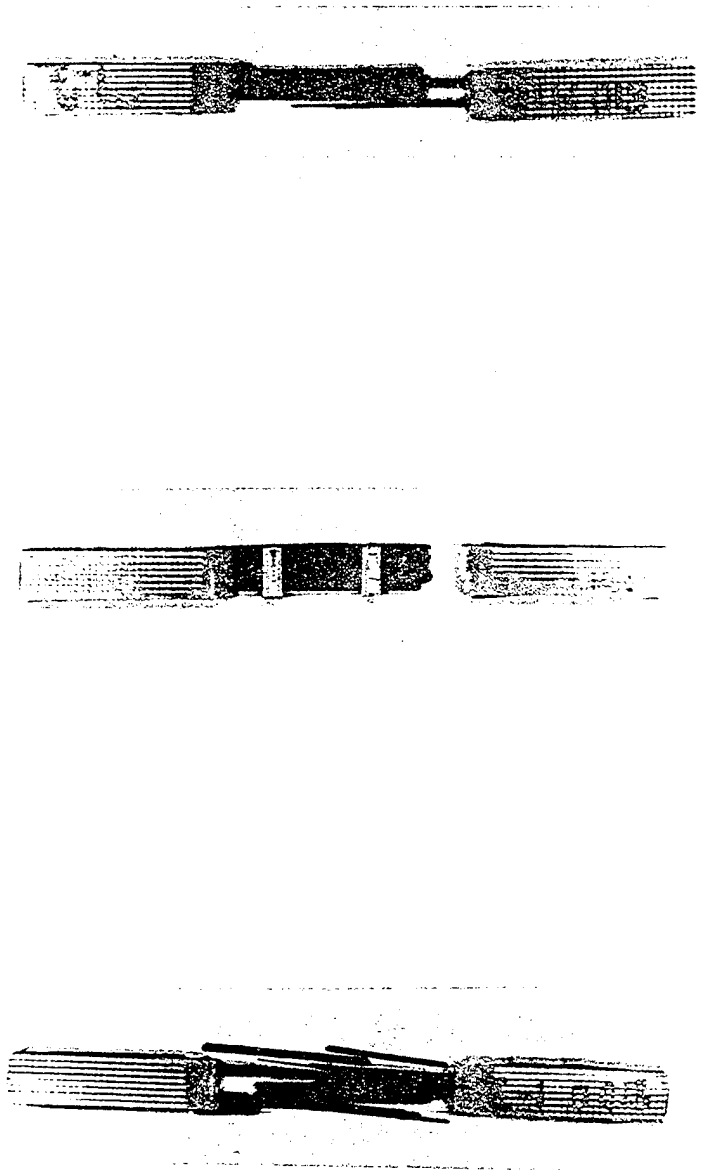

Figure 6 Photograph of failed $(0)_8$ unidirectional laminates;Top : 810 A; Middle : 820 A; Bottom: 810 O

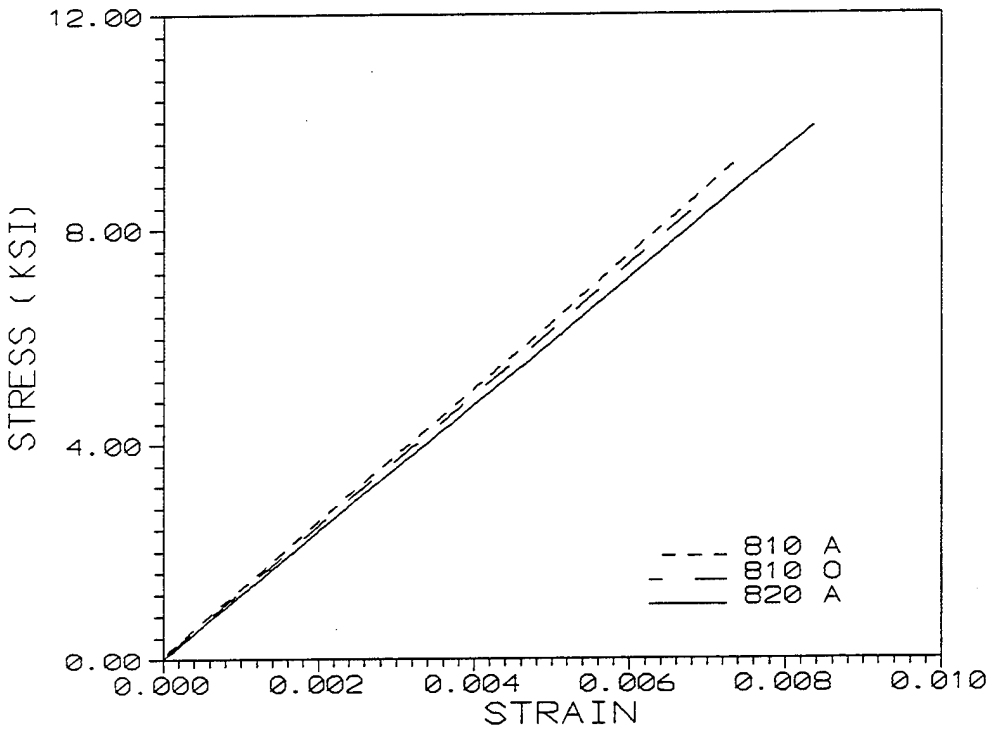

Figure 7 Typical stress-strain diagrams of $(90)_{12}$ unidirectional laminates

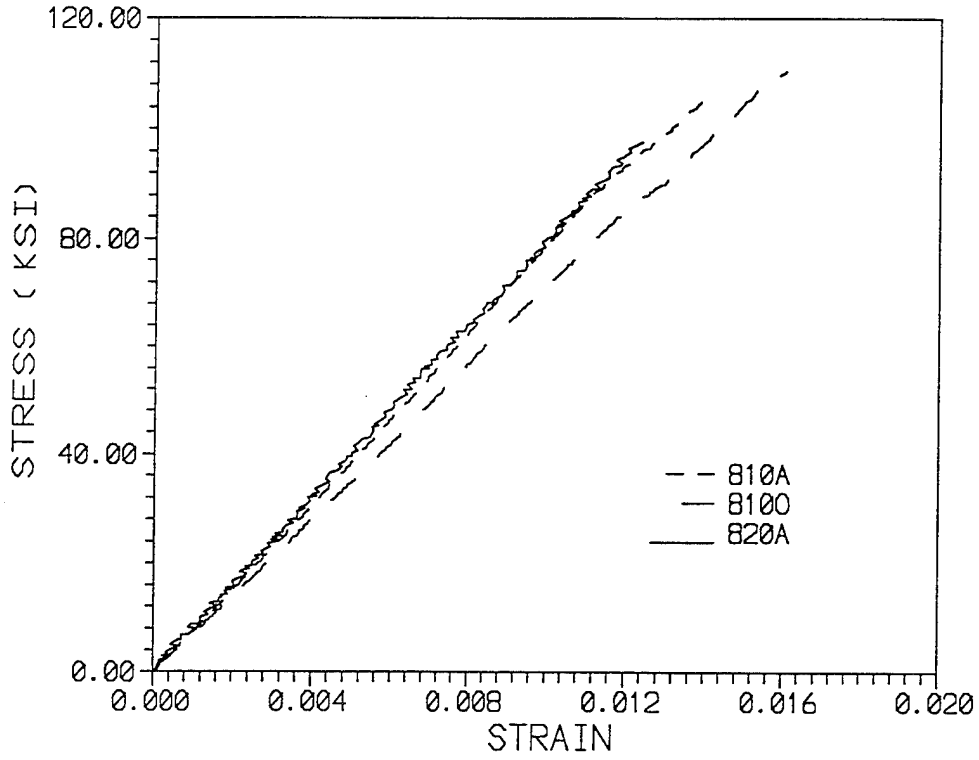

Figure 8 Typical stress-strain curves for the 810 A, 820 A and 810 O cross-ply laminates

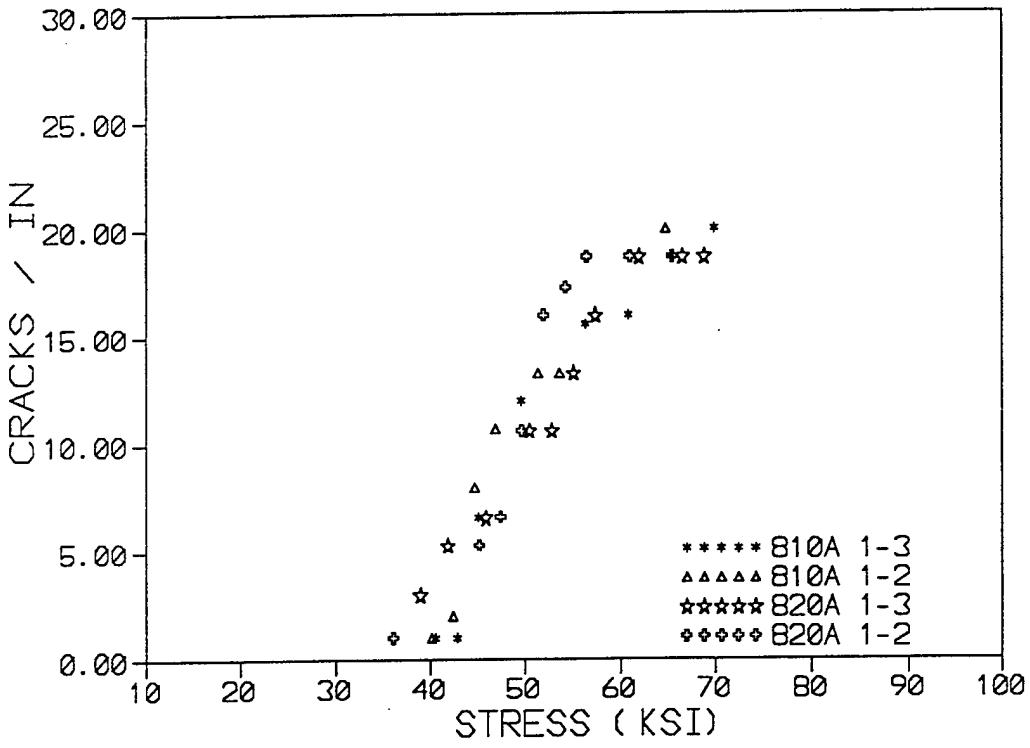

Figure 9 Variation of transverse crack density as a function of applied load for 810 A and 820 A cross-ply laminates

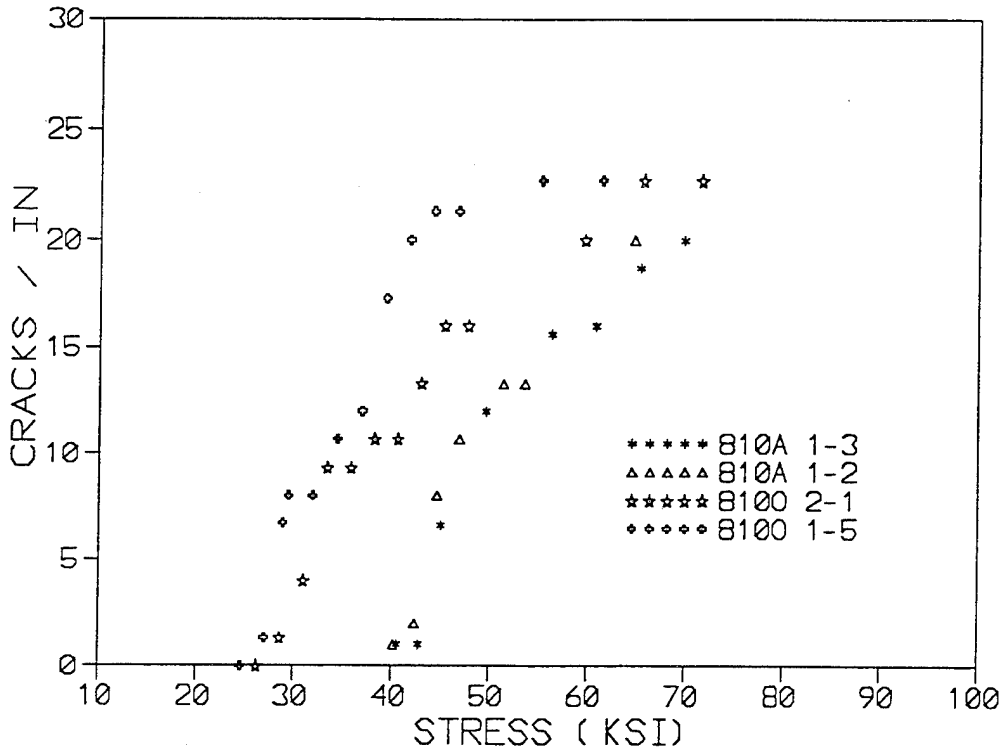

Figure 10 Variation of transverse crack density as a function of applied load for 810 A and 810 O cross-ply laminates

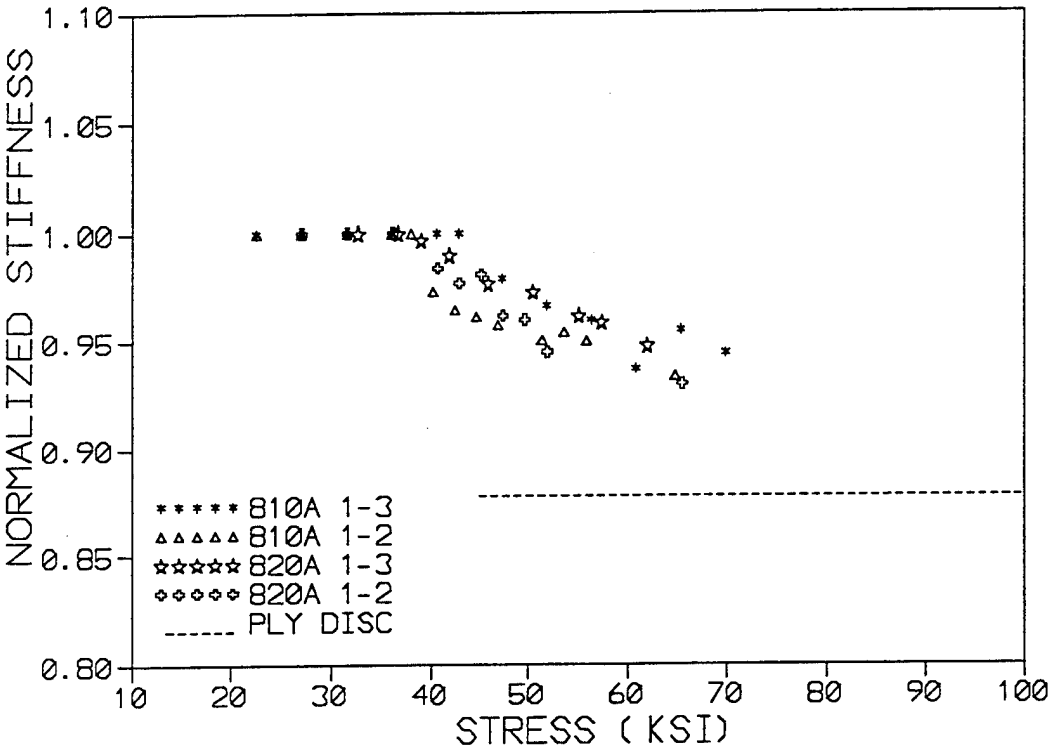

Figure 11 Variation of axial stiffness as a function of applied load for 810 A and 820 A cross-ply laminates

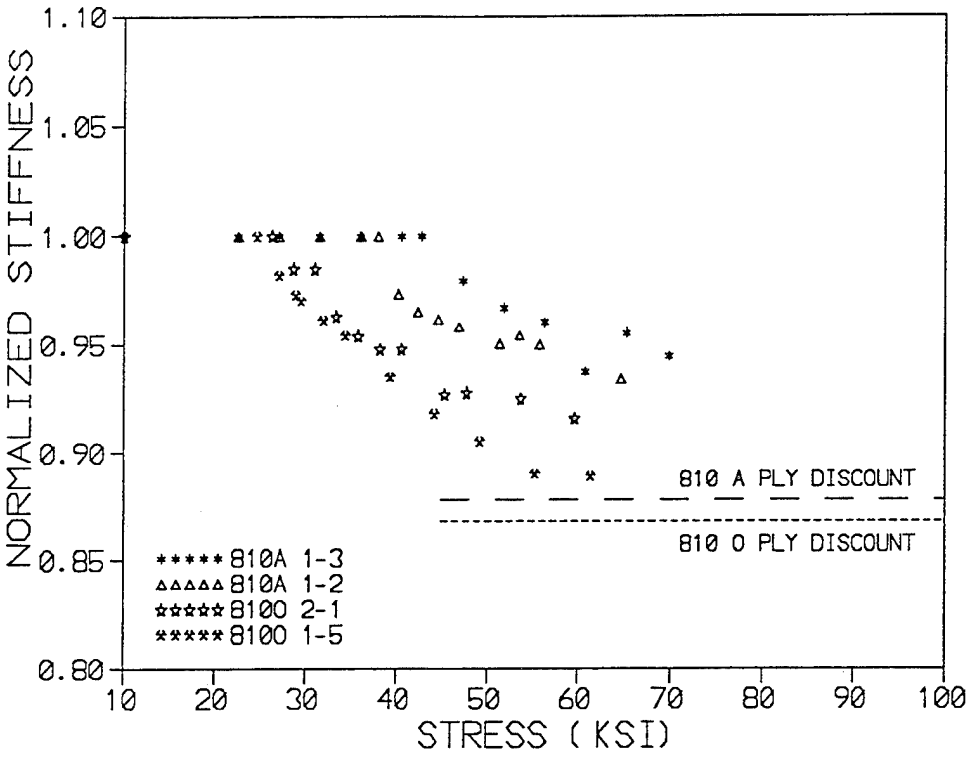

Figure 12 Variation of axial stiffness as a function of applied load for 810 A and 810 O cross-ply laminates

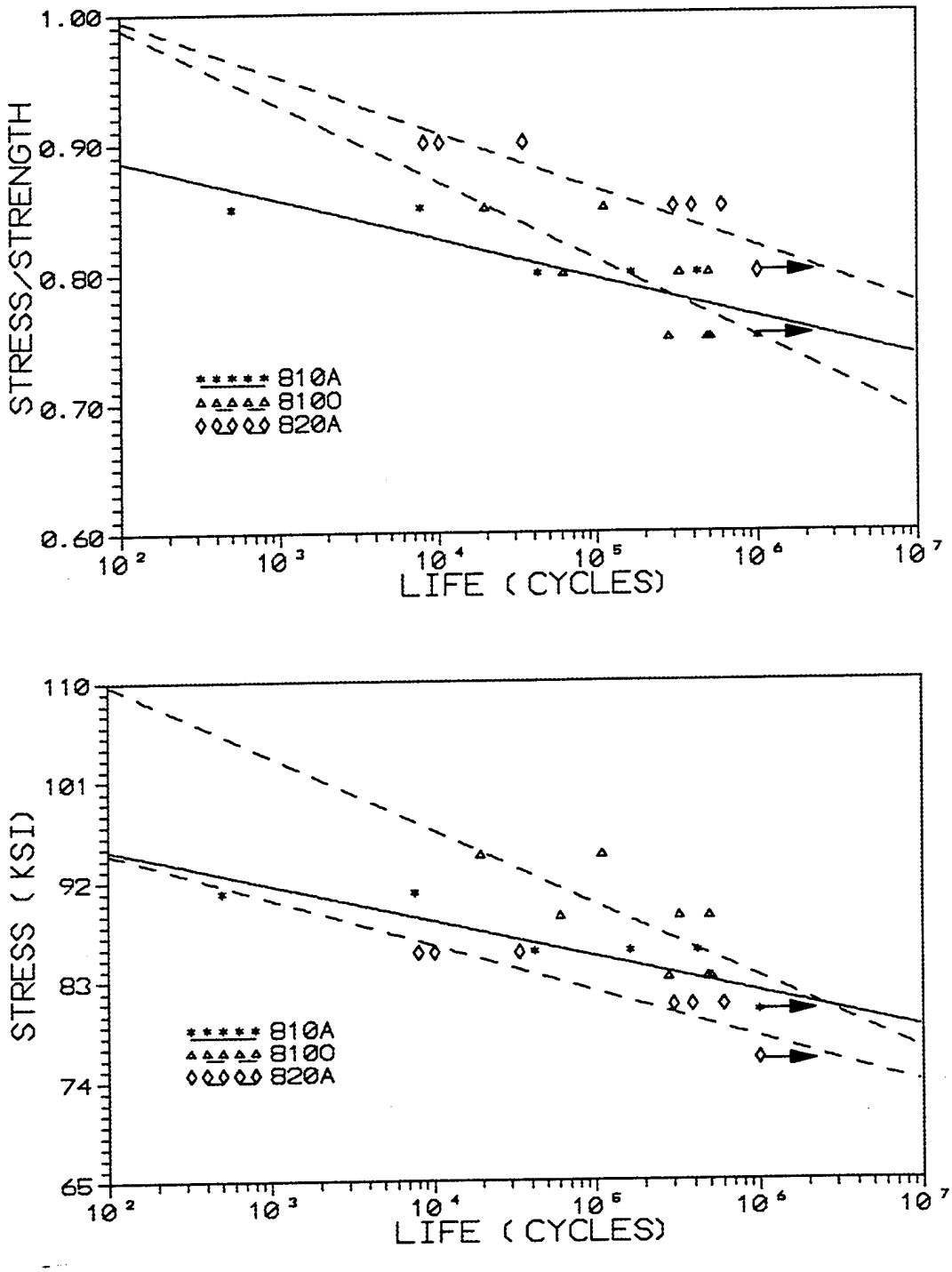

Figure 13 Comparison of the S-N curves of the 810 A, 810 O and 820 A cross-ply laminates

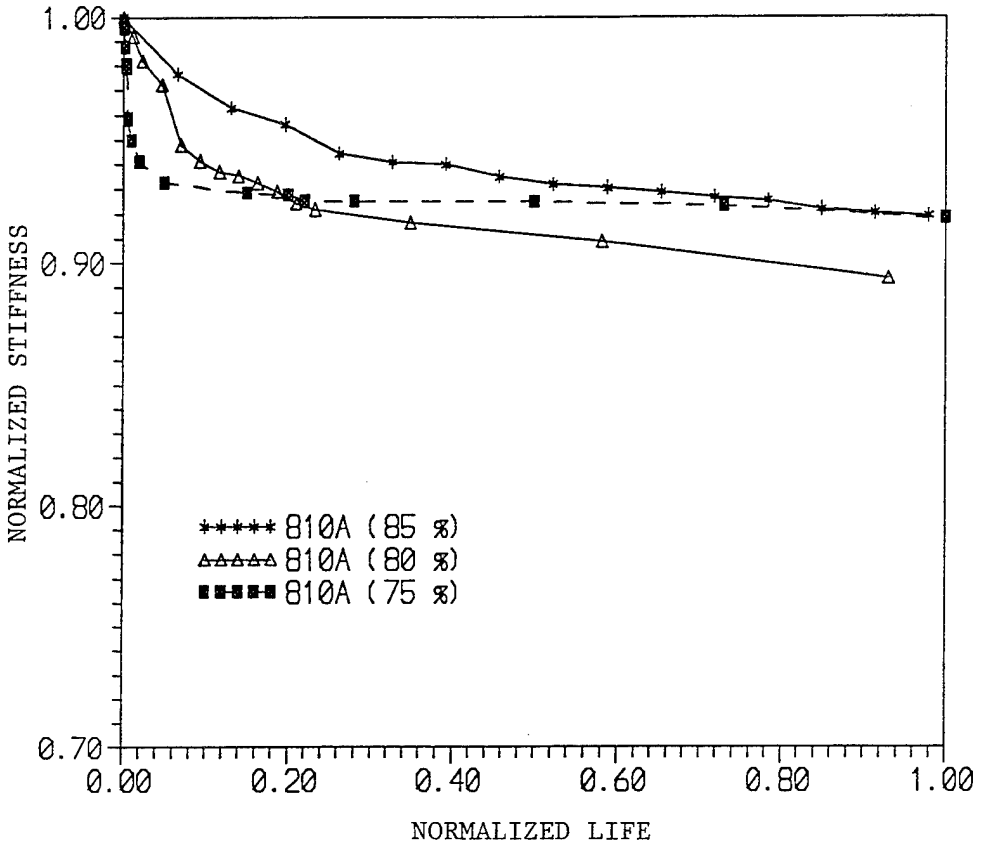

Figure 14 Variation of normalized stiffness as a function of normalized cycles for the 810 A cross-ply laminates at various load levels

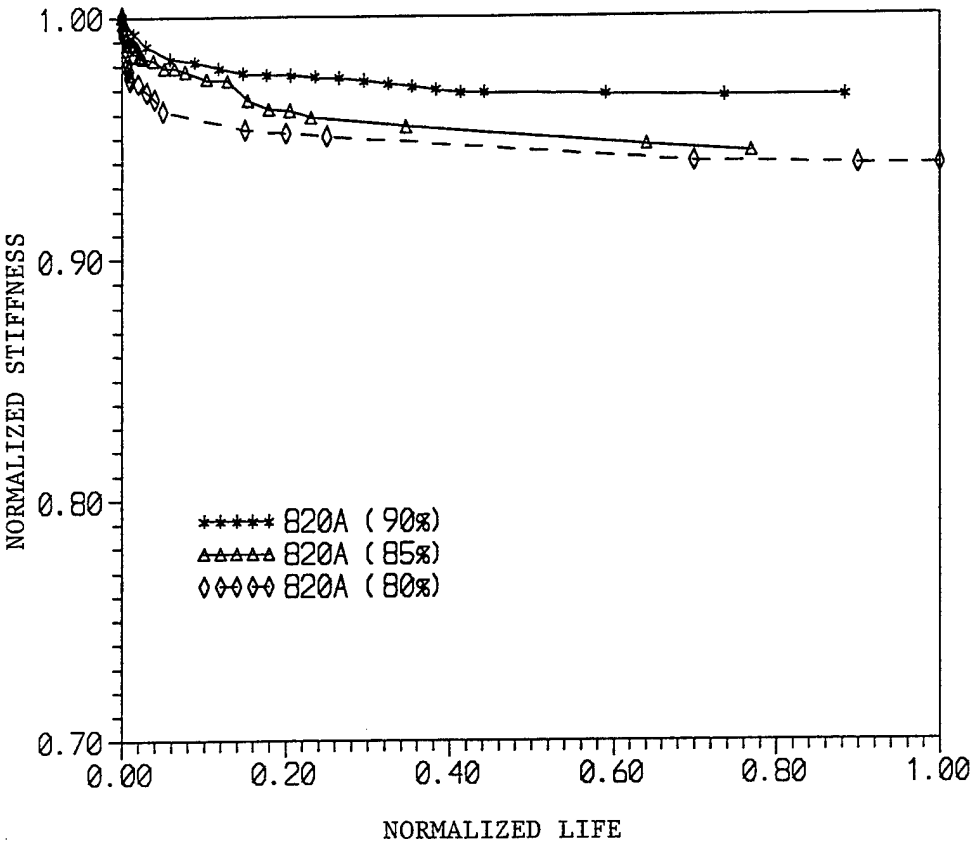

Figure 15 Variation of normalized stiffness as a function of normalized cycles for the 820 A cross-ply laminates at vrious load levels

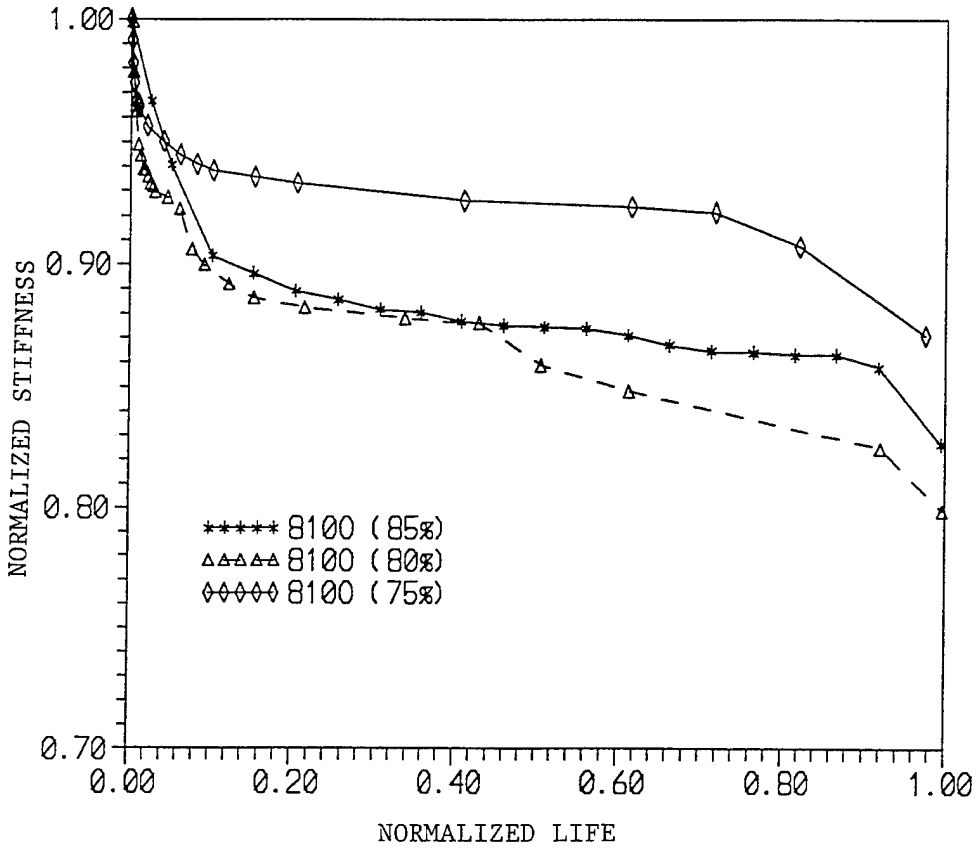

Figure 16 Variation of normalized stiffness as a function of normalized cycles for the 810 O cross-ply laminates at various load levels

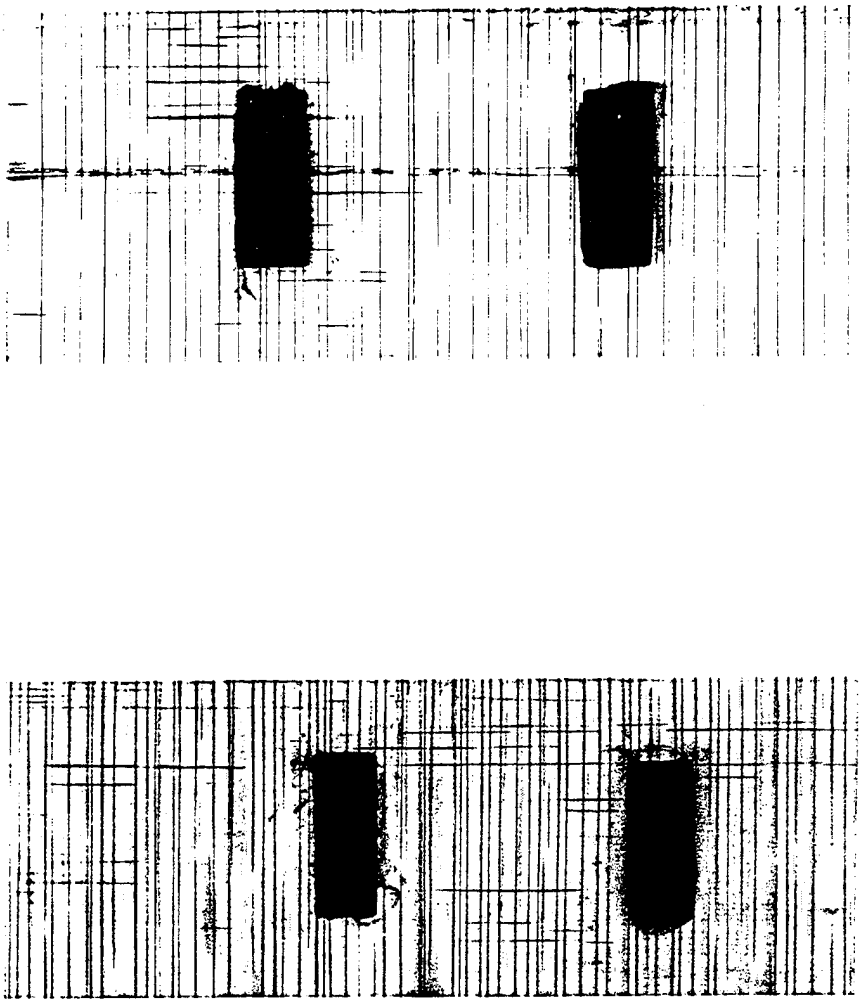

Figure 17 X-ray radiograph of the 810 A cross-ply laminate Top: 80 % load level after 50000 cycles. Bottom : 75 % load level after 1 million cycles

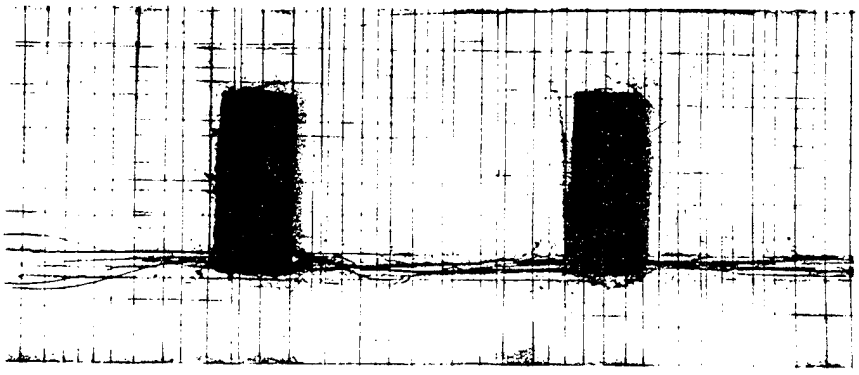

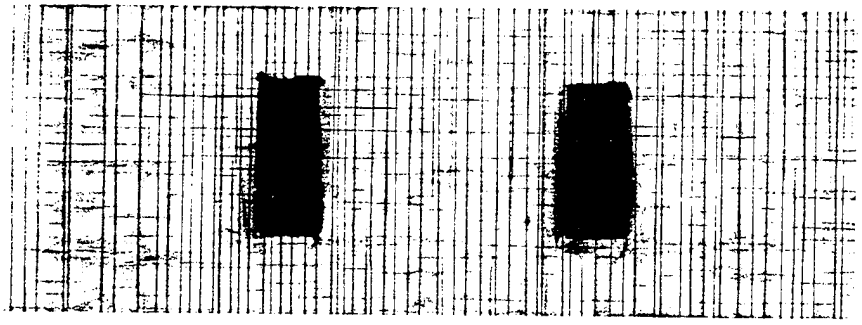

Figure 18 X-ray radiograph of the 810 O cross-ply laminate Top: 80 % load level after 50000 cycles.Bottom : 75 % load level after 200000 cycles

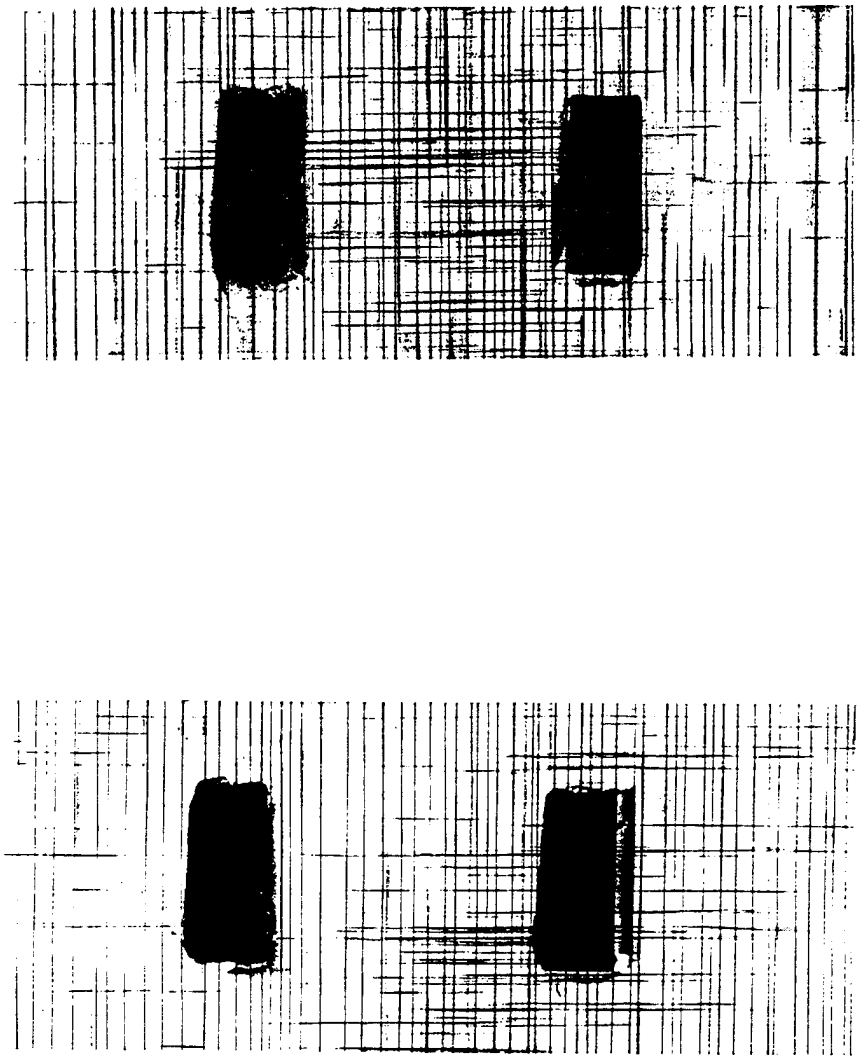

Figure 19 X-ray radiograph of the 820 A cross-ply laminate Top: 85 % load level after 250000 cycles. Bottom : 80 % load level after 1 million cycles

Figure 20 Photograph of failed 810 A cross-ply laminate Top : 85 % load level. Middle : 80 % load level. Bottom : 75 % load level

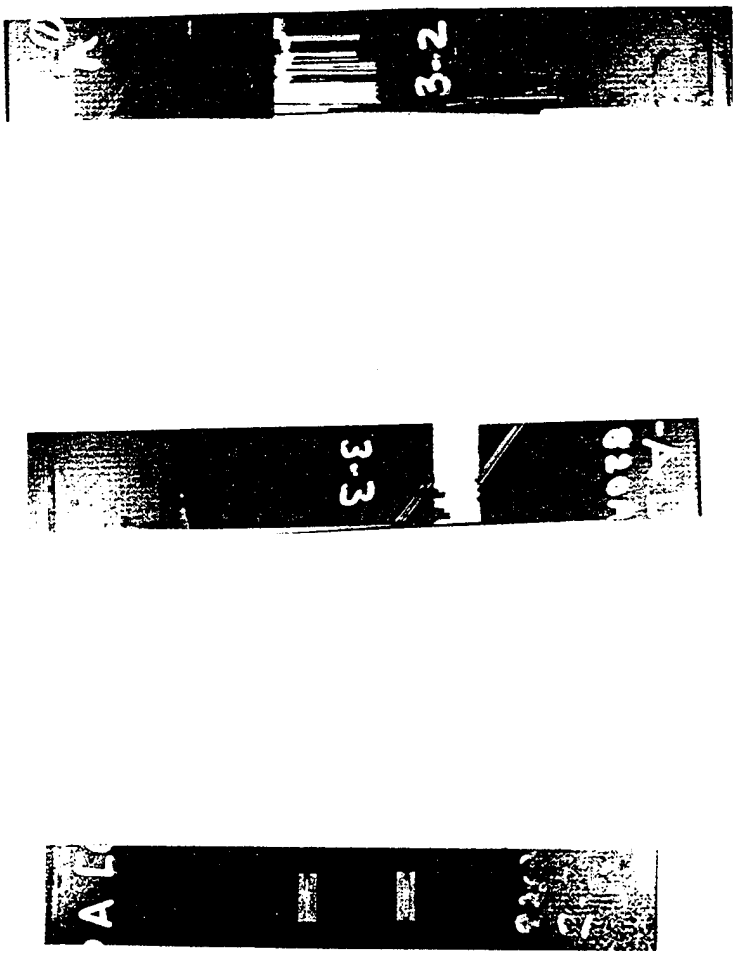

Figure 21 Photograph of failed 820 A cross-ply laminate Top : 90 % load level. Middle : 85 % load level. Bottom : 80 % load level

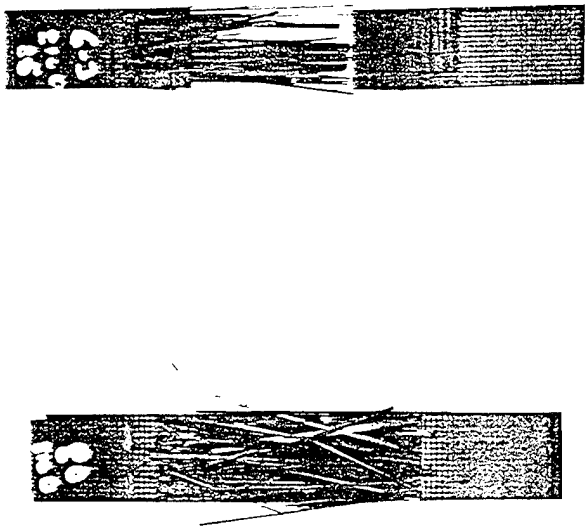

Figure 22 Photograph of failed 810 O cross-ply laminate Top : 85 % load level. Middle : 80 % load level. Bottom : 75 % load level

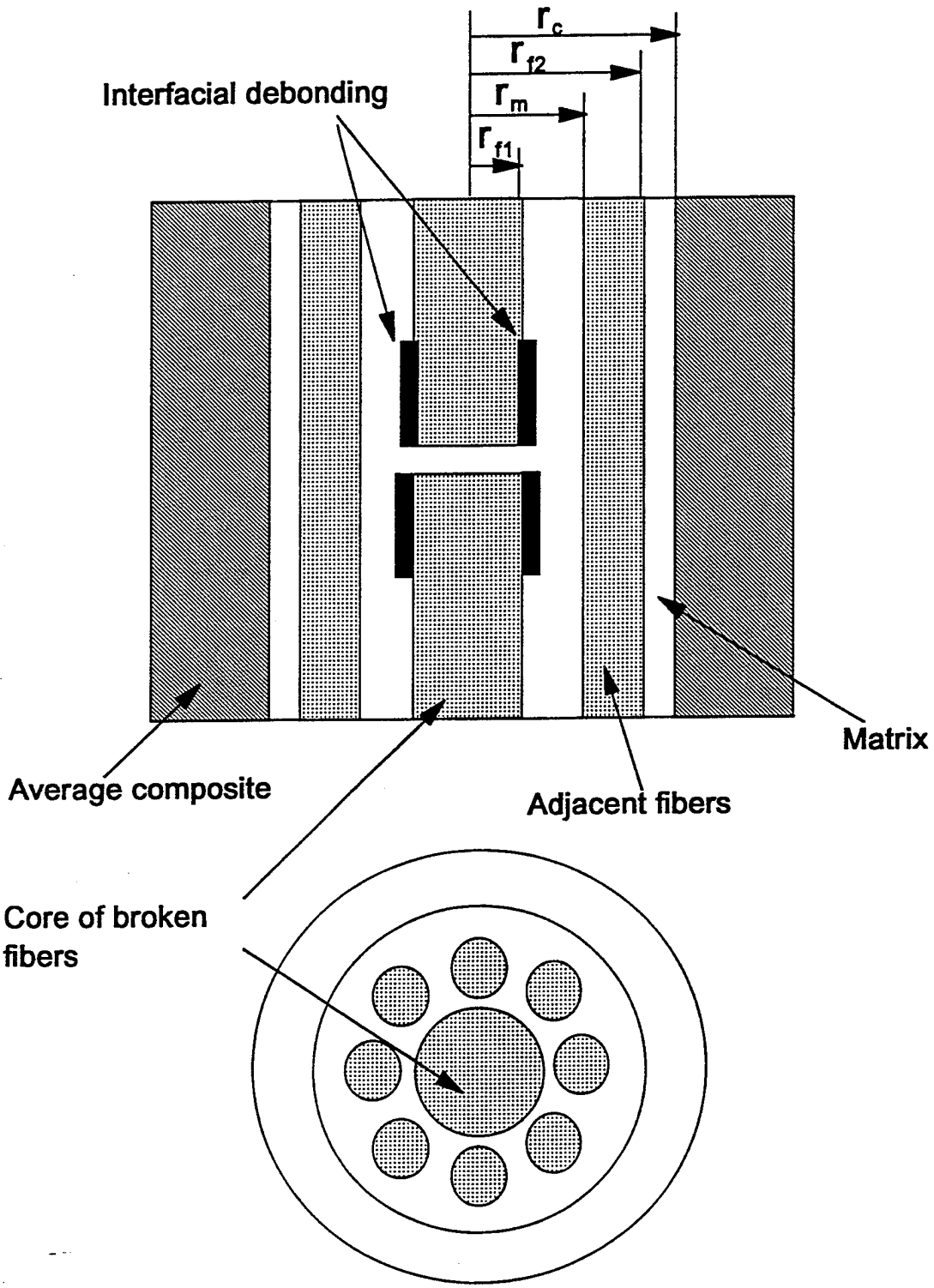

Figure 23 Schematic of unidirectional laminate with a core of broken fiber

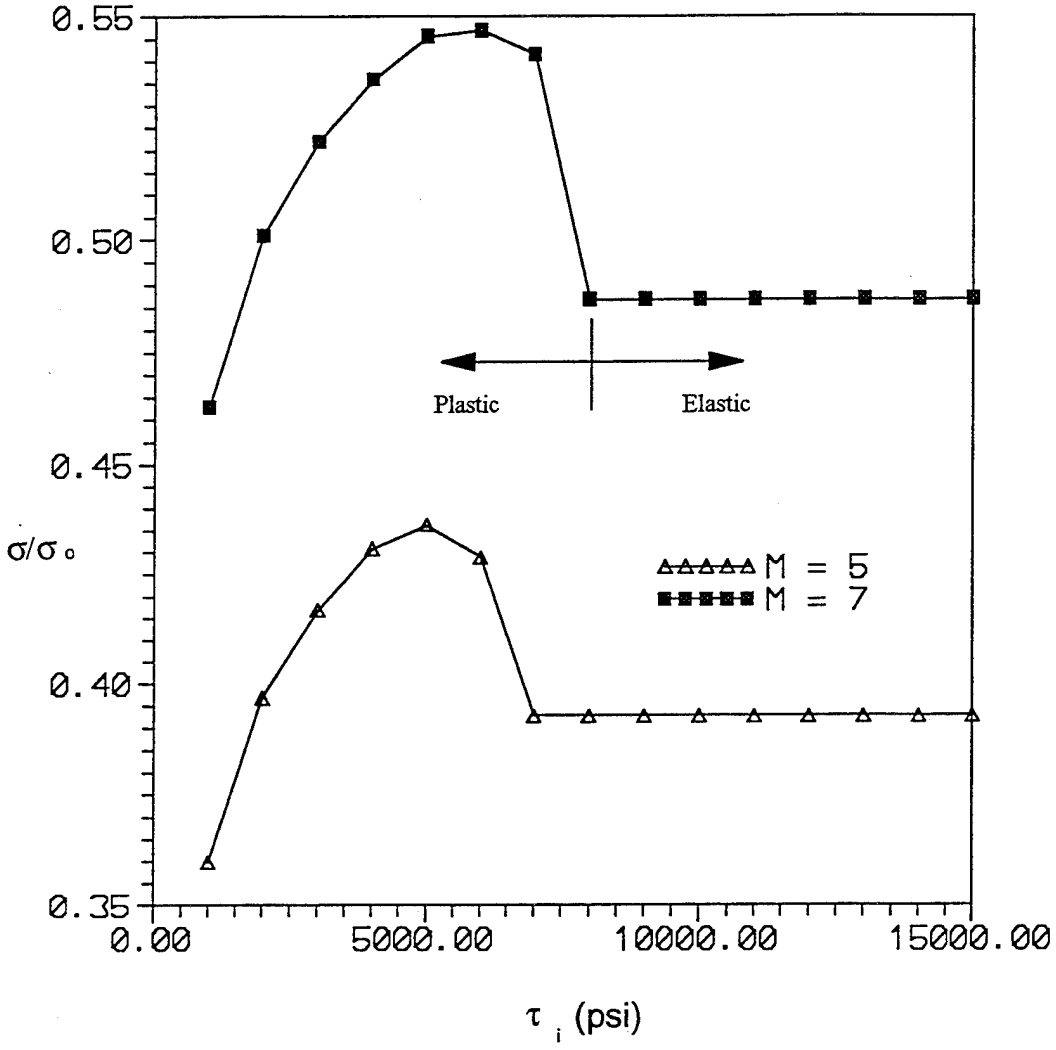

Figure 24 Variation of predicted tensile strength as a function of τ_m.

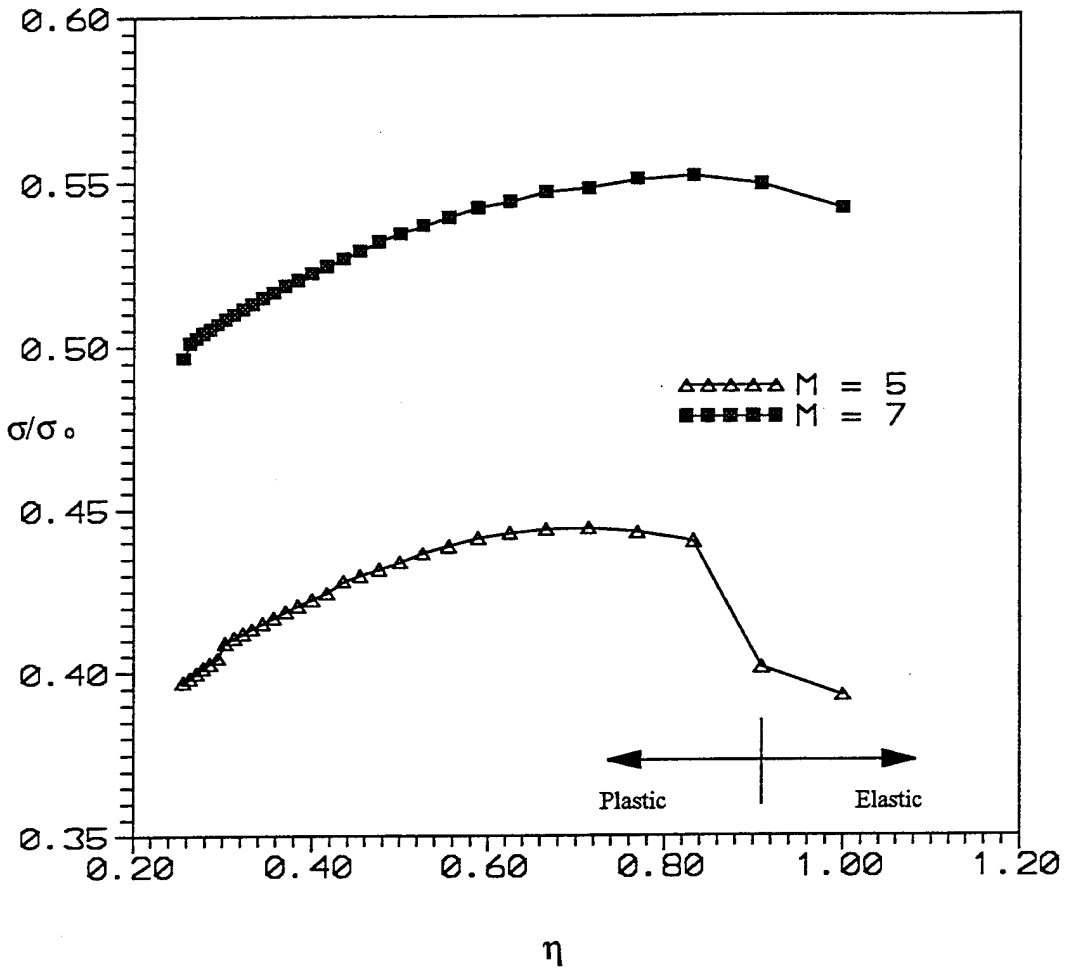

Figure 25 Variation of predicted unidirectional tensile strength as a function of η

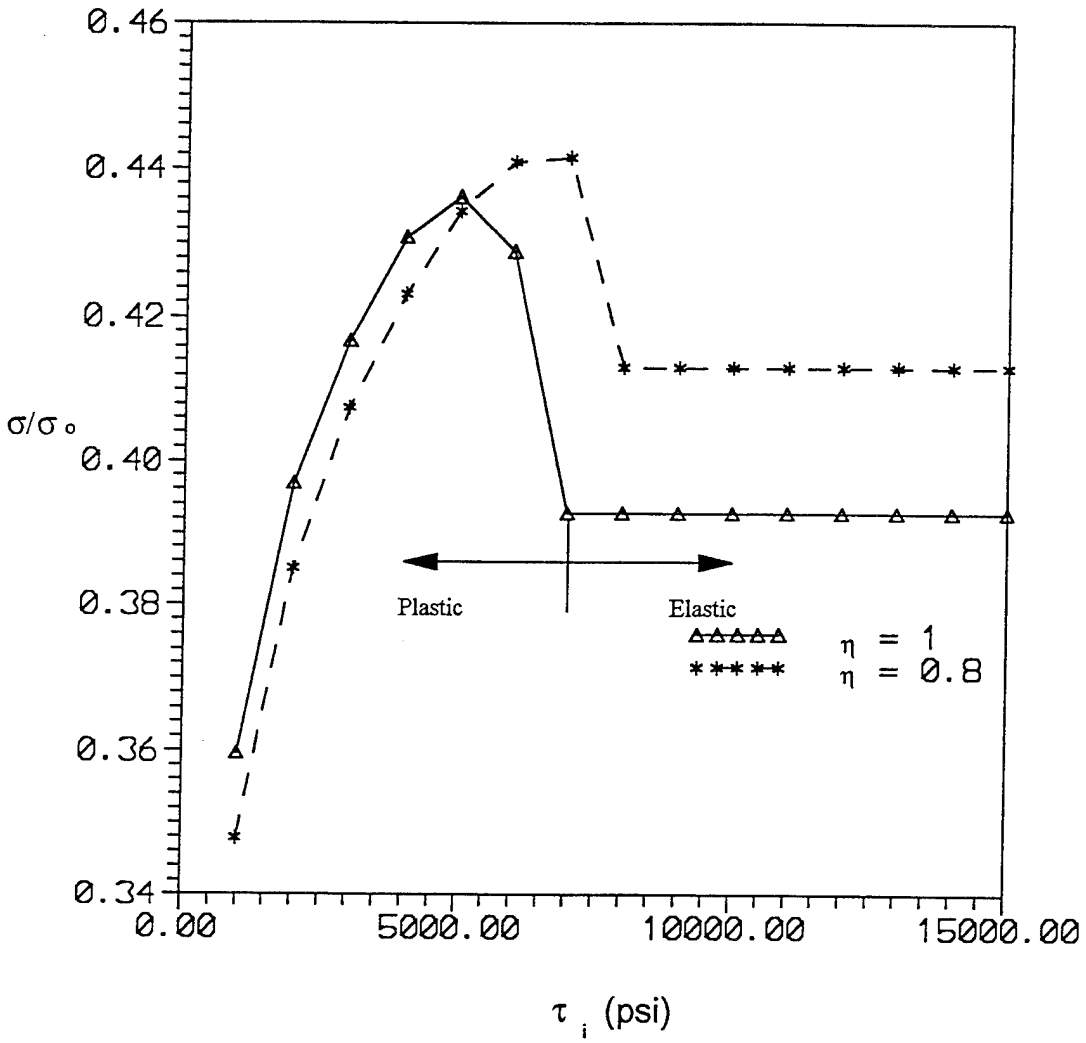

Figure 26 Predicted variation of unidirectional tensile strength as a function of τ_m for different η

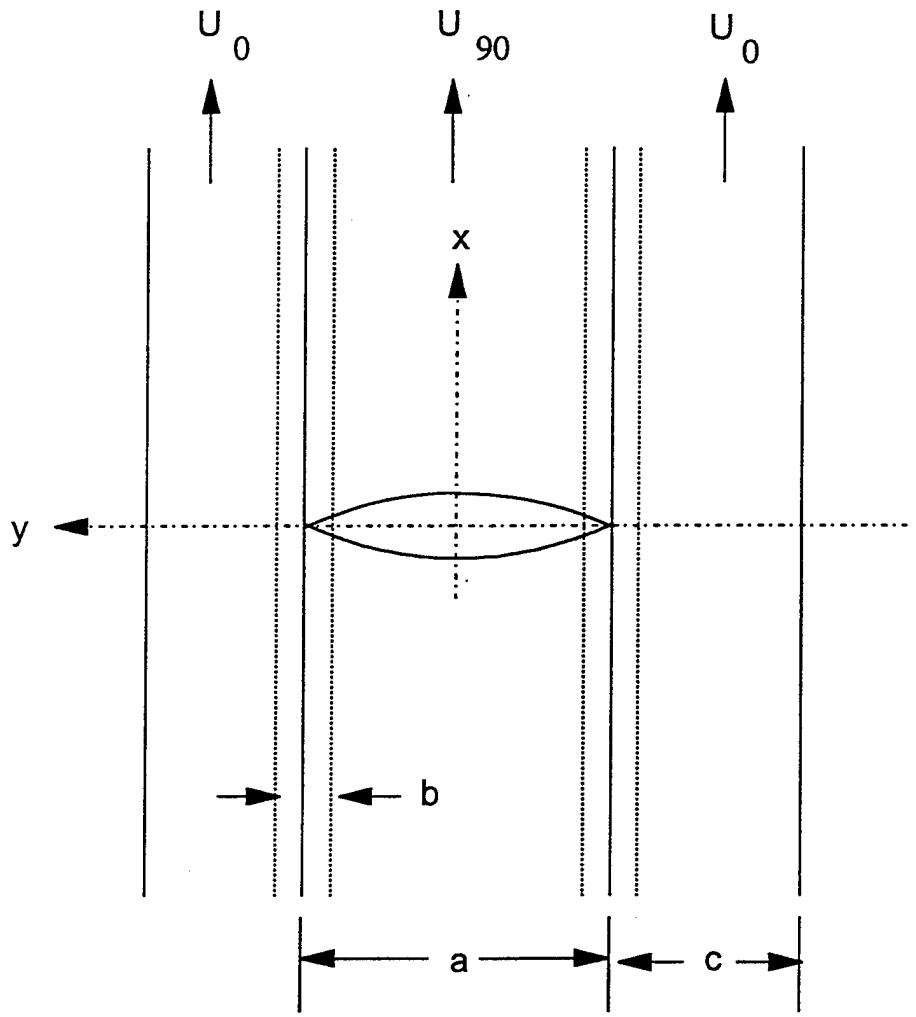

Figure 27 Schematic of the shear lag model showing a transverse ply crack in the central 90° ply with the constraining 0° plies

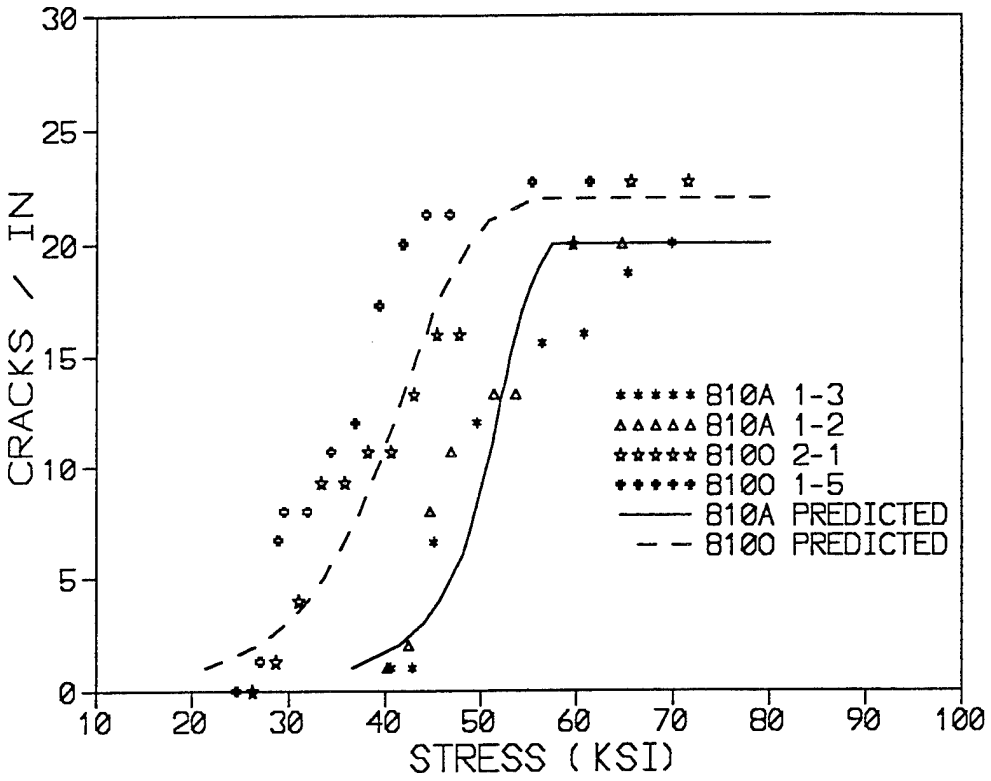

Figure 28 Comparison of experimental and predicted variation of static transverse crack density in the 810 A and 810 O cross-ply laminates

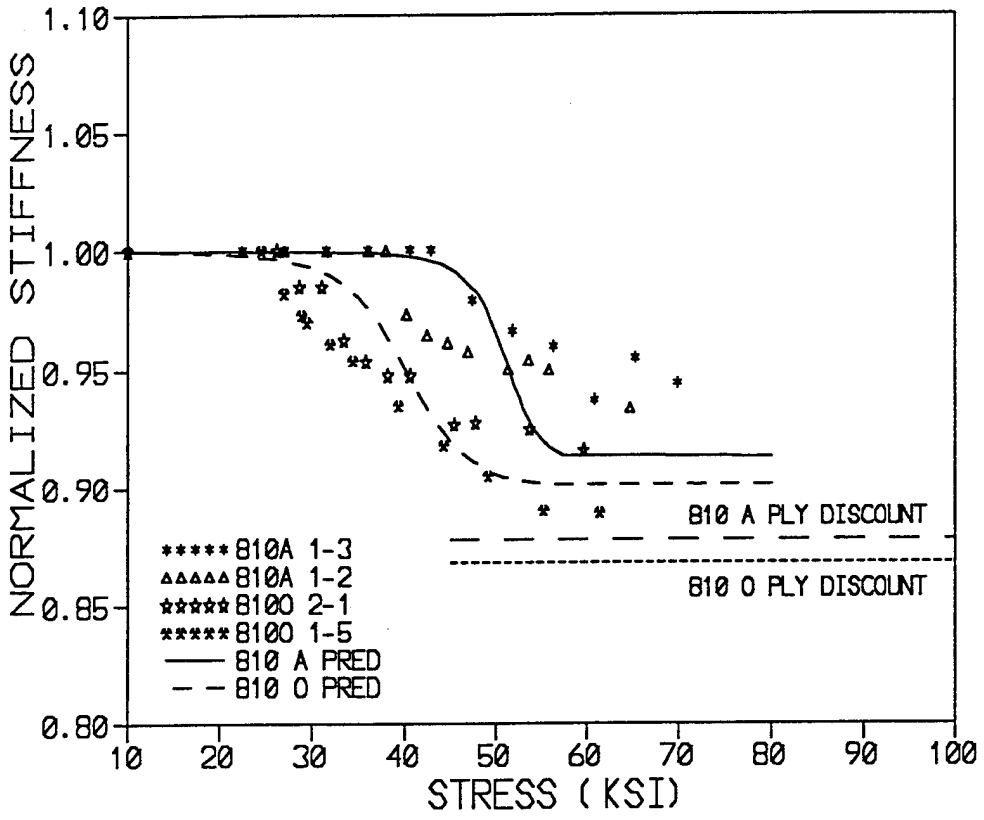

Figure 29 Comparison of experimental and predicted variation of static stiffness reduction in the 810 A and 810 O cross-ply laminates

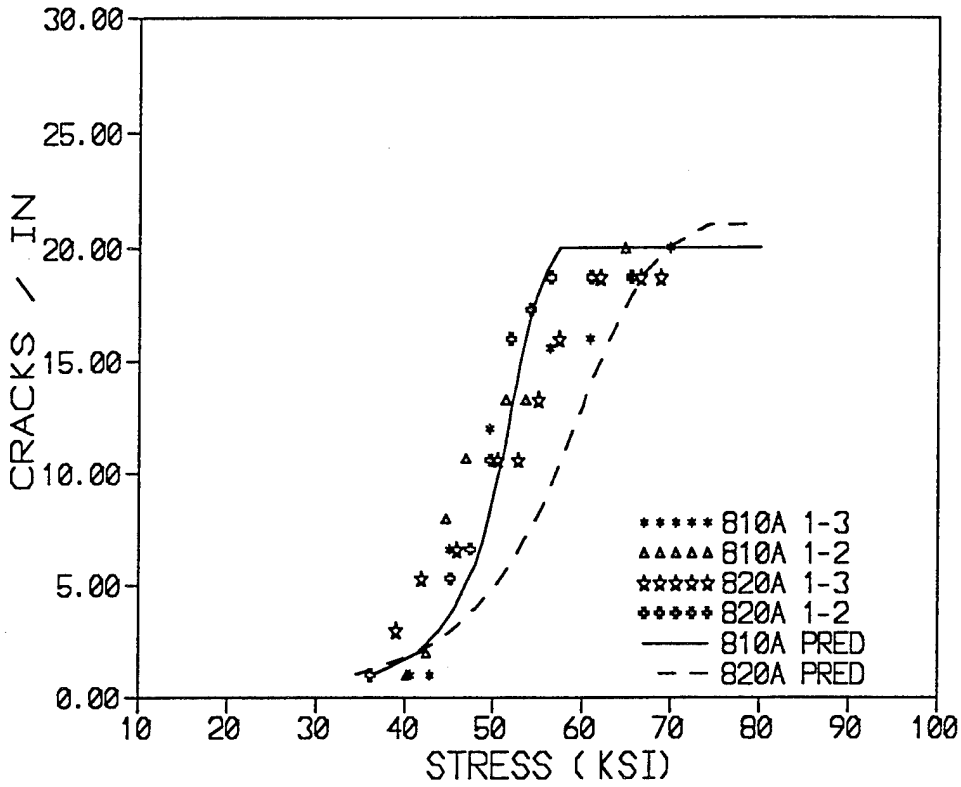

Figure 30 Comparison of experimental and predicted variation of static transverse crack density in the 810 A and 820 A cross-ply laminates

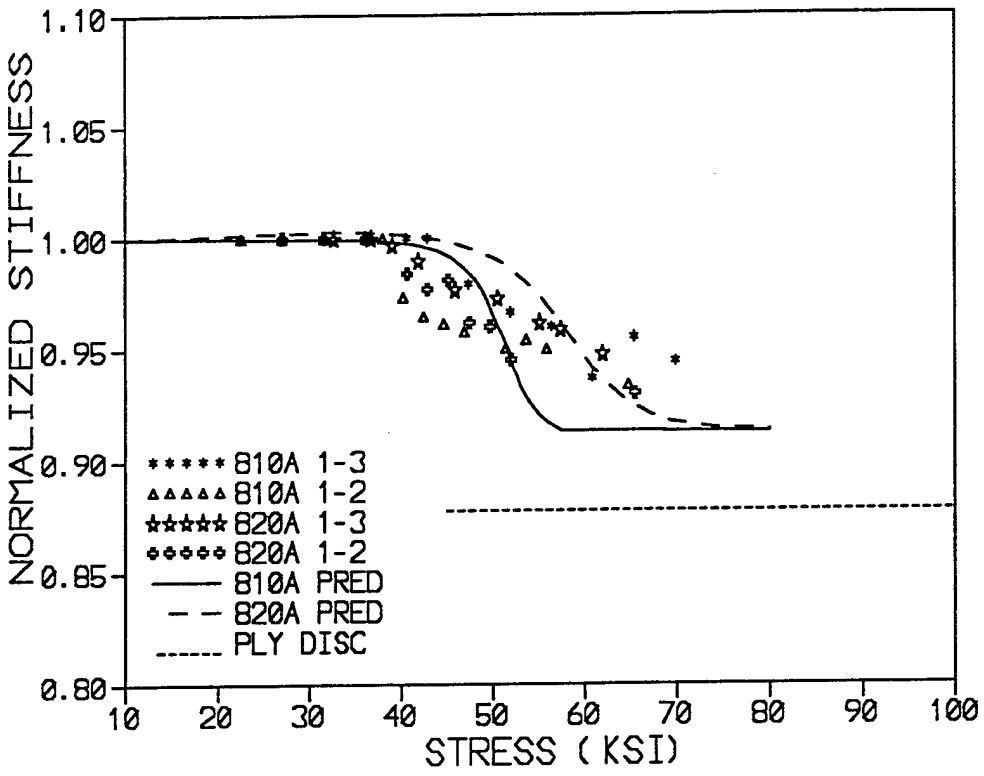

Figure 31 Comparison of experimental and predicted variation of static stiffness reduction in the 810 A and 820 A cross-ply laminates

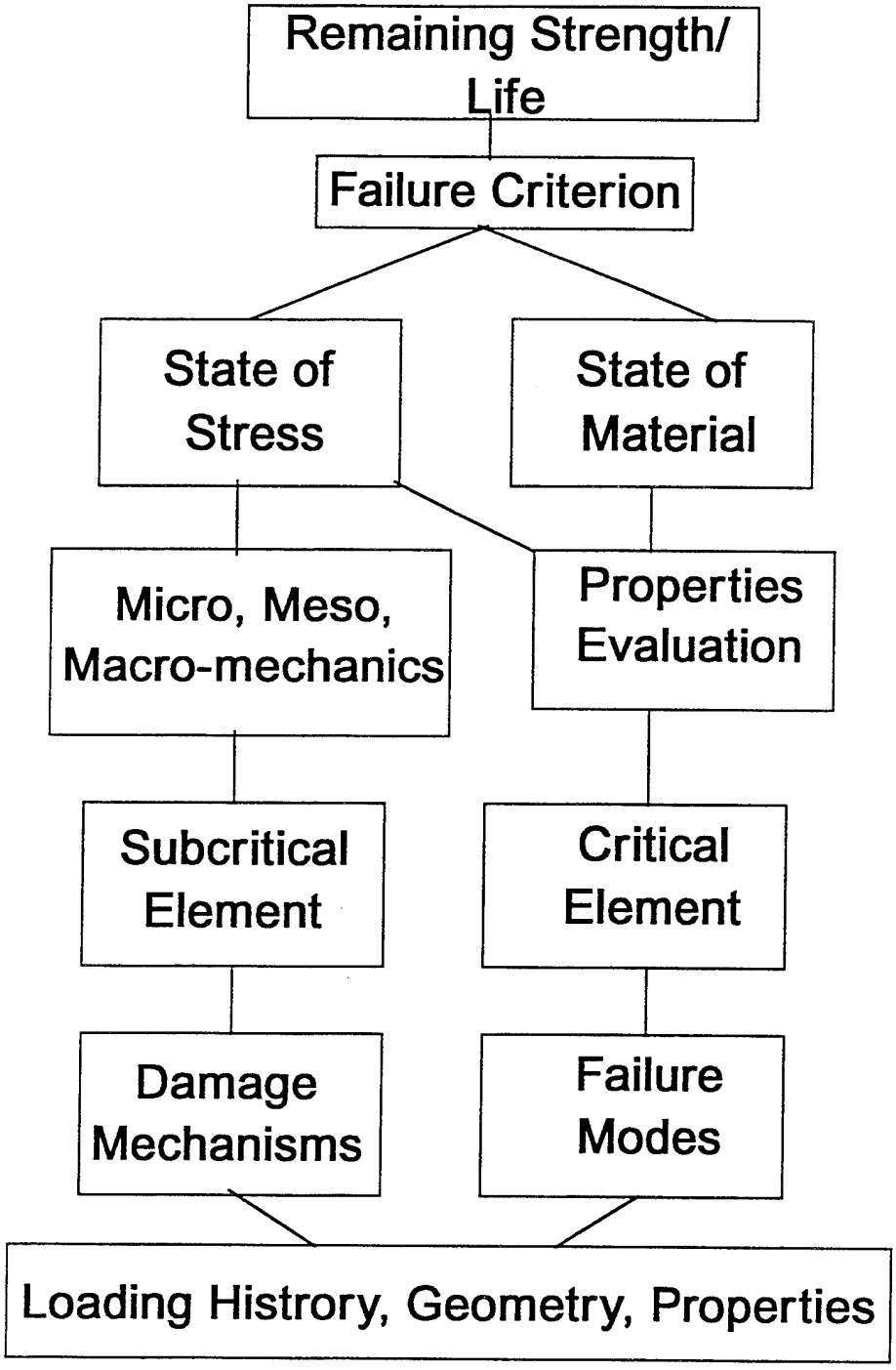

Figure 32 Schematic of Critical Element Model

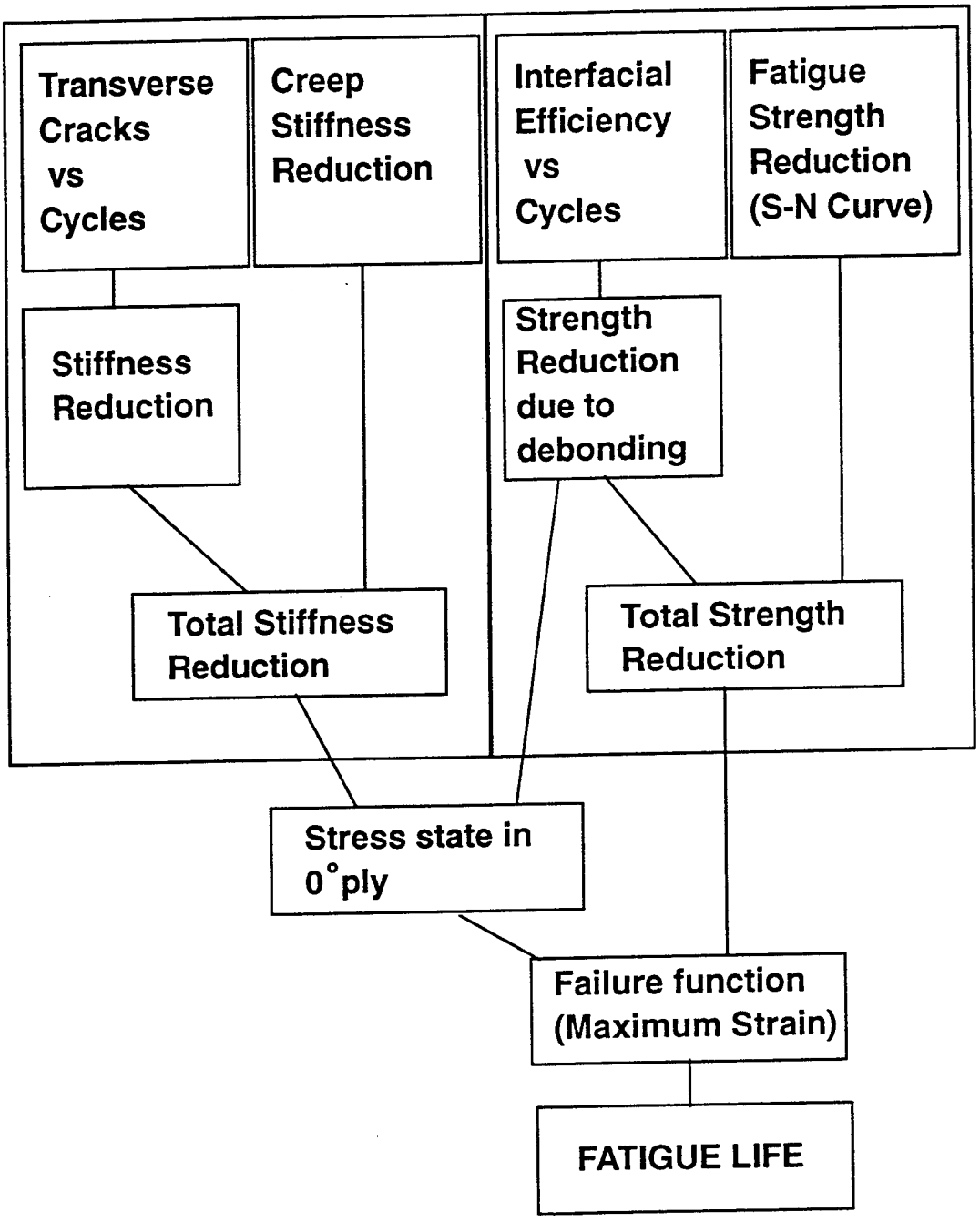

Figure 33 Schematic of cumulative damage scheme used for fatigue life prediction

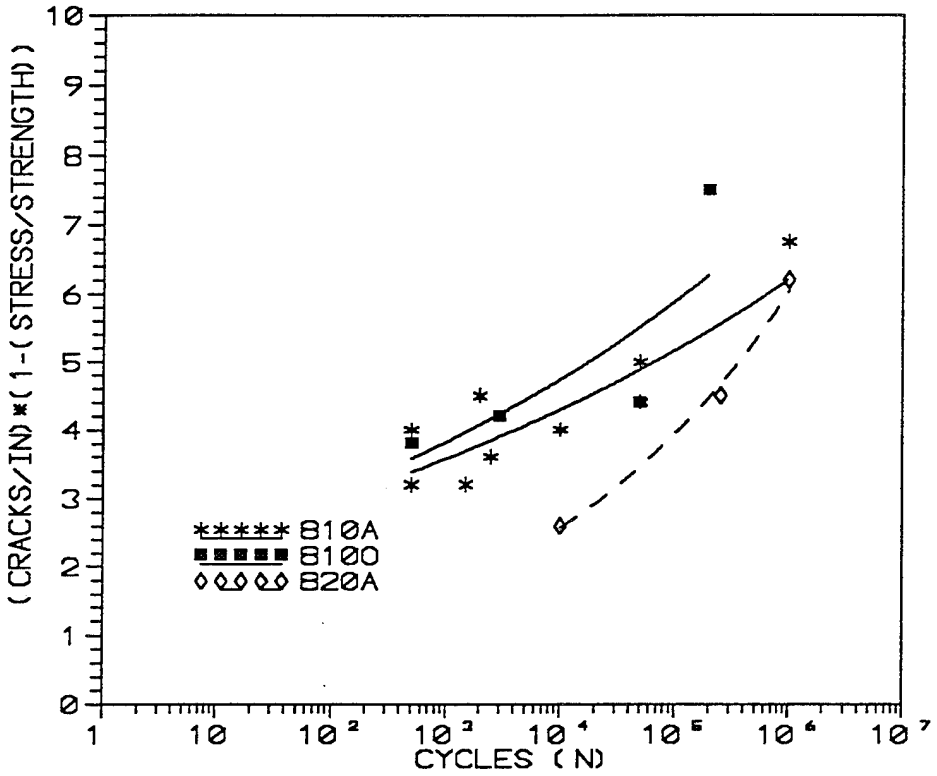

Figure 34 Variation of transverse crack density as a function of cycles in the cross-ply laminates of 810A, 820 A and 810 O system

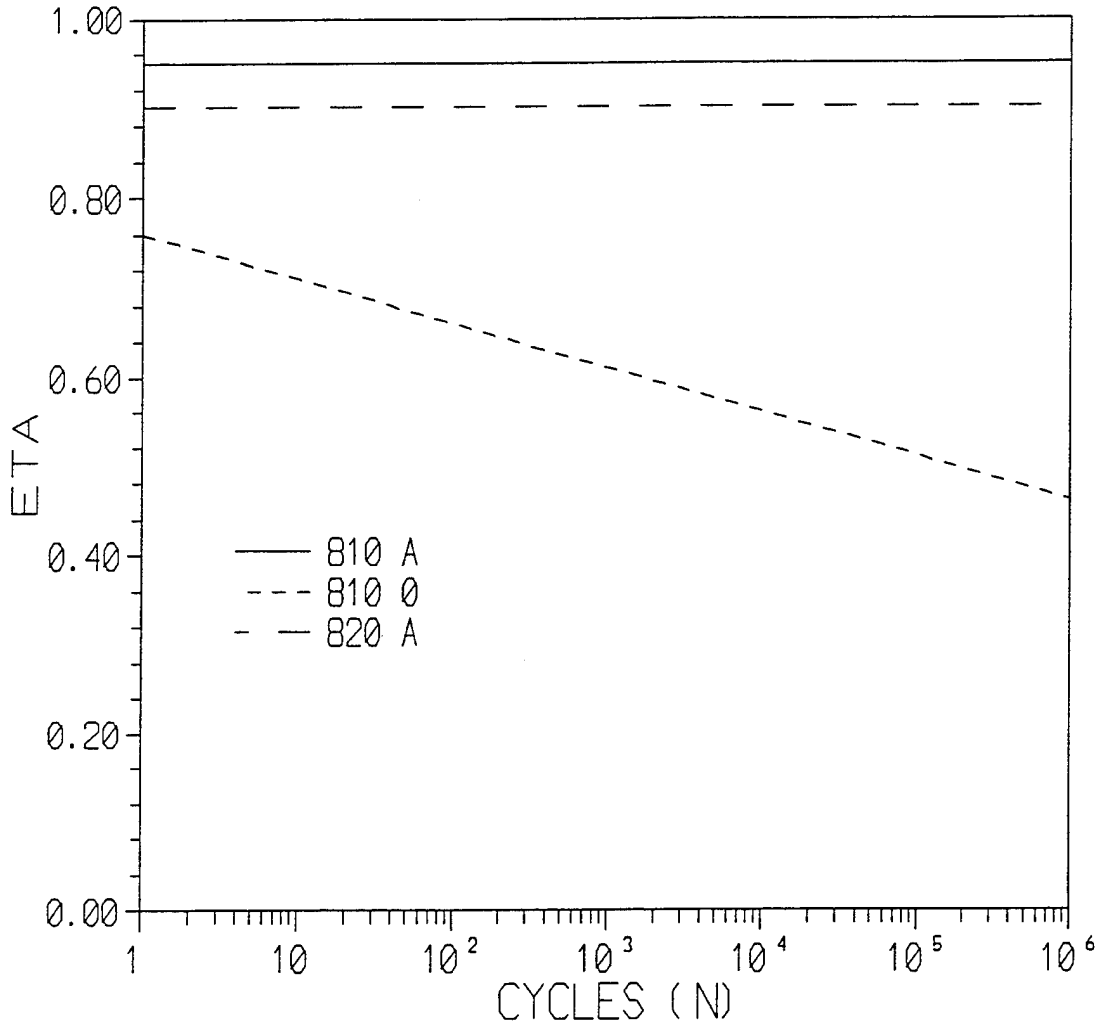

Figure 35 Variation of η as a function of cycles in the 810 A, 820 A and 810 O system

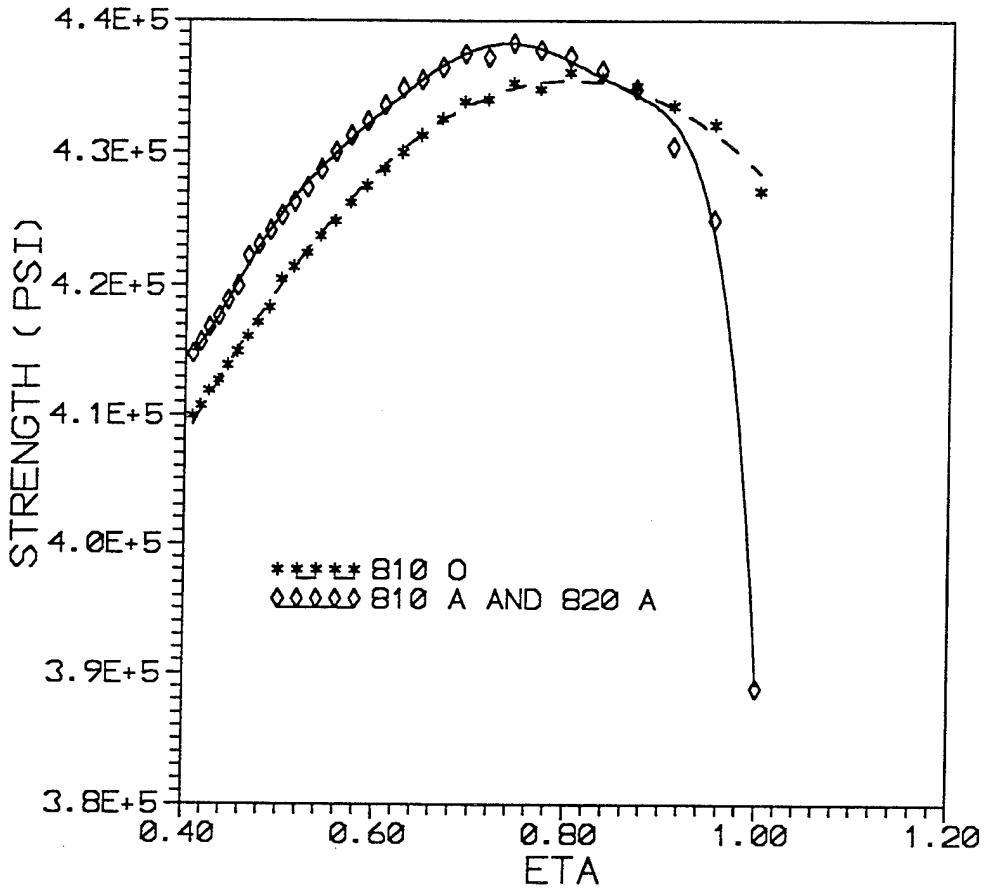

Figure 36 Variation of unidirectional tensile strength as a function of efficiency factor η for the 810 A, 820 A and 810 O system

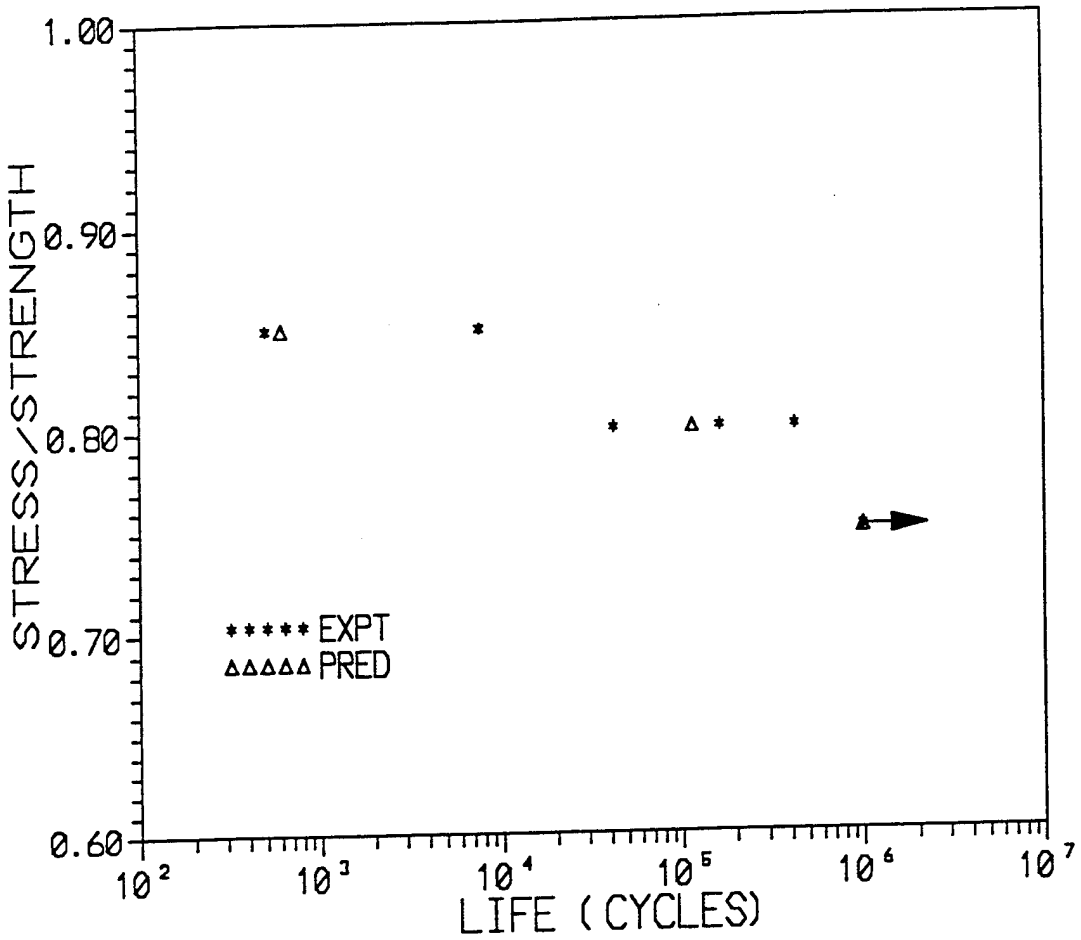

Figure 37 Comparison of the experimental and predicted fatigue life of the 810 A cross-ply laminates

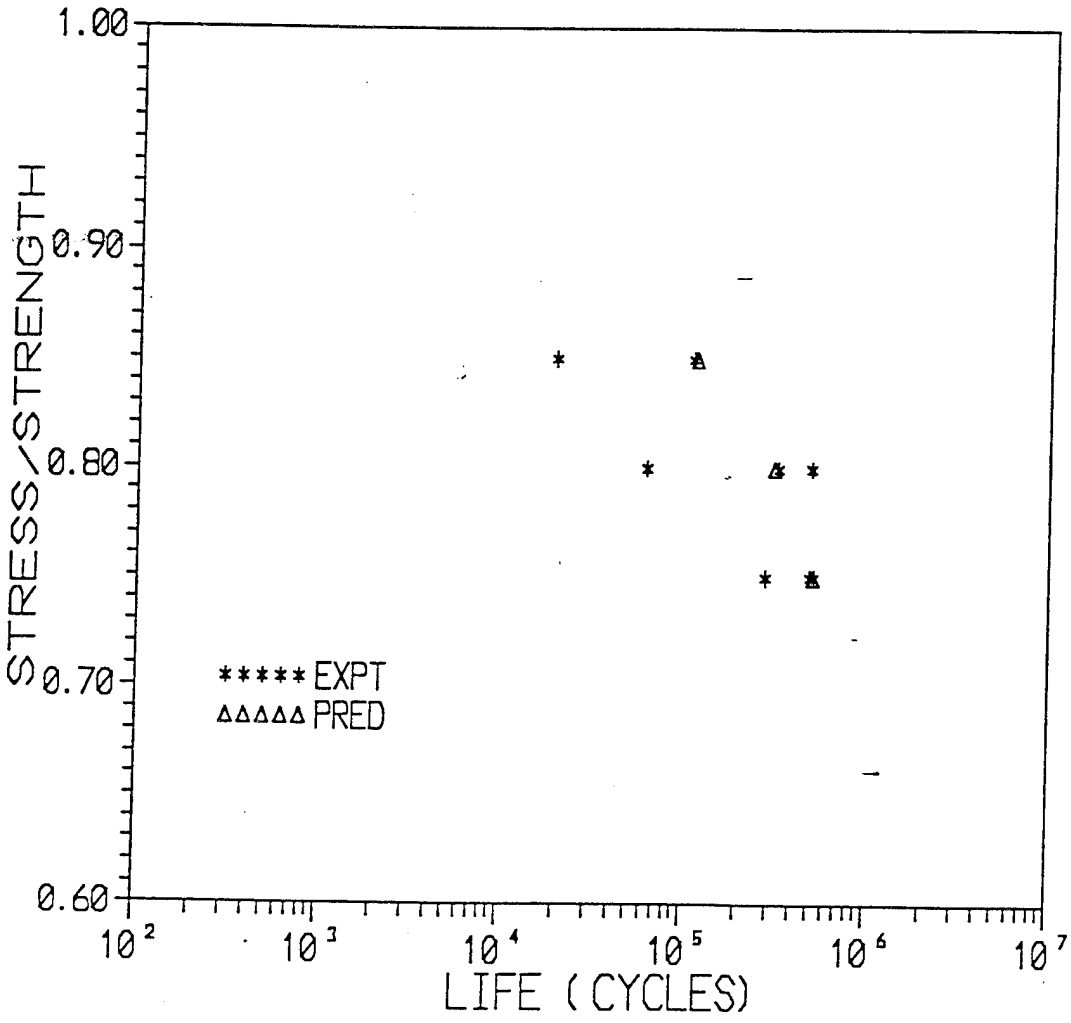

Figure 38 Comparison of the experimental and predicted fatigue life of the 810 O cross-ply laminates

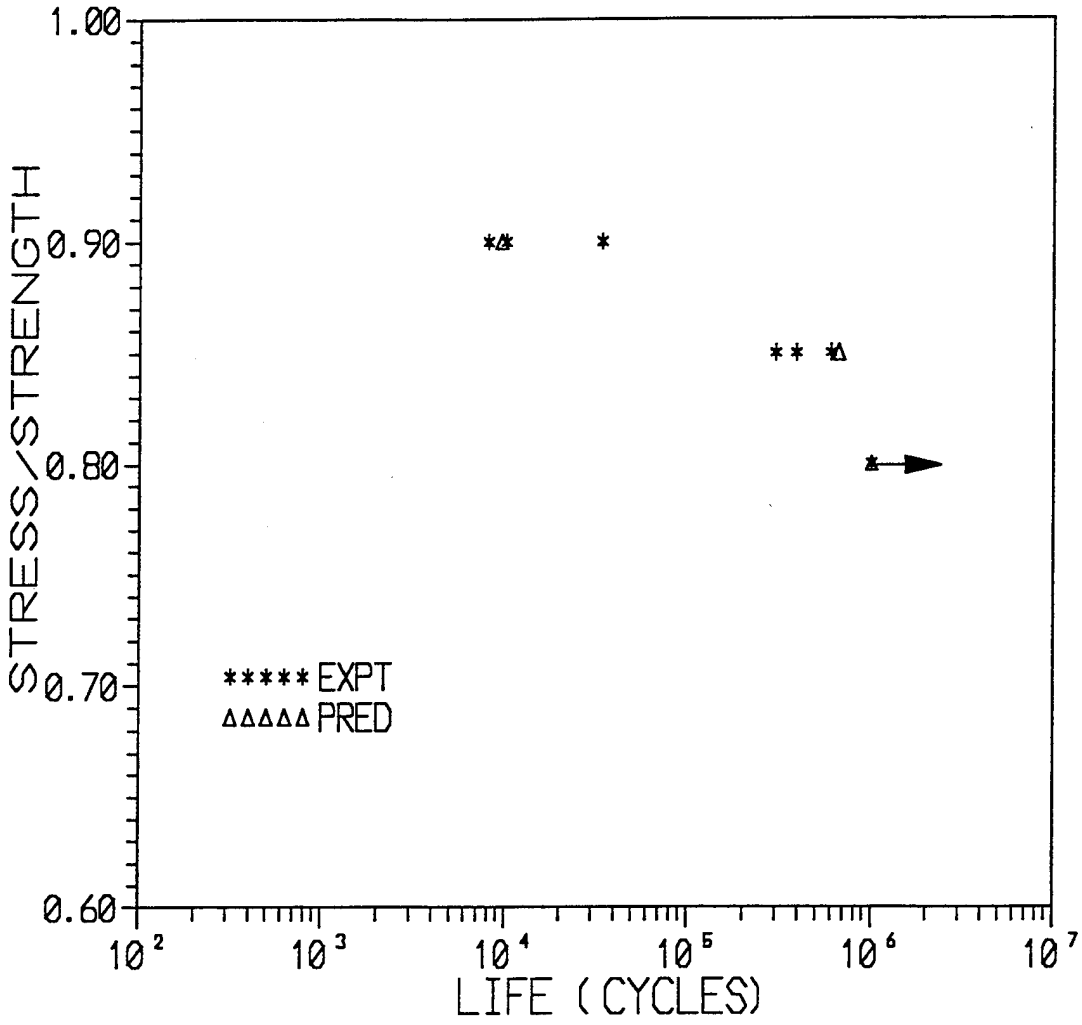

Figure 39 Comparison of the experimental and predicted fatigue life of the 820 A cross-ply laminates

5.0 CLOSURE

In this study, the influence of fiber surface treatment and fiber sizing, on the mechanical properties of unidirectional and $(0,90_3)_s$ cross-ply laminates was studied. Three material systems having the same Apollo carbon fiber and HC 9106-3 toughened epoxy matrix, but with different fiber surface treatment and fiber sizing, were used in this study. The presence of different interphase in the three material system was confirmed using a permanganic etching technique. The single fiber fragmentation test (SFFT) results indicate that the interfacial shear strength (ISS) of the 810 O system is significantly lower than that of the other two system. The 810 A and 820 A material system possess similar ISS.

The longitudinal tensile tests results indicate that the longitudinal tensile strength and strain to failure of the 810 O system is greater than that of the other two systems, while the stiffness of this material system is lower than that of the other two material systems. The 810 A and 820 A system possess similar longitudinal tensile strength and failure strain and longitudinal stiffness. The transverse tensile tests indicate that the 820 A system has the greatest strength, while the 810 O system has the lowest strength. The tensile test results on cross-ply laminates indicate that the 810 A and 810 O systems possess similar strength, while the strength of the 820 A system is significantly lower. The 810 O laminates have the highest failure strain while the 820 A laminates have the lowest failure strain. The stiffness of the 810 A and 810 O cross-ply laminates are similar, while the 810 O laminates have a significantly lower stiffness. ***Non-destructive test results reveal that the damage mechanisms and failure modes in cross-ply laminates with different fiber-matrix interphase are different.***

The fatigue life of cross-ply laminates are sensitive to the nature of interphase present in the material system. The cross-ply laminates with different fiber-matrix interphase exhibit varied damage mechanisms and failure modes. The 820 A laminates have greater life at all load levels used in this study. A comparison of the fatigue lives of the 810 A and 810 O laminates reveals that the 810 O laminates have longer fatigue lives at higher load levels and lower lives at lower load levels. Damage analysis results indicate that all three material system exhibit extensive transverse ply cracking at all load levels. In addition, the 810 A laminate reveals edge delamination at high load levels, very little longitudinal splitting and no local delaminations. The 820 A laminates exhibit moderate amount of longitudinal splitting and no local or edge delaminations. In contrast, the 810 O laminates exhibit extensive distributed longitudinal splitting and local delaminations at all load levels. The stiffness reduction results also confirm the presence of greater amount of damage in the 810 O. The failure of the 810 A and 820 A laminates are controlled by stress concentration effects in the 0° ply while the failure of the 810 O laminate is controlled by the global strain to failure of the 0° ply.

In this study, a model was developed to predict the tensile strength of unidirectional laminates including the effect of interphase. The model uses a shear lag analysis in conjunction with Batdorf's tensile strength prediction scheme. The model predicts the tensile strength, failure mode (presence/absence of fiber-matrix debonding prior to final failure) and the number of fiber fractures. The tensile strength and failure mode predicted using this model agrees well with the experimental observations for the 810 A, 810 O and 820 A material systems. **Results indicate that the tensile strength of the unidirectional laminates can be optimized by tailoring the interphase.** The onset and progression of transverse matrix cracking in cross-ply laminates was predicted using a modified form of 1 dimensional shear lag model. A novel scheme that uses the weibull strength statistics of the 90° ply, was used to predict the number of transverse matrix cracks and the corresponding stiffness reduction as a function of applied load. The predicted matrix cracking characteristics for the 810 A, 810 O and 820 A laminates agree well with the experimental values. The above models were used in a cumulative damage scheme, to predict the fatigue life of cross-ply laminates. The cumulative damage scheme used in this study is based on the critical element model. The influence of fiber-matrix interphase on the fatigue life of cross-ply laminates was predicted using the cumulative damage scheme. The predicted fatigue life matches well with the experimental values for all three material systems at different load levels.

Appendix 1

NOMENCLATURE USED IN THE MODEL

r_f = Fiber radius

r_{fl} = Radius of inner core

E_{f2} = Fiber modulus

E_{fl} = Stiffness of the inner core

i = Number of broken fibers in the inner core

v_f = Fiber volume fraction in the average composite

v_f' = Fiber volume fraction in the inner core

u_{fl} = Displacement of inner core

u_{f2} = Displacement of adjacent fiber

u_c = Displacement of the average outer composite ring

$d = r\,(1/v_f) - 1))$

b = Thickness of the matrix region over which stress transfer occurs (2*d)

η = Efficiency factor

G_m = Shear modulus of the matrix material

E_x = Axial modulus of the average composite material

σ_a = Applied external stress

E_m = Young's modulus of matrix

τ_i = Interfacial shear strength

m = Weibull shape factor for the fiber

σ_0 = Weibull location parameter for the fiber

N = Total number of fibers in the composite

L = Length of the test specimen

δ_i = Elastic ineffective length

δ_i^* = Plastic ineffective length

C_i = Elastic stress concentration factor

C_i^* = Plastic stress concentration factor

n_i = Number of nearest neighboring fibers

Appendix 2

Calculation of geometric parameters

Consider a single fiber with matrix material around it. If the radius of the fiber is r_f, and the fiber volume fraction is v_f, then the thickness of the matrix layer is calculated as follows

$$v_f = r_f^2 / r_m^2$$

$$r_m = r_f / (v_f)^{0.5}$$

The thickness of the matrix layer is obtained as

$$d = r_m - r_f$$

$$d = r_f \left(\frac{1}{\sqrt{v_f}} - 1 \right)$$

Consider an inner core of radius r_{fl} that consists of i broken fibers. Let r'_m be the radius of the matrix material that surrounds the inner core of broken fibers. For this arrangement, the various geometric parameters are calculated as follows

$$v_f = i\, r_f^2 / r'^2_m$$

$$r_{m'} = \frac{\sqrt{i}\, r_f}{\sqrt{v_f}}$$

The radius of the inner core of broken fibers can be written as

$$r_{fl} = r_{m'} - d$$

$$r_{fl} = \frac{\sqrt{i}\, r_f}{\sqrt{v_f}} + r_f - \frac{r_f}{\sqrt{v_f}}$$

$$r_{fl} = r_f \left[\frac{\sqrt{i} - 1}{\sqrt{v_f}} + 1 \right]$$

The various geometric parameters used in the tensile strength prediction model are listed below

$$d = r_f \left(\frac{1}{\sqrt{v_f}} - 1 \right)$$

$$r_{fl} = r_f \left(\frac{\sqrt{i} - 1}{\sqrt{v_f}} + 1 \right)$$

$$r_m = r_{fl} + 2d$$

$$r_{f2} = r_m + 2 r_f$$

$$r_c = r_{f2} + 2d$$

The damaged modulus of the inner core is calculated using the rule of mixture. However, the fiber volume fraction in the inner core is different from that of the composite material. The fiber volume fraction of the inner core is calculated as follows

$$v_f' = i\, r_f^2 / r_{fl}^2$$

This new volume fraction is used to estimate the stiffness of the inner core as

$$E_{fl} = (v_f' * E_f) + (1 - v_f') * E_m$$

Appendix 3

Longitudinal stiffness prediction using Concentric Cylinders Model (CCM)

1. Auxiliary Problem

A solution (using CCM) to the problem of a single fiber embedded in an infinite matrix is outlined in this section. The solution procedure used in this analysis is similar to that described in reference [25]. A displacement formulation is used to solve the problem, and the external loads are applied in the form of tractions. Figure A1 shows the schematic of the concentric cylinders assemblage model. Since the problem is axisymmetric, the polar coordinates are used to solve the problem. Throughout this section, superscripts f and m represent the quantities in the fiber and matrix phases respectively. It is assumed that the fiber and matrix are homogeneous, linearly elastic materials. The matrix is assumed to be isotropic and the fiber transversely isotropic. Due to axisymmetry, the displacement field in the two domains can be expressed in the following form

$$u_r^{(m)} = B_1^{(m)} r + \frac{B_2^{(m)}}{r}$$
$$u_\theta^{(m)} = 0$$
$$u_z^{(m)} = D z$$

(a1)

$$u_f^{(m)} = B_1^{(f)} r + \frac{B_2^{(f)}}{r}$$
$$u_\theta^{(f)} = 0$$
$$u_z^{(f)} = \eta D z$$

Note that in writing the above displacement fields, it has been assumed that the axial displacement is not continuous at the fiber-matrix interface. The efficiency factor η has been introduced in these relationships such that $\eta = u_f/u_m$. For such a displacement field, the equations of elasticity reduce to the following simple form

Strain-Displacement Relationship

$$\varepsilon_{rr}^{(n)} = \frac{du_r^{(n)}}{dr}$$
$$\varepsilon_{\theta\theta}^{(n)} = \frac{u_\theta^{(n)}}{r} \qquad \text{(a2)}$$
$$\varepsilon_{zz}^{(n)} = \frac{du_z^{(n)}}{dz}$$
$$\varepsilon_{rz} = \varepsilon_{\theta z} = \varepsilon_{r\theta} = 0$$

Constitutive Relationship

$$\sigma_{zz}^{(n)} = C_{11}^{(n)}\,\varepsilon_{zz} + C_{12}^{(n)}\,\varepsilon_{rr}^{(n)} + C_{13}^{(n)}\,\varepsilon_{\theta\theta}^{(n)}$$
$$\sigma_{rr}^{(n)} = C_{12}^{(n)}\,\varepsilon_{zz} + C_{22}^{(n)}\,\varepsilon_{rr}^{(n)} + C_{23}^{(n)}\,\varepsilon_{\theta\theta}^{(n)} \qquad \text{(a3)}$$
$$\sigma_{\theta\theta}^{(n)} = C_{12}^{(n)}\,\varepsilon_{zz} + C_{23}^{(n)}\,\varepsilon_{rr}^{(n)} + C_{22}^{(n)}\,\varepsilon_{\theta\theta}^{(n)}$$

where $C_{ij}^{(n)}$ are the elements of the reduced stiffness matrix of the constituent phases. Substituting the assumed displacement functions in equations a2 and a3 yields the various components of the stress tensor in the fiber and matrix phases.

In order to evaluate the constants that appear in the assumed displacement functions, the displacement and traction continuity conditions are enforced at the fiber-matrix interface. It is required that the radial displacements and radial stresses in the fiber and matrix be equal at the fiber-matrix interface. This is expressed as

$$u_r^{(f)} = u_r^{(m)} \qquad \text{(a4)}$$
$$\sigma_{rr}^{(f)} = \sigma_{rr}^{(m)} \qquad at \qquad r = r_f \qquad \text{(a5)}$$

In this analysis, loads are applied in the form of tractions. Since the stresses in the fiber and matrix are different, the traction boundary condition is applied by considering that the applied longitudinal load is equal to the sum of the volume averaged stresses in the longitudinal direction. This expressed mathematically as

$$\int \sigma_{zz}^{(f)}\, dV + \int \sigma_{zz}^{(m)}\, dV = \sigma_{zz}^{app} \qquad \text{(a6)}$$

It is also required that the radial stress σ_{rr} vanish as r -> ∞. This is expressed as

$$\left(\sigma_{rr}^{(m)}\right)_{r \to \infty} = 0 \qquad \text{(a7)}$$

In order for the displacement to be finite at the center of the fiber, the constant $B_2^{(f)}$ is set equal to 0. The other four constants $B_1^{(f)}$, $B_1^{(m)}$, $B_2^{(m)}$ and D are evaluated by solving equations a4-a7.

2. Complete Solution

The fiber-fiber interactions are accounted for in an approximate sense using the Mori-Tanaka average stress scheme. A detailed description of this method is available in reference [25]. The general procedure is outlined here for completeness.

The solution of a single fiber embedded in an infinite matrix subjected to uniform longitudinal loading, is obtained first using the method outlined in the previous section (Auxiliary problem). The stresses obtained from the auxiliary problem are written in the following form

$$\sigma_{rr}^{(n)} = h_{rr}^{(n)}\, \sigma_0 \qquad \text{(a8)}$$

$$\sigma_{zz}^{(n)} = h_{zz}^{(n)}\, \sigma_0 \qquad \text{(a9)}$$

where h_{rr} and h_{zz} are defined as the concentration factors in the fiber and matrix phases. These concentration factors are averaged over the entire volume of the composite to obtain the volume averaged concentration factors as follows

$$\left\langle h_{\alpha\beta}^{(n)} \right\rangle = \frac{1}{\pi \left(r_o^2 - r_i^2\right)} \int_0^{2\pi} \int_{r_i}^{r_o} h_{\alpha\beta}^{(n)}\, r\, dr\, d\theta \qquad \text{(a10)}$$

where n = fiber, matrix

$\alpha\beta$ = rr and zz

In order to account for the fiber-fiber interactions in an approximate sense, the applied external load is replaced by the unknown average stress $\langle\sigma_{zz}^{(m)}\rangle$ and $\langle\sigma_{rr}^{(m)}\rangle$. These average stresses are estimated using

the solution to the auxiliary problem and the rule of mixtures approximation written in the following form

$$V_f \left\langle \sigma_{zz}^{(f)} \right\rangle + V_m \left\langle \sigma_{zz}^{(m)} \right\rangle = \sigma_0 \tag{a11}$$

$$V_f \left\langle \sigma_{rr}^{(f)} \right\rangle + V_m \left\langle \sigma_{rr}^{(m)} \right\rangle = 0 \tag{a12}$$

The volume averaged stresses $<\sigma_{zz}^{(n)}>$ and $<\sigma_{rr}^{(n)}>$ can be written in terms of the volume averaged concentration factors in the following form

$$\left\langle \sigma_{\alpha\beta}^{(n)} \right\rangle = \left\langle h_{\alpha\beta}^{(n)} \right\rangle \left\langle \sigma_{zz}^{(m)} \right\rangle \tag{a13}$$

where n = fiber, matrix

$\alpha\beta$ = rr and zz

Using equation a13 in equations a11 and a12 we obtain

$$V_f \left\langle \left\langle h_{zz}^{(f)} \right\rangle \left\langle \sigma_{zz}^{(m)} \right\rangle \right\rangle + V_m \left\langle \sigma_{zz}^{(m)} \right\rangle = \sigma_0 \tag{a14}$$

$$V_f \left\langle \left\langle h_{rr}^{(f)} \right\rangle \left\langle \sigma_{zz}^{(m)} \right\rangle \right\rangle + V_m \left\langle \sigma_{rr}^{(m)} \right\rangle = 0 \tag{a15}$$

The average stresses $<\sigma_{zz}^{(m)}>$ and $<\sigma_{rr}^{(m)}>$ are estimated by solving equations a14 and a15. The complete solution to the problem is obtained by replacing the applied external load with $<\sigma_{zz}^{(m)}>$ and $<\sigma_{rr}^{(m)}>$. The longitudinal stresses in the fiber and matrix are written as

$$\sigma_{zz}^{(n)} = h_{zz}^{(n)} \left\langle \sigma_{zz}^{(m)} \right\rangle \tag{a16}$$

The strains in the fiber and matrix are estimated using the constitutive relationships (equation a3). The average strain in the composite is estimated using the rule of mixtures as

$$\varepsilon_{zz}^{tot} = V_f \, \varepsilon_{zz}^{(f)} + V_m \, \varepsilon_{zz}^{(m)} \tag{a17}$$

The average stiffness of the laminate in the longitudinal direction is calculated as

$$E_{11} = \frac{\sigma_0}{\varepsilon_{zz}^{tot}} \tag{a18}$$

Note that the average stiffness estimated using the above equation is a function of the efficiency factor η. The efficiency factor can be estimated using this equation, if the longitudinal stiffness of the

unidirectional composite is known. Using the properties for the Apollo fibers and HC 9106-3 matrix [16] in the above analysis, the variation of longitudinal stiffness with η was determined and is plotted as figure A2. Results indicate that the longitudinal stiffness is a non-linear function of η. As $\eta \rightarrow 1$, the stiffness of the composite approaches the value predicted by the rule of mixtures, which assumes perfect bonding. As $\eta \rightarrow 0$, the stiffness of the composite approaches the stiffness of the matrix. This is because no load is being transferred to the fiber, and all the load is being carried by the matrix material. The efficiency factor η for a given material system can be estimated using the longitudinal modulus (determined from a tensile test on a unidirectional composite) in equation a18.

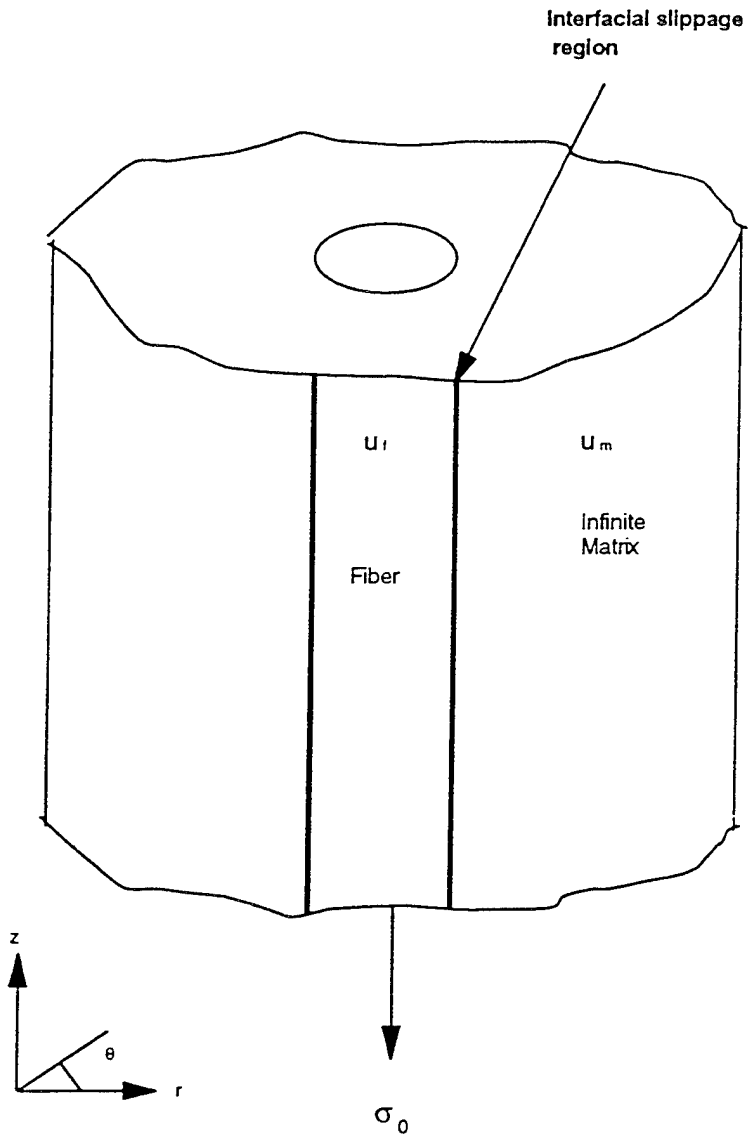

Figure A1 Schematic of the Concentric Cylinders Model Assemblage Model.

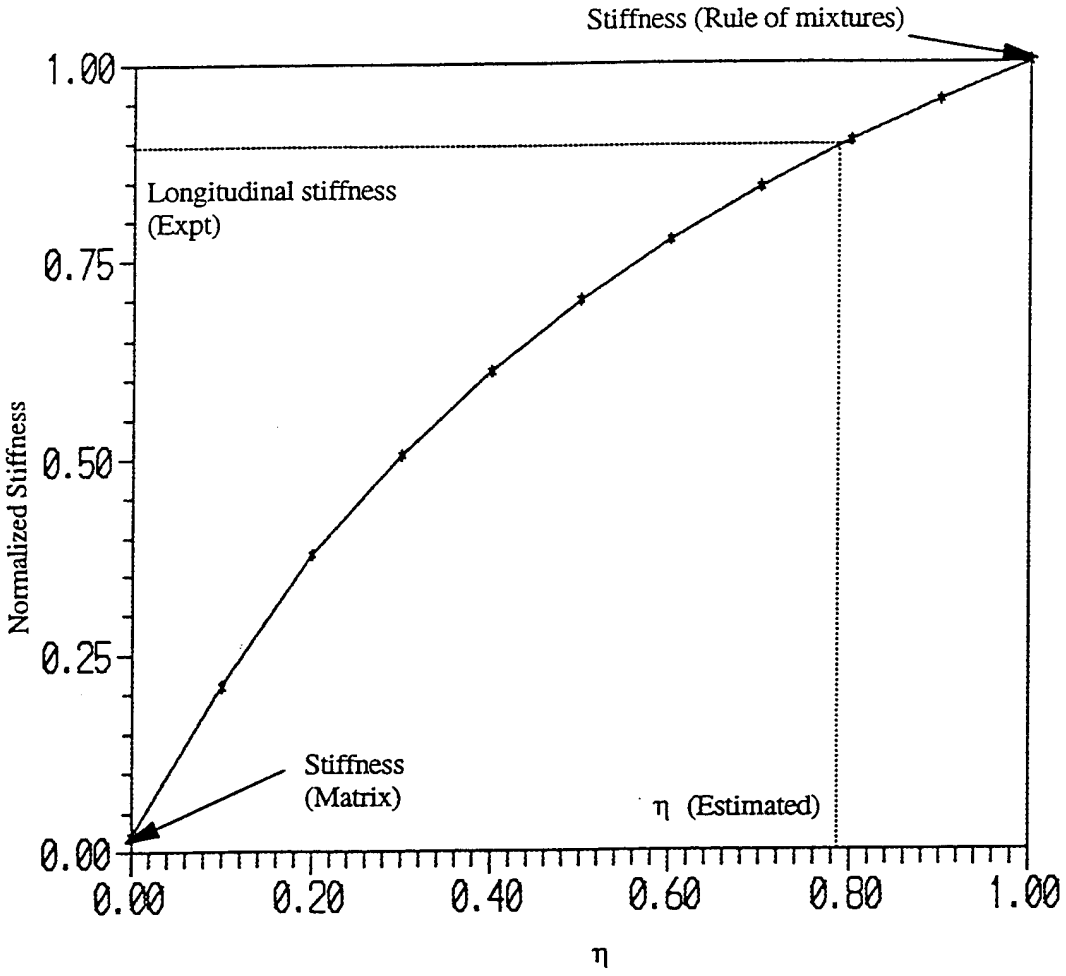

Figure A2 Variation of longitudinal stiffness with η

REFERENCES

1. Subramanian, S., " Effect of fiber-matrix interphase on the long term performance of cross-ply laminates," Ph.D. Dissertation, Virginia Polytechnic Institute and State University, 1994.

2. Lesko, J. J., Swain, R. E., Cartwright, J. M., Chin, J. W., Reifsnider, K. L., Dillard, D. A., and Wightman, J. P., "Interphases developed from fiber sizings and their chemical-structural relationship to composite compressive performance," Submitted to the Journal of Adhesion, February, 1993.

3. Swain, R. E., " The Role of the Fiber/Matrix Interphase in the Fatigue Behaviour of Polymeric Composite Laminates," PhD. Dissertaion, Virginia Polytechnic Institute and State University, 1992.

4. Olley, R. H., Bassett, D. C., Blundell, D. J., "Permenganic Etching of PEEK," Polymer, Vol. 27, March 1986, pp. 344-348.

5. Peters, P. W. M, and Albertsen, H., "The Fiber-Matrix Interphase in CFRP with a phase separating Matrix System," Interfacial Phenomena in Composite Materials, Leuven, Sept. 17-19, 1991, p. 101-104.

6. Hahn, G., Wong, R., Hwang, W.-F., Hartness, T, Drzal, L. T., Robinson, R., and Smith, S., " "Development of Ultrlightweight Materials," Tenth Quarterly Interim Technical Report, Air Force Contract No. F 33615-88-C-5452, Nov. 1990.

7. Lesko, J. J., et al., " A global local investigation of compressive strength to determine the influence of the fiber/matrix interphase," Compression Response of Composite Structures, ASTM STP, American Society for Testing and Materials, Philadelphia, 1992.

8. S. Subramanian, J. S. Elmore, and W. W. Stinchcomb, " The influence of fiber-matrix interphase on the long-term behavior of graphite/epoxy composites," To be presented at the 12th Symposium on Composite Materials : Testing and Design, May 16-17, 1994, Montreal, Quebec, Canada.

9. Ivens, J., Wevers, M., and Verpoest, I., " An energy based model for the influence of the fiber-matrix interface strength on the interlaminar fracture toughness of UD-Composite laminates," in Local Mechanics Concepts for Composite Material System, IUTAM Symposium Blacksburg, VA, 1991, J. N. Reddy, and K. L. Reifsnider, Ed., pp. 215-228.

10. Drzal, L. T., Rich, M. J., and Lloyd, P. F., Journal of Adhesion, 16,1 (1982).

11. Ivens, J., Wevers, M., Verpoest, I., and de Meester, P., "Influence of the Fiber-Matrix Interface on the matrix crack development in Carbon-Epoxy Cross-Ply laminates," in Developments in the Science and Technology of Composite Materials, ECCM 3, Ed., A. R. Bunsell, P. Lamicq, A. Massiah, March 1989, pp. 465-471.

12. Liu, S., and Nairn, J. A., "The formation and propagation of matrix microcracks in cross-ply laminates during static loading," Journal of Reinforced Plastics and Composites, Vol. 11, Feb 1992, pp. 158-178.

13. Tan, S. C., and Nuismer, R. J., "A theory for progressive matrix cracking in composite laminates," Journal of Composite Materials, Vol. 23, Oct 1989, pp. 1029-1047.

14. Varna, J., and Berglund, L., "Multiple Transverse Cracking and Stiffness Reduction in Cross-Ply Laminates," Journal of Composites Technology and Research, Vol. 13, No.2, Summer 1991, pp. 99-106.

15. Flagg, D. L., and Kural, M. H., "Experimental Determination of the In Situ Transverse Lamina Strength in Graphite/Epoxy Laminates," Journal of Composite Materials, Vol. 16, March 1982, pp. 103-115.

16. Ochiai, S., Peters, P. W. M., Schulte, K., and Osamura, K., "Monte-Carlo simulation of multiple fracture in transverse ply of cross-ply graphite-epoxy laminates," Jounal of Materials Science, Vol. 26, 1991, pp. 5433-5444.

17. Subramanian, S., Lesko, J. J., Reifsnider, K. L., and Stinchcomb, W. W., " Damage mechanisms and failure modes in cross-ply laminates under monotonic tensile loading : The influence of fiber sizing," Accepted for publication in Applied Composite Materials, 1995.

18. Camponeschi, E. T., Stinchcomb, W. W., "Stiffness reduction as an indicator of damage in graphite/epoxy laminates," Composite Materials: Testing and Design (Sixth Conference), ASTM STP 787, I. M. Daniel, Ed., ASTM, 1982, pp. 225-246.

19. Talreja, R., "Stiffness based fatigue damage characterization, " Fatigue of Composite Materials, Ch.5, Technomic, 1987.

20. Reifsnider, K. L., and Stinchcomb, W. W., "Stiffness change as a fatigue damage parameter for composite laminates," Advances in Aerospace Structures, Materials and Dynamics, Yuceoglu, U.,Seirakowski, R. L., Glasow, D. A., eds., ASME, New York, 1983.

21. Reifsnider, K. L. and Gao, Z.,"A micromechanics model for composites under fatigue loading," Int. J of Fatigue, Vol. 13, No.2, 1991, pp. 149-156.

22. Gao, Z., and Reifsnider, K. L., "Tensile Failure of Composites : Influence of Interface amd Matrix Yielding," Journal of Composites Technology and Research, Vol. 14, No. 4, Winter 1992, pp. 201-210.

23. Reifsnider, K. L. and Stinchcomb, W. W., "A Critical Element Model of the Residual Strength and Life of Fatigue-Loaded Composite Coupons," Composite Materials: Fatigue and Fracture, ASTM STP 907, H. T. Hahn, Ed., ASTM, Philadelphia, 1986, pp. 298-303.

24. Lee, J.-W., and Daniel, I. M., "Progressive Transverse Cracking of Cross-Ply Composite Laminates," Journal of Composite Materials, Vol. 24, Vov 1990, pp. 1225-1243.

25. Parvizi, A., Garrett, K. W., and Bailey, J. E., "Constrained Cracking in Glass Fiber reinforced Epoxy Cross-Ply Laminates," J. Materials Science, Vol. 13, 1978, pp. 195-201.

26. Flaggs, D. L., "Prediction of Tensile Matrix Failure in Composite Laminates," Journal of Composite Materials, Vol. 19, January 1985, pp. 29-50.

27. Gao, Z., Reifsnider, K. L., and Carman, G. P., "Strength Prediction and Optimization of Composites with Statistical Flaw Distribution," Journal of Composite Materials, Vol. 26, No. 11, 1992, pp. 1578-1705.

28. Harlow, D. G., and Phoenix, S. L., "Probability Distribution for Strength and Composite Materials I : Two-Level Bounds," International Journal of Fracture, Vol. 17, 1981, pp.321-336.

29. Reifsnider, K. L., "Some Fundemental aspects of the Fatigue and Fracture of Composite Materials," Proceedings, 14th Annual Conference of Enginnering Mechanics, Lehigh University, Bethleham, PA, 1977, pp. 373-384.

30. Hegdepeth, J. M., and Van Dyke, P., "Local Stress Concentration in Inperfect Filamentary Composite Materials," Journal of Composite Materials, 1968.

31. Harlow, D. G., and Phoenix, S. L., "The Chain-of-Bundles Probability Model for the Strength of Fibrous Materials I : Analysis and Conjectures," Journal of Composite Materials, Vol. 12, April 1978, pp. 195-213.

32. Harlow, D. G., and Phoenix, S. L., "The Chain-of-Bundles Probability Model for the Strength of Fibrous Materials II : A Numerical Study of Convergence," Journal of Composite Materials, Vol. 12, July 1978, pp. 314-334.

33. Chang, Y. S.," The affect of the Interphase/Interface Region on Creep and Creep Rupture of Thermoplastic Composites," PhD. Dissertation, Virginia Polytechnic Institute and State University, 1992.

34. Lehmann, S., Megerdigian, C., and Papalia, R., "Carbon Fiber/Resin Matrix Interphase : Effect of Carbon Fiber Surface Treatment on Composite Performance," SAMPE Quarterly, April 1985, pp. 7-13.

35. Madhukar, M. S. and Drzal, L. T., "Fiber-Matrix Adhesion and its Affects on Composite Mechanical Properties :II. Longitudinal and Transverse Tensile and Flexure behaviour of Graphite/Epoxy Composites," Journal of Composite Materials, Vol.25, 1991, pp.958-991.

36. Greszcuk, L. B., "Theoretical Studies in the Mechanics of Fiber-Matrix Interface in Composites," Interfaces in Composites, ASTM STP 452, ASTM, Philadelphia, pp. 42-85.

37. Reifsnider , K. L., and Highsmith, A. L., " Stiffness reduction mechanisms in composite laminates," in Damage in Composite Materials, ASTM STP 775, K. L. Reifsnider Editor, pp. 103-117, 1982.

38. Zhang, J., Fan, J., and Soutis, C., "Analysis of multiple matrix cracking in $(+\theta_m,90_n)_s$ composite laminates - Part I : In-plane stiffness properties," Composites, Vol. 23, No. 5, Sept 1992, pp. 291-298.

39. Dvorak, G. J., Laws, N., and Hejazi, M., "Analysis ofProgressive Matrix Cracking in Composite Laminates-I. Thermoelastic Properties of a Ply with Cracks," Journal of Composite Materials, Vol. 19, 1985, pp. 216-234.

40. Talreja, R., "Transverse Cracking and Stiffness Reduction in Composite Laminates," Journal of Composite Materials, Vol. 19, 1985, pp. 355-375.

41. Hashin, Z., "Analysis of Cracked Laminates : A Variational Approach," Mechanics of Materials, Vol. 4, 1985, pp. 121-136.

42. Lim, S. G., and Hong, C. S., "Prediction of Transverse Cracking and Stiffness Reduction in Cross-Ply Laminated Composites," Journal of Composite Materials, Vol. 23, July 1989, pp. 695-713.